Design and Development of a Testing Machine for Compressive Creep Tests on Polymers at Elevated Temperatures

Master Thesis

by

Silvia Brunbauer

at the

Institute of Materials Science and Testing of Polymers

Supervision: Dipl.-Ing. Andreas Kaufmann
Assessor: Univ.-Prof.Dr. Gerald Pinter

Leoben, August 2016

AFFIDAVIT

I declare in lieu of oath, that I wrote this thesis and performed the associated research myself, using only literature cited in this volume.

EIDESSTATTLICHE ERKLÄRUNG

Ich erkläre an Eides statt, dass ich diese Arbeit selbstständig verfasst, andere als die angegebenen Quellen und Hilfsmittel nicht benutzt und mich auch sonst keiner unerlaubten Hilfsmittel bedient habe.

LEOBEN, August 2016

Contents

I. Abstract

In many long term applications, where polymers are used as engineering components, the creep behavior can be a dominating part of the observed material properties depending on the material and the load case. If creep tendencies are to be expected under load and temperature for a certain material, it is useful to have reliable creep measurement data available, that allow a more accurate component design.

The development, validation and calibration of a compression creep test machine is presented in this thesis. Since the test setup should fit into a prescribed environment, a modular and compact test setup is developed. The design allows, that a variable number of specimens can be applied with stress in parallel. Thus various reproductive creep measurements can be performed simultaneously at the same test conditions.

The developed testing machine is able to characterize the compressive creep behavior of polymers at load levels up to 2000 N and temperatures ranging from room temperature to 200°C. The displacement measurement range is up to 1 mm measurement distance with the currently implemented calibration. The stress in the specimen is applied by a moving piston, that is guided inside a cylinder and is loaded with pressurized air. The pressure on the piston is regulated by a proportional valve and a cylindrical specimen is positioned underneath the piston on a load cell. The time dependent displacement is detected by a sensor that is attached to the piston. For the development, three test rigs are combined to one test battery that is characterized in detail.

To quantify the measuring certainty an extensive sensor calibration and uncertainty analysis is performed. It could be shown, that with careful calibration the displacement sensor performance can be increased significantly by one decimal power. Temperature influences on the displacement sensors could be estimated by a specially developed calibration method. After the sensor calibration the test rig performance was investigated. The loading and unloading behavior of the system and the intrinsic system compliance are characterized at room temperature and elevated temperatures.

It could be shown, that the chosen test setup allows controlled loading and unloading of the specimens with high reproducibility. With modified sealing elements on the piston and a nonlinear pressure regulation an overshooting of pressure during loading and an entire unloading is enabled. With all calibration procedures the displacement sensors allow an overall measuring certainty of 1% of the maximum measurement distance and the load cells a measuring certainty of 0.2%.

II. Acknowledgment

During the work on this thesis and my studies many people have supported and inspired me and I would like to express my deepest gratitude to them.

First and foremost I want to thank Univ.-Prof.Dr. Gerald Pinter for enabling this thesis. Not only by his support during research, but also by giving me the possibility to work at his institute for many years and for awaken my curiosity and interest in material testing and polymer science.

My sincere thanks also go to Dipl.-Ing. Andreas Kaufmann for giving me guidance and support throughout the entire work and for repeatedly motivating me with his unclouded good mood. I wish you and your little family all the best for the future.

Furthermore, I would like to express my thanks to Hoerbiger Ventilwerke GmbH & Co KG and Tino Lindner-Silwester for enabling this project.

I also want to offer my warmest thanks to Prof. Paul O'Leary, who motivated me with his engagement and who opened new perspectives to me, when I needed them most.

And just like a tree can only grow upright and straight when it is not out in the fields all alone, but surrounded by others, that protect it from harm and rough winds, I owe my progress to my family and friends. I want to express heartfelt gratitude to my parents Gertrude and Gottfried and to my siblings for inspiring and supporting me and for offering a loving and caring environment one could only wish for.

Finally, my warmest and deepest thanks go to Rene, who has accompanied me during the last five years with all his love and understanding, who motivates and supports me and who gives me the protection and power to grow.

1. Introduction

During the last decades polymers have made their way into many different applications due to their wide scope of properties. They have become an alternative to other materials in more and more engineering components, since they enable economic, customized, lightweight solutions. In some applications, polymers are the first choice due to their distinct viscoelastic properties. Such as in compressors, where polymeric components are used to seal high pressure areas. Sealing elements of compressors are exposed to many different loads, such as temperature, cyclic loads due to friction and also a constant pressure gradient. To face these challenges a high performance polymer, polytetrafluorethylene (PTFE), is used. For economic reasons the maintenance intervals of compressors should be maximized. This is why the long term functionality of all used components has to be guaranteed.

To estimate the behavior of polymeric components over extended application times, the knowledge about the long term material behavior is indispensable. However, in the development phase the components behavior can not always be tested in the real application conditions, such as a compressor, over the whole service time. This is why accelerated measurements and simulation is required to enable fast development of high performance components [1]. Even if testing under application conditions is not always possible, the material should still be characterized under similar test conditions. This can sometimes be challenging, due the complexity of components and the resulting load cases and stress distributions. This is why the complex load situation is separated into different, less complex load cases and each load case is characterized individually, e.g. friction behavior and creep behavior [2].

In this thesis a test machine to characterize the compressive creep behavior of polymeric materials was designed and developed. To allow application oriented material testing, compressive creep tests can be performed at elevated temperatures. This is why a short introduction to viscoelasticity and especially creep behavior, is presented to give an overview of the time dependent phenomenon that is to be characterized. Next a general overview over compressive testing methods and the guidelines given in European and American standards are presented. To quantify the quality of the developed test machine, a measuring uncertainty analysis is performed. The proceedings on how to perform such an analysis are also documented in this thesis.

The development of a suitable test design and the advantages compared to other compressive creep testing methods are discussed. The design of the chosen mechanical test

setup is presented, as well as the instrumentation and calibration of the used sensors. The calibration of the displacement sensors is documented very extensively, since they play a central role in the acquisition of reliable creep data. To quantify the reliability of the gained material data, a measurement uncertainty analysis of the whole test equipment is performed. This analysis is performed following guidelines and recommendations of literature and standards. With the knowledge gained from this analysis, creep measurements were performed and compared to experiments on conventional test equipment.

2. Theoretical Background

An introduction to the theoretical background required for this thesis is given in this chapter. In the first section the phenomenon of the viscoelasticity of polymers is introduced. To characterize the viscoelastic properties of polymers a suitable test equipment is required. In the second section an overview over the methods and challenges for the measurement of compressive creep properties of polymers is presented. In the third section an important aspect of any performed measurement is discussed, which is the measuring certainty.

2.1. Viscoelasticity and Creep

Due to their special morphological structure, polymers show strongly time and temperature dependent material behavior, compared to other engineering materials. The morphology and the correlations between polymeric structure and mechanical, thermal and chemical properties are well represented in literature [3–5].

Owing to their molecular structure, polymers do not only show elastic, but also time dependent viscoelastic and plastic material behavior, which also might be strongly temperature dependent [1, 3, 4]. This is why in the construction of polymeric engineering components under mechanic loads, special attention should be put at the time and temperature dependent material behavior of polymers.

If load is applied, and only bond angles are changed, the energy is stored elastically and is released after unloading. This is referred to as an elastic material response. When not only bond angles change, but molecular groups start to relocate over time, the behavior is described as viscoelastic. After unloading the relocation processes are reversed. Plastic behavior, can be described by molecular chains gliding against each other. The energy that is brought in by the applied stress, is dissipated by the internal friction. This is why after unloading, no repelling forces are left and the plastic deformations remain after unloading.

When stress is applied to a viscoelastic material, relocation processes in the molecular chains take place, to access a new equilibrium state. Relocation processes of different molecular groups take a specific amount of time. For several relocation processes in a material, relaxation or retardation spectra can be detected, that describe the material behavior over time [1, 6]. Therefore a material-specific relaxation or retardation time τ_0

is defined. The relaxation or retardation time τ_0, describes the time that is required, to either reduce the stress σ within a material to 1/e or 0.368 of the initial applied stress σ_0 (relaxation), or to increase the strain ϵ_{rel} to 0.632 $\sigma_0/\varepsilon_{rel}$ of the initial strain due to a constant stress (retardation or creep). With this relaxation and retardation mechanisms also the loading rate dependent material behavior can be explained [4].

Two main time dependent effects appear due to viscoelasticity, which are relaxation and creep. The deformation of a specimen due to an applied stress is known as creep or retardation, as depicted in figure 2.1. The material response to an applied strain, which is decreasing stress over time, is referred to as relaxation, as shown in figure 2.1. There are two common two-parameter material models to describe creep and relaxation processes in polymers. For creep or retardation behavior the Voigt Kelvin model is often used. This model describes the material behavior by a damping element and a spring in parallel connection. The equivalent circuit is depicted below. Though it is not quite applicable for relaxation processes. This is why a second model, the Maxwell model, is used to describe relaxation processes of materials. In this model a spring and a dash pot are connected in series [5].

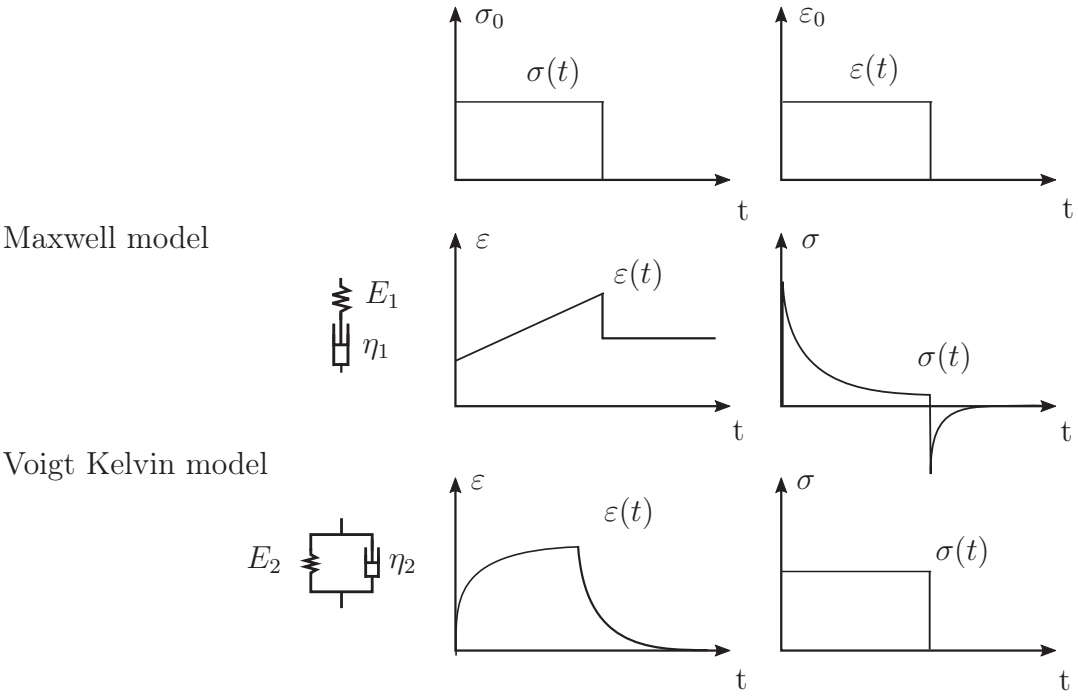

Figure 2.1.: Schematic representation of Maxwell and Voigt Kelvin model for retardation and relaxation, following [5].

For most polymers, not only viscoelastic, but also elastic and viscous or plastic deformation mechanisms can be detected. This is why more complex models than the Maxwell and Kelvin Voigt models are used, to depict the behavior more accurately.

One well established model is the 4 parameter model or Burger model, to describe viscoelastic-plastic material behavior [3]. Or the Zener model, a standard for linear solids [5].

Figure 2.2 shows the 4-parameter or Burger model for viscoelastic material behavior. If stress σ_0 is applied, the response is an instant, reversible deformation ε_{el}, which is σ_0/E_0. Due to the viscoelastic behavior, the strain ε_{rel} increases over time, but is also entirely reversible after unloading. Many materials also show viscous behavior. This results in an irreversible, time dependent strain ε_v as response. When unloading, as depicted in figure 2.2 the linear stain ε_{el} declines instantly, while the viscous strain ϵ_{rel} declines over time and the irreversible, plastic strain ε_v remains after unloading, based on [4].

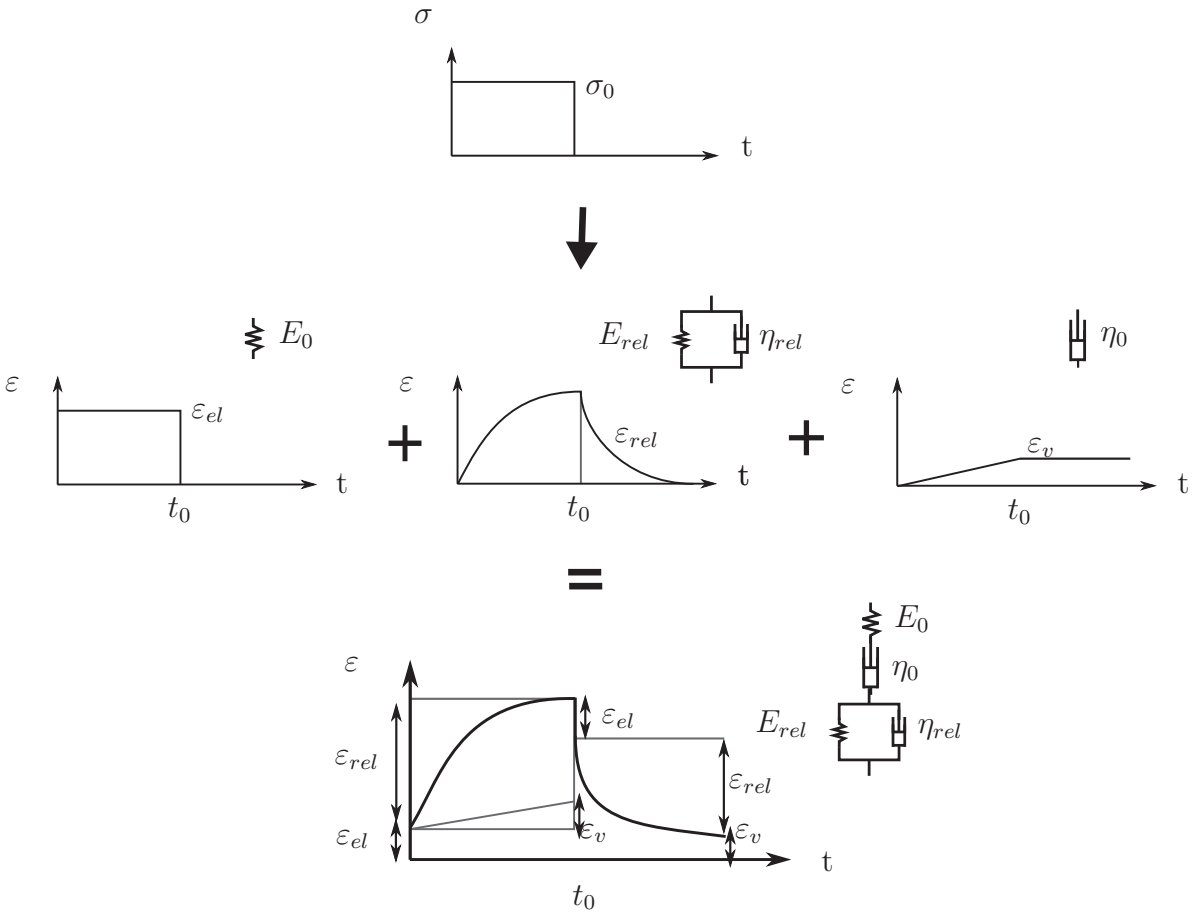

Figure 2.2.: Schematic diagram of 4-parameter model (Burger Model) for viscoelastic-plastic material behavior under constant stress σ_0.

The main principle on which the viscoelastic theory is built on, is the Boltzmann superposition principle [1]. It describes, that for linear viscoleastic material behavior, the material response for superimposed loads can also be superimposed. If a stress σ_1

leads to a time dependent deformation ε_1, and a second stress σ_2 causes the deformation ε_2, than an applied load of $\sigma_1 + \sigma_2$ results in a deformation of $\varepsilon_1 + \varepsilon_2$. Many polymers do not only react time dependent to an applied load, but the material response may also be depend on the load level. In this case, the Boltzmann superposition principle is theory no longer applicable [1].

For linear viscoelastic materials, the correlation between stress and strain is not load dependent, which means that the modulus is independent from the applied load. If the material behavior is nonlinear, the correlation between stress and strain changes depending on the load level. This can be illustrated by performing creep measurements at different stress levels. With this data, isochronic stress-strain diagrams can be constructed. For small strains, when the isochronic stess-strain correlation is linear, the material behavior is linear viscoelastic, following [3].

In addition to time and load, the mechanical properties of polymers also highly depend on the temperature [3, 4]. In the polymeric structure the molecular groups and bonds, in the side branches as well as in the backbone, move with a certain temperature dependent frequency. The time required for relocation processes τ_0 can be calculated according to equation 2.1. Where f_0 is the frequency with which the molecular groups swing at equilibrium, R is the gas constant for ideal gases, E_a is the activation energy for the observed relocation mechanism and T is the temperature. With the assumption, that certain relocation mechanisms have specific activation energies [1], it can be seen, that according to equation 2.1, the relaxation or retardation time τ_0 decreases with increasing temperature T.

$$\tau_0 = \frac{1}{2f_0} e^{\frac{E_a}{RT}} \tag{2.1}$$

The activation energy is specific for each relocation process. And according to equation 2.1, the time required for the relocation processes decreases with elevated temperature. This is why at higher temperatures, creep and relaxation processes proceed faster. Based on this observation, accelerating methods for creep experiments were developed. Two main approaches for accelerated material characterization by using the time temperature dependency in polymers are the Arrhenius and the William-Landel-Ferry (WLF) time-temperature correlation principles. While Arrhenius uses an energy based method, the WLF approach is based on the specific volume of polymers [1].

2.2. Compression Test Systems

2.2.1. General Requirements and Challenges

Characterizing the viscoelastic material properties of polymers can be challenging and requires sophisticated and application-specific measurement solutions. Depending on the

measurement method and the tested material high requirements concerning tolerances and measurement precision must be met. Various standards give an overview of the challenges in compression testing.

A detailed guideline for compression testing is for example given in the standard ISO 604 [7], which defines the terminology used, gives recommendations for compression testing equipment and specimen types and provides instructions for the test procedure. General requirements to the test equipment, such as the tolerances on the load direction, the parallelism and evenness of the test plates and the displacement measurement devices, are documented. According to ISO 604 section 5.1.3 the load direction in a compression test is required to be maximum of 1:1000 off-axis by polished steel plates, of an evenness, parallelism and perpendicularity smaller than 0.025 mm. In the following, compression testing in a test setup is discussed, where the specimen is positioned between two parallel surfaces. Other clamping situations, such as a specimen fixed between two pneumatic, mechanical or hydraulic clamps, is further not discussed in detail.

In the section 9.3 of ISO 604 guidelines dealing with the friction between the specimen and the plates are given. It is recommended to either use lubrication between the specimen and the test equipment to reduce friction or to use sand paper to prevent sliding entirely. The influence of the friction at the front surfaces on the results depends on the investigated material. For thermoplastic materials (e.g. for polyethylene [8]), several specimen types and lubrication methods were investigated to reduce friction.

To deal with this issues, several different compression test systems were developed. Each system has different advantages. All testing methods share the same difficulties, which is the load application, the parallelism, a proper specimen geometry and a proper displacement measurement technique [7–10].

The displacement measurement technique is also dependent on the specimen type used. In the ISO 604, a rectangular cylindrical, prismatic or pipe-shaped specimen geometry is recommended and specifically a prismatic shaped type, made from the universal specimen types A or B as documented in ISO 3167 [11]. A displacement measurement equipment is to be chosen, that fulfills the geometric framework conditions of the testing machine and the requirements of the accuracy. For soft materials, contacting extensiometers for local strain determination should be avoided, due to local stress concentration as a consequence of local indentations. This is why for soft materials, contact-less displacement measurement techniques are to be preferred, such as optical measurement methods, or other solutions [9]. If no optical method is used and the displacement measurement device can not be attached to the specimen, the compliance of the equipment, which contributes to the measurement displacement ought to be considered. It is recommended to consider the machine compliance C_m in the data evaluation [7].

Another critical point of compression test systems is the load application, since in compression effects such as buckling may appear [7]. The load application is often

dependent on the specimen geometry and the chosen clamping situation. The critical buckling load F^* depends on the material stiffness E_c, the geometrical moment of inertia I and the Euler buckling length l, that is defined by the clamping situation, as given in equation 2.2.

$$F^* = \frac{\pi^2 E_c I}{l^2} \tag{2.2}$$

The larger the buckling length for specimens with a low stiffness and a constant geometrical moment of inertia is, the lower is the critical buckling force F^*, and the more important is the alignment of the load direction and the specimen. However the shorter the specimens are, and the larger the ratio of diameter to specimen length gets, the more critical are stress influences on the specimen endings due to friction on the contact surface or the clamping situation [7, 8].

The stiffness and toughness of the tested material, and the mechanical workability pay an important role in the choice of specimen geometry. This creates entirely different requirements to the specimen preparation. For brittle materials, e.g. ceramics, it is important to avoid notches at the surface due to cutting or polishing and further small misalignments that may influence the test results [12]. For polymers, depending on the specimen type, different aspects come to the fore. For rectangular prismatic specimen geometries, e.g. the ones milled or cut of the ISO specimens, the parallelism of the front surfaces may be very challenging for soft materials.

If stiff materials are to be characterized, the choice of a proper displacement measurement device is important, since very small strains should be detected. For brittle and stiff polymeric materials, the similar issues to the measurement of ceramics arise, when it comes to alignment and parallelism. Since the stiffness is high, stress can not be redistributed by deformation. And if local stresses appear, they easier lead to damage, since the strain at break is lower for brittle materials [2, 12]. Materials with high crack resistance and low stiffness, are less sensitive so small misalignments. Local stresses can be redistributed by deformation. However, at high deformation levels, the friction gets more critical and may lead to inhomogeneous stress distributions. One effect of inhomogeneous stress distribution is for example barreling. In this case, the calculation that the stress is load per area is no longer unlimitedly valid. Since this would assume, that the stress is homogeneous over the whole specimen.

All those material- and test procedure dependent requirements must be met by an applicable testing device. This is why several different compression testing machines have been developed in the past and a selection is presented in the following section.

2.2.2. Different Test Systems

For performing only a few compression creep characterization measurements, it may be more economic to use conventional test equipment. This can be universal testing machines with a mechanical screw drive, or might be a hydraulic conventional test setup. Conventional test equipment is usually calibrated annually by the manufacturer, and has a well known measurement uncertainty and user friendly handling. Though, for a longer measurement period, universal testing machines might be too expensive or have limited availability, since they are often also used for more complex material tests. If a furnace is needed in addition, to measure at elevated temperature, the equipment costs per hour increase additionally. This is why testing machines specifically designed for creep measurements are also available on the market [13–15]. However those machines are associated with high acquisition costs and must not necessarily fit into the available infrastructure.

A more economic option, is to apply weight to the specimen, and measure the deformation over time. For this solution a displacement measurement device is needed, and defined weights in various steps. Sometimes, especially for soft materials, the realizable specimen geometries have a lower limit, due to limitations in the manufacturing process. This is why for some materials a minimum specimen size is required, to ensure proper tolerances. To test those specimens under higher stresses, the needed weights increase rapidly as well as their volume. This may exacerbate the handling, at room temperature and especially at elevated temperature. Another challenging issue is, that dynamic shocks of the specimen or an overshooting of the applied load must be avoided when applying the weight. And if measurements are to be performed in a furnace at high stress levels, the limited space due to the weights has to be taken into consideration.

Lever systems are very precise tools, where a weight is applied at one end and the load is transmitted to the other end of the lever system, where the specimen is placed [13]. The stress level in the specimen can be varied, by shifting the weight along the lever with small linear engines. This way, a nearly step less modification of the stress level can be realized. However, the lever system can be placed in a furnace depending on the engineering. But if the stress is regulated manually, the regulation must either be possible from outside the furnace, or the specimen can not be loaded and unloaded at elevated temperature.

Another method is to use a media to transfer pressure onto a moved specimen holder. This media can be, for example pressurized air. If the regulation valve can be positioned outside the furnace, a piping system can transfer the pressurized air into the test chamber and the pressure piston. One downside for sealed systems working with compressed air, is that sealings are often only technically leak proof, but do mostly loose pressure over time. A solution is, to work with permanent leakage of air and constantly regulate the pressure in the system. If the leakage can be kept moderate, the economic aspect of the

compressed air that goes missing can be neglected.

Other, interesting methods, that work for example for inducible materials, is to use the Lorenz force to apply tension or compression loads. Or use the centrifugal force of a fast rotation to apply constant bending or compression loads [16–20].

Depending on the chosen testing system different error sources may arise, that are to be considered in the measurement uncertainty. This is why in the following section an introduction on measurement errors and on how to estimate measuring certainty is given.

2.3. Measuring Certainty

2.3.1. Introduction

In measurements it is not only important to detect values, but also to estimate how reliable those measurement results are. Some errors, that reduce confidence in a measurement are obvious during the procedure. For example, if the specimen fails near the clamping, slipping between the clamping and the specimen appears or if large temperature drifts are detected [7, 21]. In any of these cases, the measurement results are to be rejected. Other measurement errors are more difficult to determine.

During a measurement, a physical phenomenon, such as a change in displacement, force, velocity, thermal conductivity, etc. is detected. The currently observed phenomenon is referred to as variable. In a repeated measurement, all measurement conditions are kept constant, and one variable is characterized to estimate measurement errors. For example in a creep experiment more than one repeated measurement is performed, where the stress, the specimen geometry, loading rate, temperature etc is kept constant and one variable, which is the displacement over time is investigated.

There are two main groups of measurement errors that appear: Systematical, or bias errors and random errors. A systematic error, is an error, that appears over several repeated measurements of the same variable [22]. While a random error, is an error that changes randomly during repeated measurements of the same variable. The uncertainty that comes from random errors can be determined by performing repeated measurements under constant test conditions, and evaluating the deviation between the results. Systematic errors are much more difficult to detect and can be estimated by comparing the result to an accompanying measurement of the same variable.

Often the repeatability of one experiment is characterized by the standard deviation. But if a systematic error is involved, a standard deviation does not cover the whole measurement error. An example given by Figliola (2011) for random and systematic errors, is the dart player, as depicted in figure 2.3 [22].

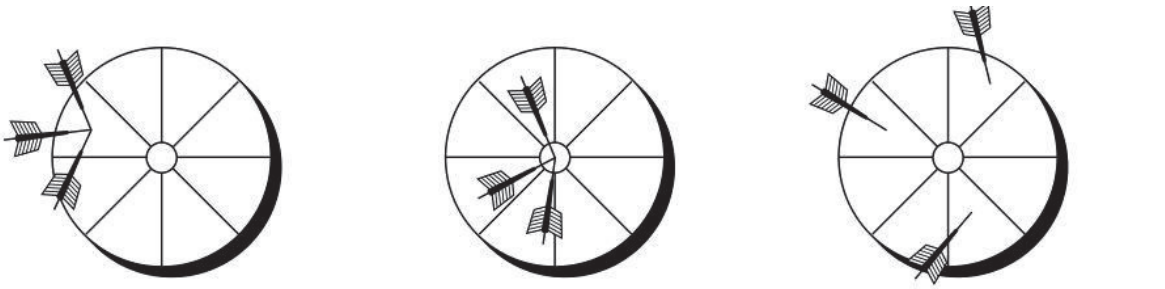

(a) High repeatability gives low random error but no direct indication of accuracy.

(b) High accuracy means low random and systematic errors.

(c) Systematic and random errors lead to poor accuracy.

Figure 2.3.: Picture of dart-player example, pointing out the difference between accuracy and repeatability [22].

The absolute error ε describes the ability of a measurement system to indicate a true value correctly and is given by

$$\varepsilon = true\,value - indicated\,value. \tag{2.3}$$

The *accuracy* of the system can be estimated during calibration. The relative accuracy A can be found from

$$A = 1 - \frac{\varepsilon}{true\,value}. \tag{2.4}$$

The error ε in a measurement can consist of a random error, or *precision* error, which occurs during repeated but independent application of an input value to the measurement system. And the error ε can contain the difference between an average error of several calibration measurements and the true value, which can be considered as a systematical error or *bias*, as shown in figure 2.4.

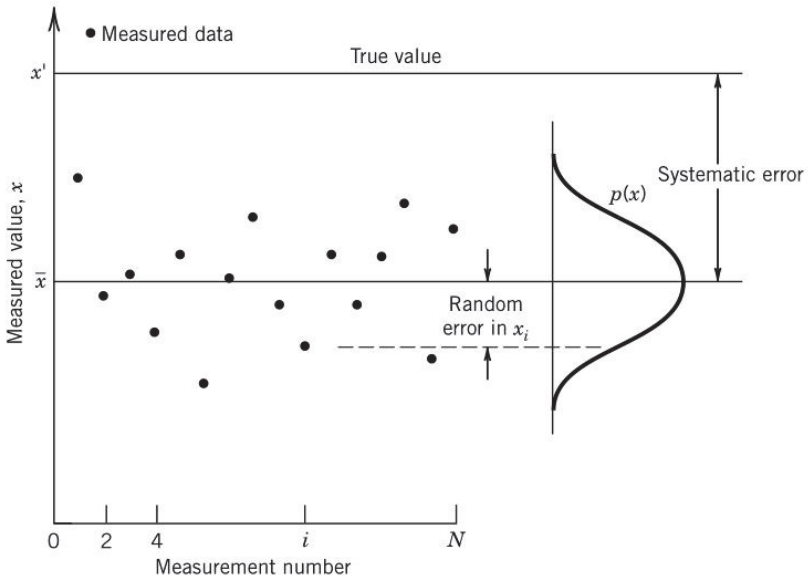

Figure 2.4.: Diagram showing systematic and random errors [22].

To calculate the error ε the assumption, that the true value is known, has been made. But during calibration the true value usually not known. Hence an estimation for the true value is required. During calibration a *sample* of data is obtained. This sample is a representation measurement systems behavior, but not a full description, since there is only a limited amount of data points detected. In a given sample the true value x' can be estimated by

$$x' = \overline{x} \pm u_x \, (P\,\%), \tag{2.5}$$

where $\overline{x}$ is the most probable estimate for x' and u_x is the confidence interval or the uncertainty at a given confidence level P. Discrete, random variables, that show a central tendency towards one value, can be described by mean value and variance regardless of the underlying distribution function.

The mean value for discrete data is given by

$$x' = \lim_{N\to\infty} \frac{1}{N} \sum_{i=1}^{N} x_i. \tag{2.6}$$

The variance σ^2, which represents the width of the density function reflects the data variation and is given by

$$\sigma^2 = \lim_{N\to\infty} \frac{1}{N} \sum_{i=1}^{N} (x_i - x')^2. \tag{2.7}$$

But since no measured data has infinite sample size, the mean value and the variance need to be adopted. For the sample can only partly represent an infinite population,

the sample mean value and variance can differ from the populations mean value and variance depending on the degrees of freedom. The the finite sized sample mean value $\overline{x}$ can be computed as follows

$$\overline{x} = \frac{1}{N}\sum_{i=1}^{N} x_i. \tag{2.8}$$

The sample variance S_x^2, which represents the width of the density function reflects the data variation and is given by

$$S_x^2 = \frac{1}{N-1}\sum_{i=1}^{N}(x_i - \overline{x})^2. \tag{2.9}$$

Regardless of the sample's underlying distribution function mean value and variance provide sufficient statistical estimates. However, if N is finite, the sample needs to have a central tendency. If the sample size is big enough the assumption, that the independent random variables follow a normal distribution, can be made due to the Central Limit Theorem. However William S. Gosslet (1876-1937) [22] found out, that for small samples the theory of the Normal distribution was not reliable and he developed the *Student-t distribution*. The value t is a function probability P, given by the Student-t distribution, and depends on the degrees of freedom ν. The variable t is called estimator. It can be said, that the variable x_i statistically lies with a certain probability P within in interval around the sample's mean value $\overline{x}$. The interval, dependent on the probability P for the Student-t function, is given by the estimator t times the sample standard deviation S_x defined as $\sqrt{S_x^2}$. So for the variable x_i can be stated that it lies with the probability P within the given interval

$$x_i = \overline{x} \pm t_{\nu,P} S_x (P\,\%) \tag{2.10}$$

To allow reliable statistical statements on the standard deviation a minimum number of repeated measurements N should be performed depending on the required confidence level P.

$$N \approx \left(\frac{t_{\nu,P} S_x}{d}\right)^2 (P\,\%) \tag{2.11}$$

To estimate a measurement uncertainty, it is necessary to identify the main error sources, since those contribute most to the final result. Important error sources are data acquisition errors, calibration errors and data reduction errors [22]. Data acquisition errors can be errors caused by the measurement equipment or any unknowns or changes in the test environment. Calibration errors are caused by the errors the standard is fraught with, or errors that appear during the calibration process. Errors in reading, or alignment or the calibration curve fit are considered. The third main error source, the data reduction, where errors may appear during curve fitting or signal modeling, or

interpolation.

2.3.2. Calibration

During a calibration a known input value called *standard* is applied to the measurement system and the output is detected. A correlation between the standard and the output is generally given by $y = f(x)$. The calibration can itself be considered as a measurement and the measurement errors can be qualified. The calibration is performed within a certain *measurement range*. In this range the correlation between the input and the output is determined.

In the ASTM standard E2309 [23] the calibration procedure for displacement measurement equipment is documented. Recommendations, concerning the calibration procedure, calibration devices and verification methods are given. Requirements are, that the compared standard must be equal or less than one third of the required certainty level. There are also guidelines for preliminary procedures, for example as how to ensure proper alignment and considering temperature effects.

According to the ASTM standard E2309 a calibration is only valid, if it is performed on the test machine and if the calibrated sensor is not removed during calibration. However, in many cases a calibration on the test machine is not possible. Therefore it has to be considered, that there are errors in the calibration due to the changed setup. Errors, that are caused by the calibration setup should not be included in the sensor calibration.

2.3.3. Uncertainty Analysis

In this section an introduction on how to approach an uncertainty analysis is given. The focus is on the measurement equipment and the test method itself an not on uncertainties due to the operator, the specimen manufacturing or other influences.

In every measurement the sensor equipment, the test setup, the calibration process and many other effects contribute to the uncertainty of a measurement. This is why the measurement uncertainty is a property of the result [22]. The better the measurement uncertainty is known, the more information about the reliability of the test results is available. Therefore, an uncertainty analysis for the whole test setup should be performed. Figliola points out, that there is a difference between errors and uncertainties: Errors are a property of the experiment, and they lead to uncertainties, which are properties of the results [22].

To estimate the uncertainty of the whole testing machine, the uncertainties of the individual components are calculated first and then combined. For each sensor, a design stage uncertainty u_d can be estimated. It can be calculated from the information available in the sensors data sheet. The design stage uncertainty u_d includes two different

sorts of uncertainties: i.) the zero order uncertainty, u_0, that can be estimated without any repeated measurements, and that is related to every single measurement point. It includes for example the uncertainties due to resolution errors of an amplifier or an analog- digital (AD) converter. ii.) The second group is the instrument uncertainty u_c. It defines the uncertainties that appear over the whole measurement range, for example due to errors in linearity, or due to hysteresis, gain or signal drifts. This is why zero order uncertainty and the instrument uncertainty are to be combined. Every measurement point is fraught with u_0, and several measurement points show effects that lead to the uncertainty u_c. Therefore, the design stage uncertainty of a measurement equipment u_d is given by equation 2.12:

$$u_d = \sqrt{u_0^2 + u_c^2}. \tag{2.12}$$

During a calibration, an unknown measurement is compared to a known standard. However, it should be considered, that the standard itself is also fraught with uncertainty. That e.g. an analog micrometer cannot be more accurate than the line width of the markers, that picture certain distances. Or that gauge slides also have an uncertainty due to the manufacturing process. Hence the uncertainty of the standard should also be considered during calibration. However, in the ASTM standard E2309 a recommendation is given, that the uncertainty of a standard for the calibration of a displacement measurement device should be at least one third of the expected uncertainty.

Usually the calibration is performed stepwise, so that discrete data sets are available. However, in a measurement a continuous correlation of the physical phenomenon and the sensor output is needed. This is why a model for the measured data is required. The model is a function, that represents the input output behavior sufficiently. But by applying this correlation, an uncertainty due to the model is raised. This uncertainty also has to be considered in the final results [22].

3. Experimental Work

In this chapter the experimental proceedings are documented. In the first section a stepwise elaboration of the test concept is presented. The mechanical test setup, the used measurement equipment and the software concept for the testing machine are introduced. The calibration of the displacement sensors and load cells is documented in the second section. In the third section an uncertainty analysis for the test machine is performed.

3.1. Development of Test Concept

The requirements, that are to be met by the developed system, are that compression creep measurements with a maximum load of 2000 N should be possible. The equipment has to cover a temperature range from room temperature ranging to 200°C and should perform both, creep tests during loading and unloading. Since the investigated materials undergo large deformations in the applications, a maximum strain of 10 % is to be realized on the test equipment.

For creep experiments at room temperature a universal testing machine is available. However, due to the long testing time it is too expensive to use the available universal testing machine, because of the high costs/hour. Furthermore, an attachment for the machine would be required, to allow more than one measurement simultaneously and the equipment cannot perform tests at elevated temperature. To perform experiments at elevated temperature, the developed test equipment should be compatible with the available infrastructure, e.g an available furnace. Therefore a new test equipment was developed, to allow reliable measurements for an economic prize. Due to availability and costs a prescribed furnace is to be used for the measurements at elevated temperature.

3.1.1. Mechanical Test Setup

Both, creep behavior and the behavior after unloading shall be characterized at various temperatures from 25°C to 200°C and several stepwise stress-profiles over time shall be realized. Therefore a method for a proper load application is needed, that allows to load and unload the specimen in a controlled and flexible way also at elevated temperature. A schematic overview of the chosen mechanical test setup is depicted in figure 3.1. A aluminum piston is gliding inside a cylinder. The piston is equipped with a sealing

element, to build up pressure. And a guiding element is attached to prevent misalignment. The displacement sensor is attached to the piston and measures the distance to a measurement target. The specimen is placed in a specimen cup, which is a polished steel cup that keeps the specimen in a central position. It is screwed on the load cell and fixed with a counter nut.

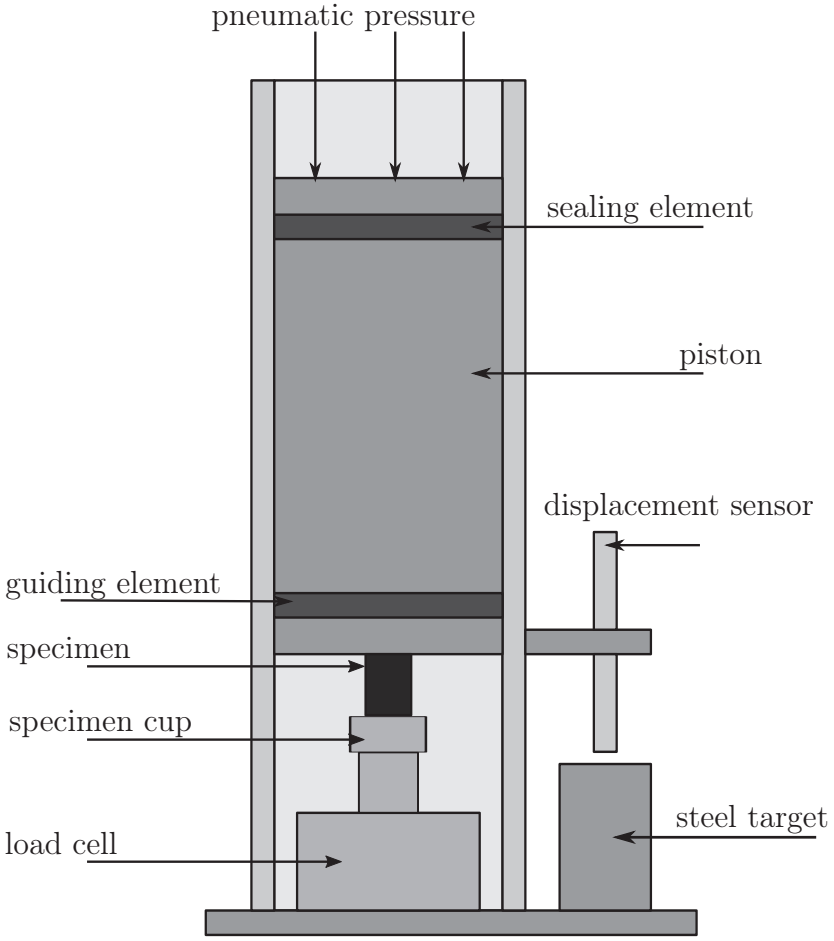

Figure 3.1.: Schematic picture of one test rig of the developed test setup.

Since loading and unloading experiments at elevated temperature are required, the most common method, of applying defined weights manually on the specimen is discarded. For the chosen specimen type with a diameter of 10 mm, 1960 N are required to reach a stress of 25 MPa. And a steel weight of approximately 200 kg, with e.g. a diameter of 20 cm, is about 80 cm high. The controlled handling of the weights, also at higher temperatures and the limited space in the furnace, were the reasons why this method was rejected. It is not desired to enable loading and unloading by opening the furnace door, since slight changes in temperature influence the material behavior significantly.

Different options are to use mechanical load transmission by for example a lever system. A lever system steered with a linear engine, may ease loading and unloading, but

was also rejected due to limited space and handling. If the weights of the lever system were positioned inside the furnace, the door must be opened and closed at elevated temperature to apply the weight, or the specimen is heated under load. Or, if the weight was positioned outside the furnace, the load transfer and transmission are difficult to realize. Another option often used for conventional test equipments are either spindle drives or hydraulic systems, but those were rejected due to high costs, occupational safety and missing infrastructure.

To achieve 25 MPa in the specimen, at very limited space in the furnace, the option of compressed air was chosen. The load is applied by compressed air to piston, gliding inside an aluminum cylinder. The pressure is regulated with a proportional valve. This enables an almost continuously adjustable load application. The cylinder equipped with a sealing element and guiding elements. The sealing element is necessary for the pressure build-up inside the system. The guiding elements improve the parallelism of the system. Due to the high requested parallelism, the piston was designed as long as possible, to avoid inclined positions inside the cylinder. With the limitations given by the geometry of cylinder, piston, sealing and guiding element, a maximum misalignment angle can be computed. Though, it is unlikely, that the piston remains in an misaligned position after loading, due to the high pressure in the system, that is applied to the sealing element and piston symmetrically.

To allow measurements at low stresses (from 0.25 MPa to 25 MPa) and also the characterization of the unloading behavior, the sealing element must not hold the piston in position. But the piston should be gliding inside the cylinder with as little friction as possible. To allow good behavior during unloading, it is useful if the piston glides up and down inside the cylinder due to it's own weight. To enable measurements at low stresses, the weight of the piston should be as little as possible, since the piston weight always rests on the specimen. This is why the piston is not made of steel but of aluminum and has a cavity inside. The sealing elements of the three pistons were modified to ease gliding.

The chosen test setup, with the specimen positioned between two parallel plates, brings one downside with it. The issue of friction between the specimen and the steel plates has to be investigated. Since the material behavior is to be characterized up to high strains, the consideration of friction and the assurance of homogenous stress distribution in the specimen are requirements for reliable material data. As suggested in the ISO 604 standard, the friction can be either reduced to 0 by using lubrication, or it can be maximized by using sand paper at the contact surface.

For PTFE specimens, the influence of friction was investigated by using different lubrication methods in a compression test setup. The transverse strains were measured during compression with an optical displacement measurement method. Depending on the friction, more or less barreling appears during compression, as depicted in figure 3.2. The barreling appears, as a result of the friction forces on the contact surface, that

hinder the transverse strain in the contact area. Therefore, the stress increases in this region and the specimen puts up more resistance against compression, than without friction.

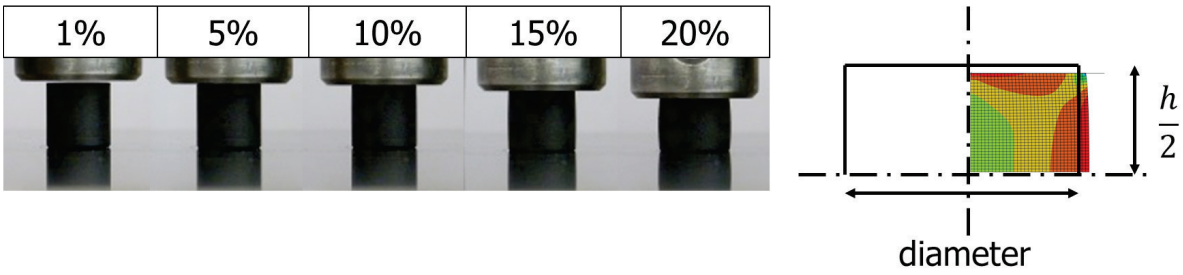

Figure 3.2.: Picture of specimen (10 mm diameter, 10 mm height) compressed at different strains (%) and a picture of the stress distribution in an axial symmetric model of the specimen under compression considering friction in the contact surface [24].

The specimen was modeled with a finite element (FE) simulation software, and the different test conditions were reconstructed by varying the friction coefficient in the simulation. With the simulation it could be shown, that by neglecting the hindering of transverse strain in the contact surface due to friction, the material stiffness measured can be overestimated up to 5% [24].

It is often necessary for creep experiments to measure over long time periods. For statistical safety of a measurement series, more than just one specimen should be characterized. This is why it is useful, if several measurements can be performed simultaneously to shorten the time for a whole measurement series. Another advantage of simultaneous measurements is, that the environmental conditions can be correlated to the measurements easier, if any inconsistencies occur.

To get more replications during one measurement, a setup was chosen where a third test rig is implemented, that has no load cell. In the test rigs one and two, where a load cell is implemented, the pressure in the pipes can be controlled by the applied load on the load cell. It is assumed, that in the third rig, the applied pressure is equal, since all pipes are connected to one another. Since the loading process, and the pressure regulation works with small regulation steps, it is assumed, that no feedback effects or overshooting are to be expected. The chosen test setup also allows a modular design, since more than three test cells can be attached to the pressure supply. If it can be shown, that the calibration in the third rig, with no load cell, is consistent with the other two rigs, the price per measurement can be reduced significantly by exchanging the load cells with dummies. For more advanced setups, for example one load cell can control the pressure for up to five simultaneous measurements.

A schematic picture of the test setup is depicted in 3.11. The test battery, consisting

of three test rigs, is positioned inside a furnace (dashed line). The signal amplifiers and the CPU are mounted in a control cabinet (bold black line), that is placed next to the furnace. The pressure valve, that is supplied by the compressed air system is also located outside the furnace. The CPU is controlled by a software on a computer next to the test setup.

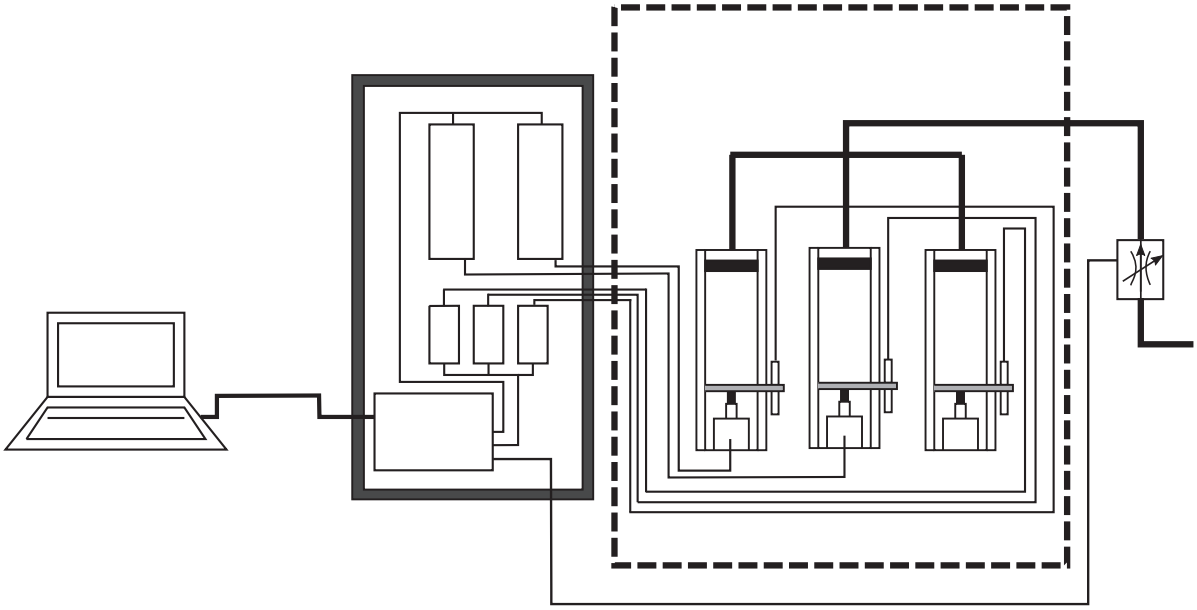

Figure 3.3.: Schematic picture of the test concept including computer, circuit cabinet (bold line) with amplifier and CPU, furnace (dashed line) and test battery with 3 test rigs.

To keep the stress level on the specimen constant, a sufficiently accurate pressure regulation in the test machine is required. But it is difficult to design an almost frictionless moving piston, that still has no leakage. Therefore a design was chosen, where there is a minor constant leakage, so that the pressure in the piping system is constantly regulated by a proportional valve. However, this leakage can cause difficulties during the pressure build up, since the valve has to compensate the increasing leakage. But with increasing pressure, the sealing element gets pushed against the cylinder walls and the leakage decreases to a constant value. To avoid an overshooting of the regulated pressure and the applied force on the specimen, a regulation mechanism is implemented. Therefore a potential function was chosen, that allows a fast pressure built up at the beginning, and that reduces the regulation steps near the final value. Depending on the implemented time constant τ, the loading time and the overshooting can be regulated.

To estimate the maximum possible misalignment, the geometry of the piston equipped with sealing and guiding elements is required. Figure 3.4 shows the construction data of the piston. The piston has a diameter of 49.7 mm and is moving inside a cylinder with 50 mm diameter. The guiding element is positioned 14.3 mm beneath the front

surface and is 2 mm thick. The sealing element is attached to the piston on the opposite side, 11.5 mm inside the piston end and has a maximum diameter of 50 mm. With the two elements a maximum misalignment of 0.08° of the piston is possible, which is a misalignment of ± 6.6 µm on the specimen diameter.

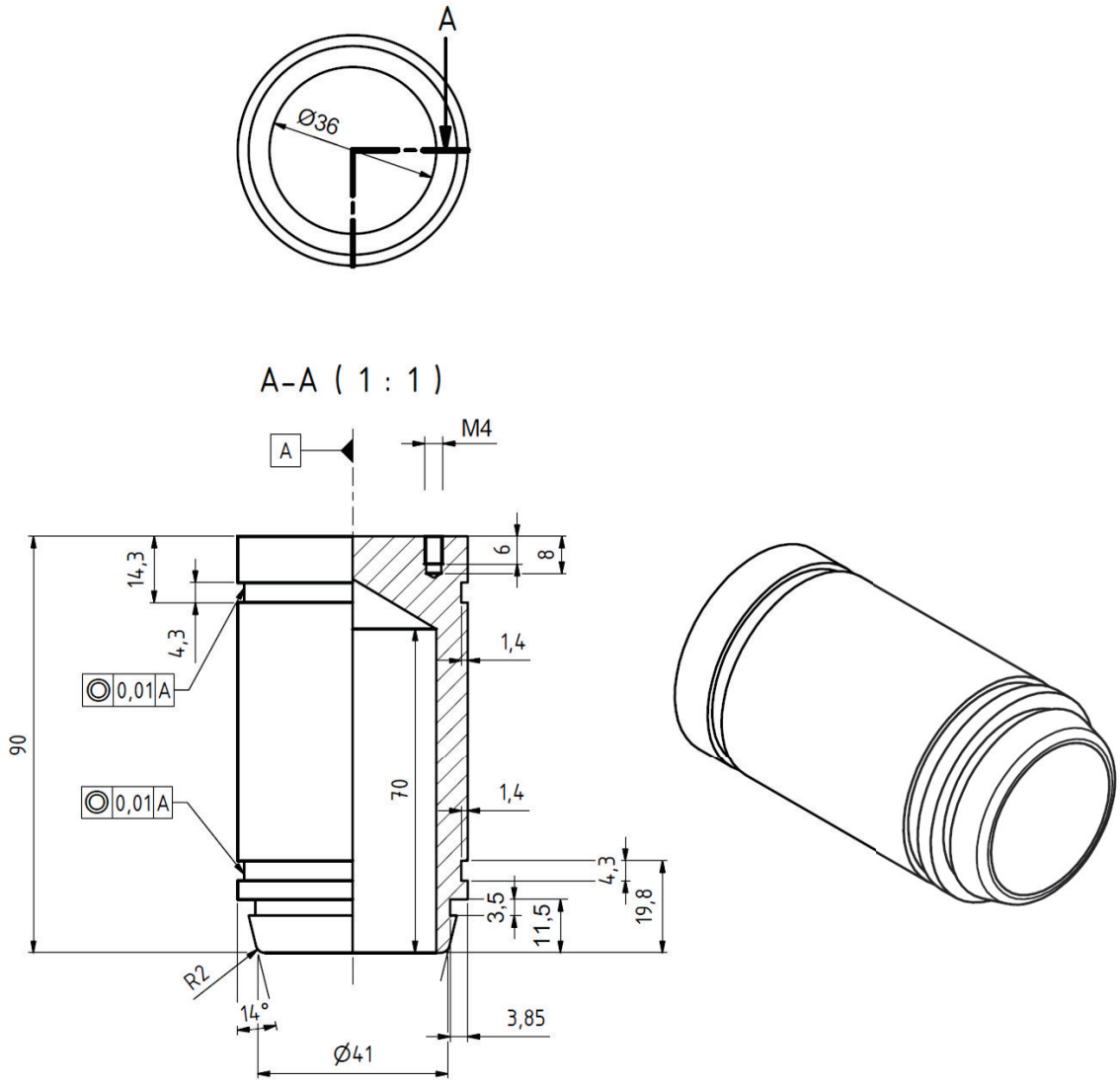

Figure 3.4.: Construction drawing of piston with 49.7 mm diameter and 90 mm height.

3.1.2. Measurement Equipment

The following section describes the test equipment used.

Load Measurement

Due to the test rig setup, a maximum load of 1963 N has to be measured. The measurement method should be reliable over time and should have no decay in performance at temperatures up to 200°C. Since piezoelectric load sensors show signal drifts over time and varying temperature, they are not suitable for high temperature applications. Sensors with strain gauges are more applicable in this environment, for the change in resistance can be compensated by a bridge circuit. Therefore a load sensor with strain gauges is used. The upper load limit of the implemented load cell is 2500 N. A measurement system with strain gauge elements by Althen GmbH (Kelkheim, Germany), type ALF256-Z4466-2,5kN with the amplifier system SG-IP-24E-B10, is used.

Displacement Measurement

For the displacement measurement a sensor is required, that allows to measure at temperatures up to 200°C over long time periods with a maximum uncertainty of 1% of the required measurement distance of 1 mm, which is 10% of the specimen height. The sensor will be put into the furnace and should have small dimensions due to the limited space. Due to the test setup, a contact less displacement measurement method is preferred. An eddy current sensor, with a measurement distance from 400 to 1500 µm is used. The sensor is made by the company Althen GmbH (Kelkheim, Germany) and is a 5CM type with the amplifier system KD-2446.

Temperature Measurement

For the temperature measurement a platinum (Pt) temperature sensor PT1000 is implemented. One main advantage of the PT1000 (and also PT100) sensor is, that the resistance over the temperature range is standardized (IEC 751 / DIN EN 60 751). PT1000 elements have a smaller relative error due to line resistance compared to measurement resistance, which is one tenth of the PT100 element. PT elements show good long term stability compared to Negative Temperature Coefficient Thermistors (NTCs) and better cyclic behavior. To reduce the errors from the line resistance, a 3 terminal sensing technique is used. The PT1000 element is implemented to the test system by a thermal resistance measurement tool by B&R (Bernegger und Rainer GmbH, Vöcklabruck, Austria).

3.1.3. Software and Hardware

A user interface for the test equipment shall be developed. An input-output system is necessary to regulate the compression valve functions, to provide the power supply for the sensors and to detect the sensor signals. The input-output system is to be operated with a graphical user interface (GUI), that enables the user to specify the test procedures and track real time sensor signal. The information gained in the measurement is combined in one output file, that can be further evaluated. To coordinate the input and output signals a bus module is configured and a CPU is connected to Automation Studio (by Bernegger und Rainer GmbH, Vöcklabruck, Austria) and via tcpip connection to the graphical user interface. A flow diagram for the data transfer is depicted in figure 7.13. The GUI is programmed in Matlab (The MathWorks, Inc., USA), with a software tool called Guide. The GUI is connected to the CPU by a tcpip protocol and the input-output modules are operated by an internal software on the CPU.

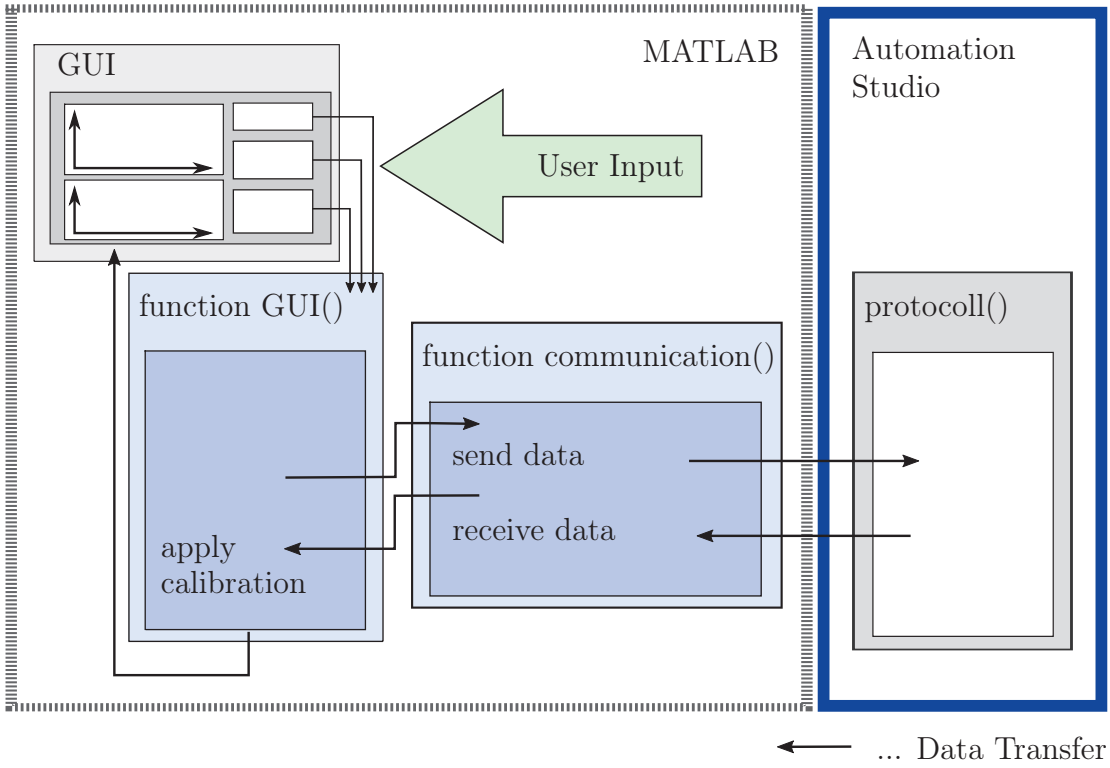

Figure 3.5.: Schematic flow diagram of the signal transfer.

The test rig can be operated by the user with a GUI that is depicted in figure 3.6.

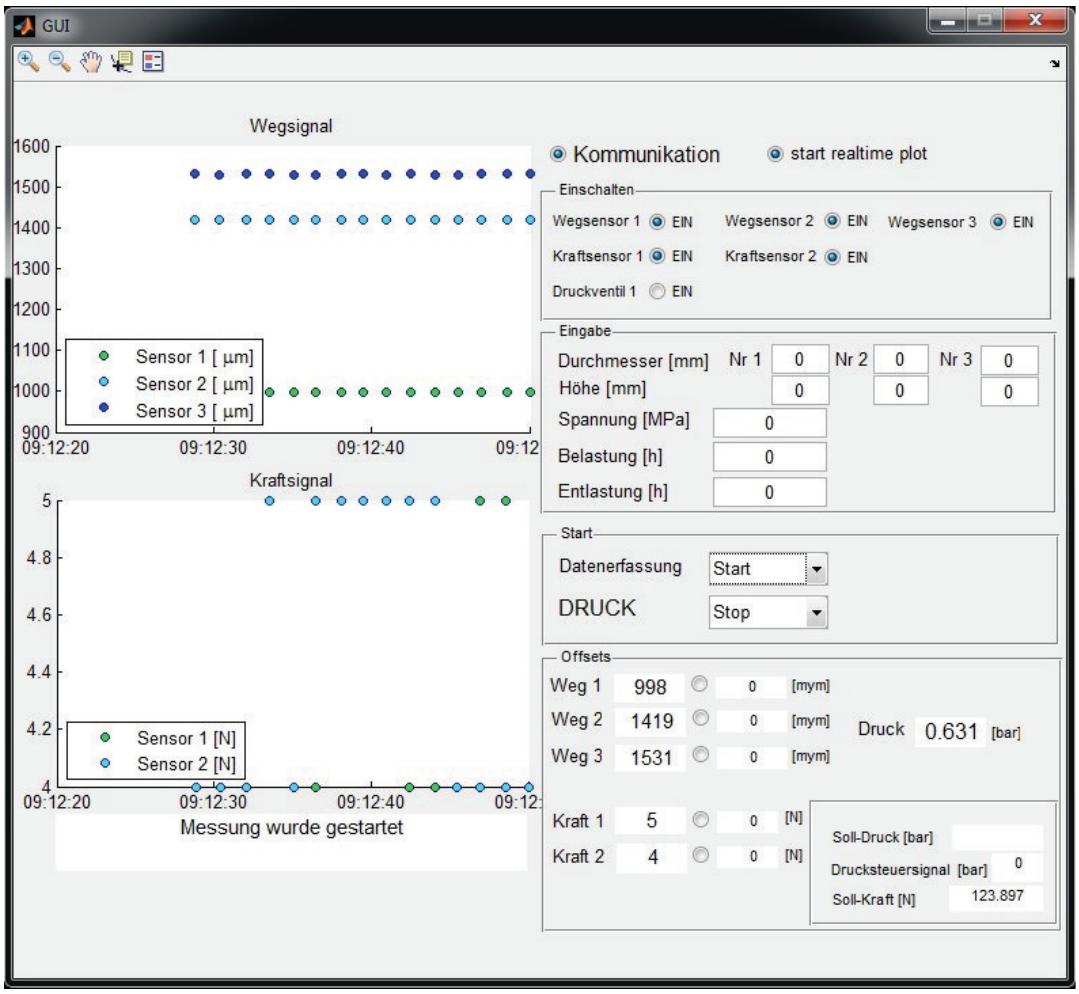

Figure 3.6.: Picture of the graphical user interface (GUI) to control the test rig.

The test procedure for a creep test should be as simple as possible so that measurements can be performed easily. For tests at elevated temperature the test procedure slightly differs, since some time is required until the test temperature in the furnace is regulated. The test procedure for a creep test at elevated temperature is described in the following:

- Plug in and switch on the Computer, the CPU (button on the control cabinet) and the furnace.
- Make sure the test system is linked to the pressure piping system.
- Start Matlab and Automation Studio and wait until Automation Studio displays *Run* in the status bar.
- Start the function GUI in Matlab. Now the user interface opens.

- □ Switch on the *Kommunication* button. Now a connection between the user interface and the CPU is established.
- □ Now switch on the displacement sensors, the load cells and the proportional valve via GUI.
- □ Measure the specimen geometries for the three specimens and type in the heights and diameters.
- □ Check if the displacement sensors show displacements between 500 to 1500 µm.[1]
- □ Type in the stress level from 0 to 25 MPa. Now the required pressure is displayed.
- □ Start *Datenerfassung* to save the measured data in *.txt* files.
- □ Switch on the furnace and wait until the temperature in the test chamber reaches a constant level.
- □ If the temperature is reached, start *Druck* and now the pressure is applied.
- □ Depending on whether the cooling phase is relevant or not, cool down the furnace before or after unloading.
- □ To end the measurement, either set the stress to 0 MPa- then the pressure will be reduced stepwise. Or stop *Druck*, and the pressure will be reduced all at once. Then stop *Datenerfassung* and the data, that is stored in the buffer, will be written to a *.txt* file.
- □ Switch of the pressure valve and the sensors and close the communication.
- □ Close the user interface and Matlab and close Automation Studio and switch of the CPU.

A circuit diagram for the analog input modules (AI), the analog output modules (AO) and the digital output modules (DO) used to provide power supply for the sensors and signal detection can be found in the appendix chapter 7.

[1] If the measurement is to be performed at higher temperature and the whole measurement range is required, the thermal expansion of the measurement target should be compensated. Therefore calculate the expected thermal expansion $\Delta\varepsilon$ of the steel target and use gauge slips, to adjust the sensors at the distance of 1500 µm + $\Delta\varepsilon$.

3.2. Calibration

In the following chapters the calibration of the displacement sensor and the load cell is presented. The used statistical theory is documented in chapter 3.2.

3.2.1. Calibration of Displacement Sensors

To get an reliable displacement signal, an extensive and cautious sensor calibration should be performed. As explained in chapter 2.3, all calibration errors contribute to the error in the final result and cause uncertainties. Therefore, two different calibration tools were developed. The first calibration tool, with which a very extensive calibration at room temperature is performed, is a micrometer screw fixed on a steel plate by a holder. On the front of the screw a measurement target is fixed, that can be moved, as depicted in figure 3.7.

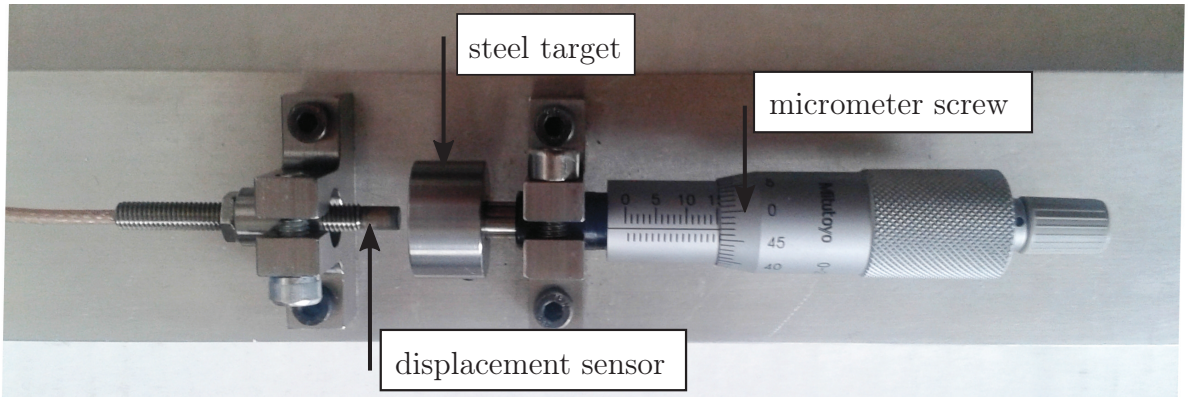

Figure 3.7.: Photograph of micrometer screw calibration tool.

The second calibration tool is a setup, were two gauge blocks are positioned symmetrically under a target block, figure 3.8. The whole tool is placed in the furnace and can be used up to 200° due to the temperature limit of the displacement sensor.

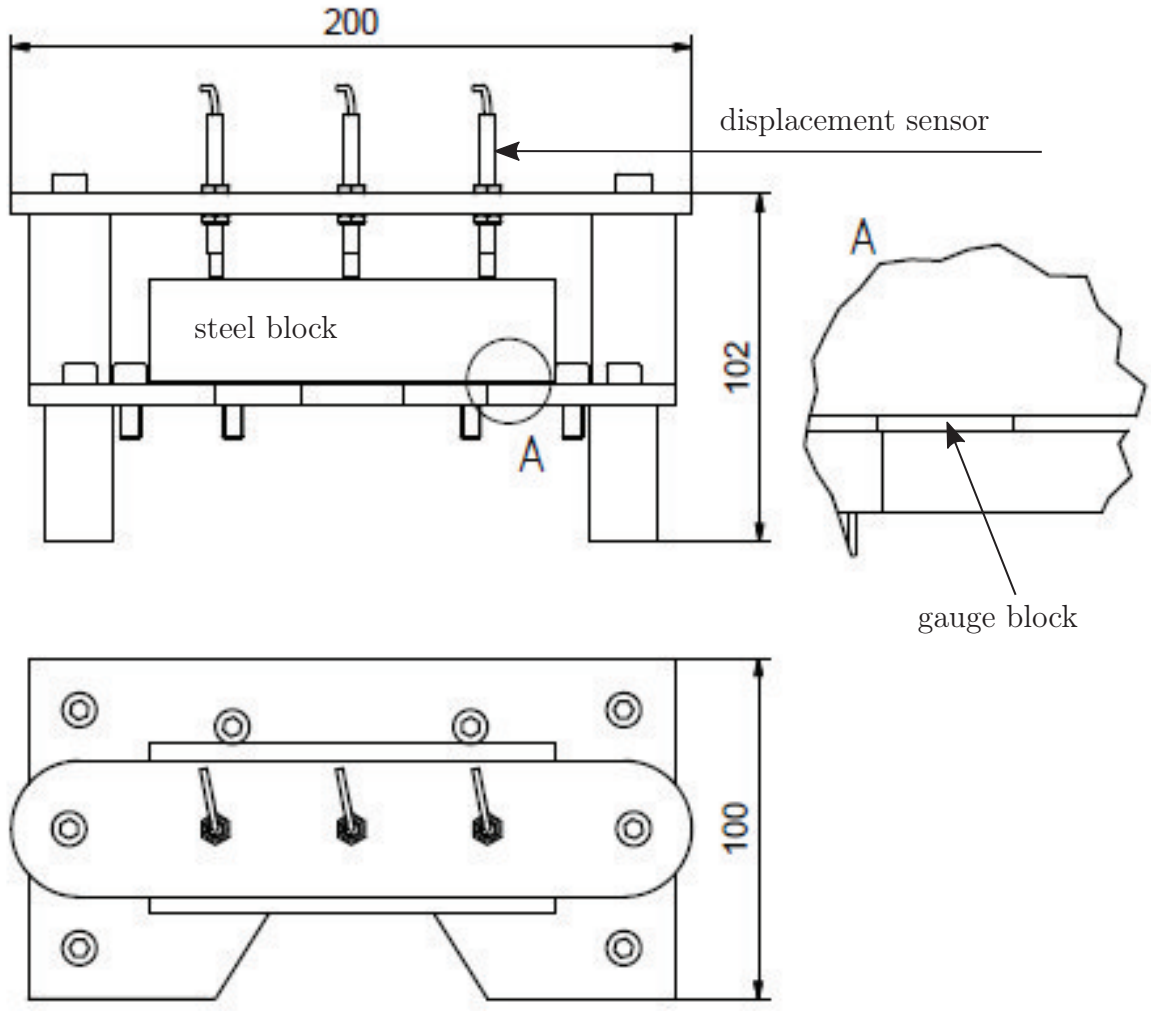

Figure 3.8.: Schematic figure of the gauge block calibration tool.

Calibration at Room Temperature

For the calibration at room temperature the three displacement sensors are calibrated by the micrometer screw. The proceeding is explained by the example of the displacement sensor on the first rig, referred to as sensor 1. The other sensors were calibrated analogously and the measurement data and diagrams can be found in the appendix, chapter 7. For the calibration with the micrometer screw the sensor is fixed on the calibration tool by a holding device and a counter nut as documented in picture 3.7. On the opposite side of the sensor a calibration target is fixed on the micrometer screw.

The target material is X20Cr13, which is a magnetizable steel and the same material as used on the rest rig. Requirements to the target, such as the ratio of target diameter to the sensor diameter were met. The sensor is fixed at a given zero position (10 mm) and the micrometer screw is moved to vary the measurement distance. The measurement equipment response is documented in bit at every 10 µm step. A measurement range from 400 µm to 1500 µm is covered.

In the first step, the data of each calibration run with increasing measurement distance is plotted, as shown in figure 3.9. Then the reading in bit is normalized between 5000 and 30000 bit to ease fitting. Since minor irregularities are detected under 500 µm measurement distance in every calibration run, the data below 500 µm is not included in the fit. Then a polynomial fit is performed using the function polyfit in Matlab, that uses a least square solving algorithm. The left plot in figure 3.9 shows the raw displacement data in µm, that is gained from reading the micrometer screw's marks, versus the normalized equipment reading in bit. The plot indicates, that a polynomial fit of at least second order might be required to represent the equipments behavior. The right plot shows displacement data in mm versus the normalized reading.

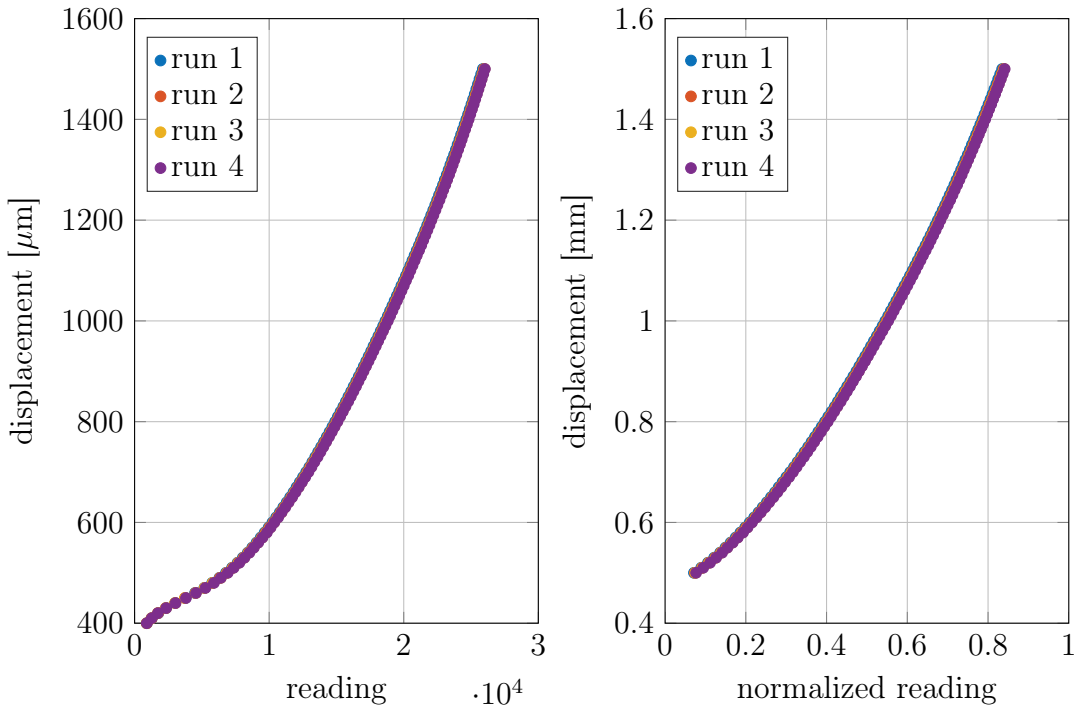

Figure 3.9.: Left figure: Calibration data from micrometer screw in µm versus reading, between 0.4 mm and 1.5 mm measurement distance.
Right figure: Calibration data from micrometer screw in mm versus the normalized reading, between 0.5 mm and 1.5 mm measurement distance.

However, when fitting a polynomial of degree = 2 and investigating at the residual as

depicted in figure 3.10, it appears, that the remaining residual has periodic properties. In the figure 3.10 two different residuals of the four calibration runs are shown. In the upper plot of figure 3.10 the individual residuals are shown. Which means, that each of the four runs is fitted individually by a polynomial of degree = 2. So the residuals in the upper figure represent and in-measurement error. In the lower part of figure 3.10, the four data sets were fitted together and the residuals between each run and the polynomial fit of all four runs is displayed. This can be seen as a measure for the measurement-to-measurement error.

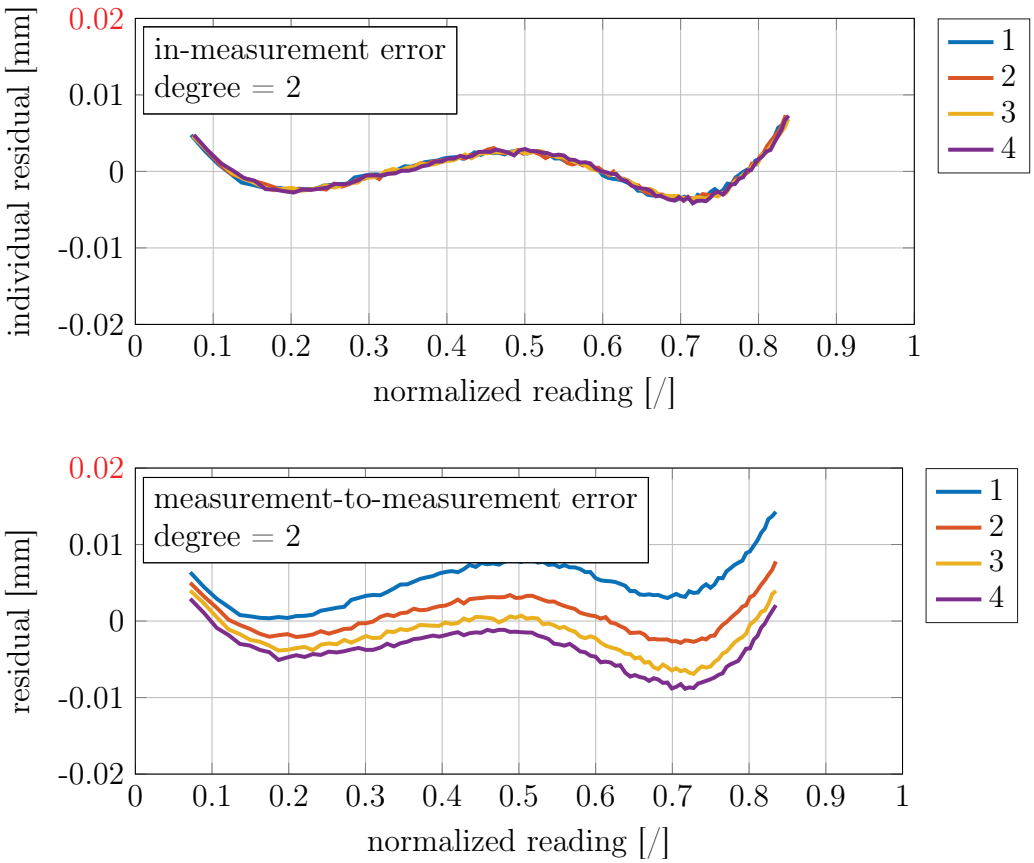

Figure 3.10.: Calibration data of displacement sensor 1 fitted with polynomial of degree = 2.

To exclude the possibility, that the periodic signal error is caused by the micrometer screw of the calibration device, the zero position for the calibration process was shifted stepwise. The step width for the offset change was one forth of the screw's rotation. In this test, no phase difference in the periodic residual could be detected, which indicates, that the periodic signal is an intrinsic error of the displacement sensor and therefore can be compensated in the calibration process.

To get a better understanding of the periodic calibration results, the signal path of

the measurement signal is investigated. The sensor's response, in this case in mV, is proportional to a physical phenomenon, which is an eddy current around the sensor tip that is influenced by a moving target. This response y is amplified and transformed from an analog signal in V to a digital signal in bit, as depicted in figure 3.11. The signal amplifier causes a noise called σ_s and the analog digital converter causes the noise σ_{ADC}. It is assumed, that the signal modifications by the amplifier and the AD converter do not produce periodic errors but independent and identically distributed (i.i.d) random errors. This can be shown by fixing the sensor at a given position and switching it on. Without moving it, no physical phenomenon has happened (except for temperature changes, which are dealt with later).

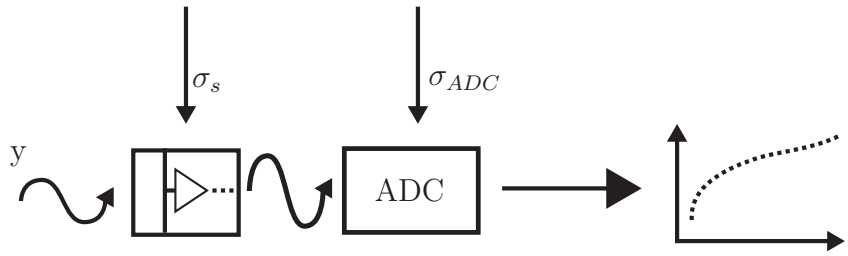

Figure 3.11.: Signal path from physical phenomenon to measurement data.

To prove, that the noise caused by the amplifier and the AD converter is an i.i.d. error, the sensor is fixed at a certain position, and the signal is detected over time. In the following figure 3.12, the sensor signal over time is plotted and in figure 3.13, a statistical test is performed on the data. The performed test is a Kolmogorov Smirnov test, that tests the null hypothesis, that the data comes from a normally distributed population. If the test is positive, the tested data has a Gaussian distribution and can be considered as an i.i.d.

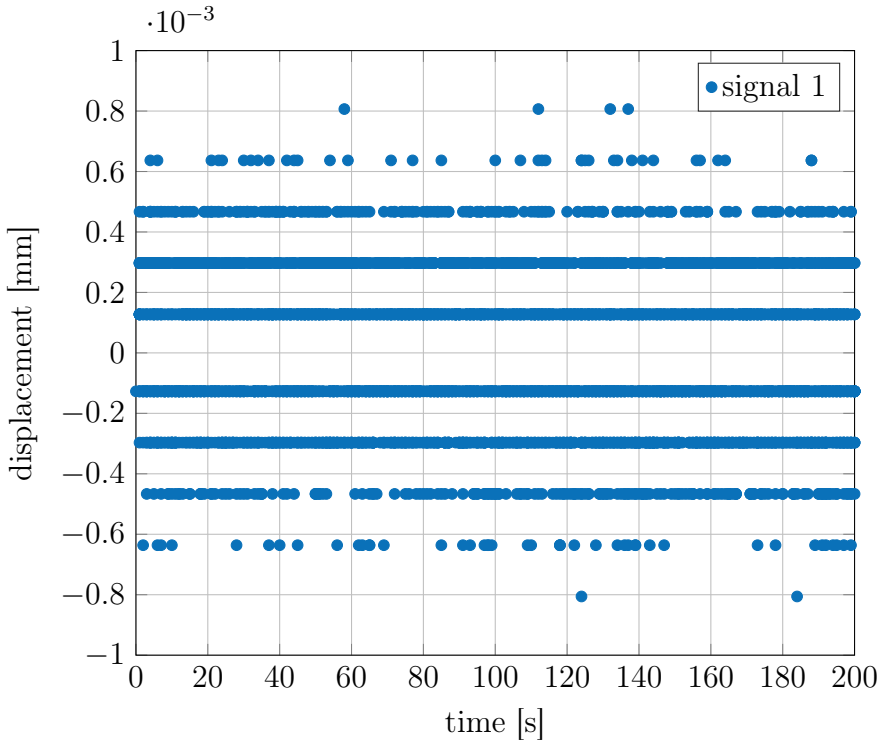

Figure 3.12.: Sensor noise of displacement sensor 1.

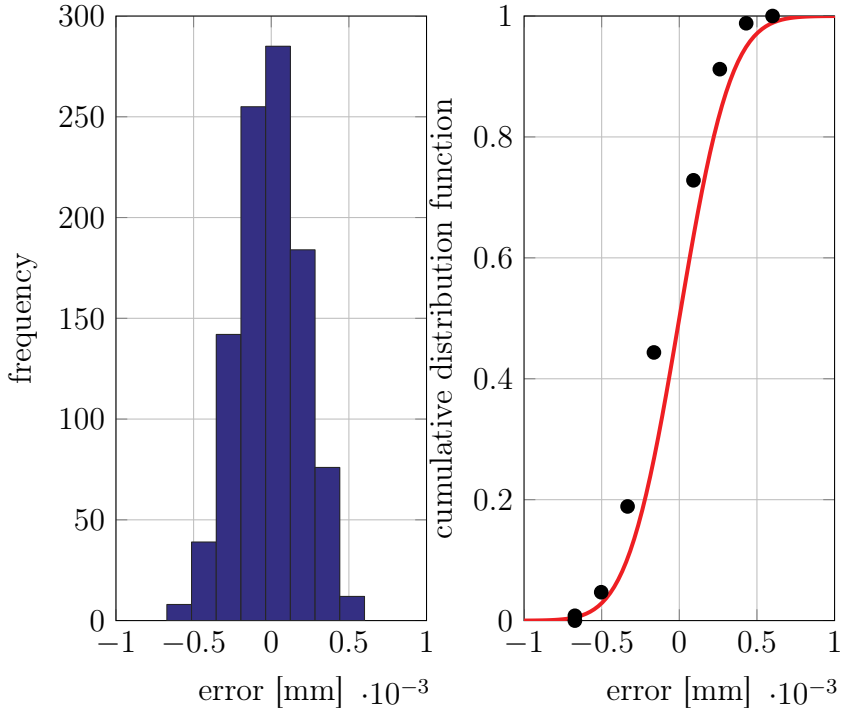

Figure 3.13.: Kolmogorow-Smirnow test for noise of displacement sensor 1.

In the figure 3.12, no periodic signal drift can be detected. And the Kolmogorov Smirnov test depicted in figure 3.13 indicates a Gaussian distribution of the noise produced by the amplifier and the AD converter. This indicates, that the periodicity does not come appear during static measurement, but appears over a measurement range. From this figure also information the resolution of the AD converter and the amplifier can be gained. According to the data shown in figure 3.12, the resolution of the displacement signal is about 0.2 µm. This measurement result will be compared with calculations in section 3.3.1.

According to figure 3.12, the periodic noise appearing in the calibration curve should be caused by the physical phenomenon of the measurement method. Since this periodic error can be seen as part of the measurement method, it ought to be considered in the calibration process. This is why a higher degree polynomial, as depicted in figure 3.14, is used to partly compensate the remaining periodic error in the data set shown in figure 3.10. It is distinguished between the error within one calibration run, as depicted in the upper part of the figure, referred to as in-measurement error. And the error between several calibration runs, referred to as measurement-to-measurement error.

The residual left by the polynomial fit of degree 5 is one tenth (shown red) of the residual in 3.10. So the accuracy can be improved significantly. However, the remaining residual in figure 3.14 still has a slight periodic shape. This is where the design stage uncertainty can be considered as a lower limit. Since the amplifier and the AD converter both have limitations in their resolution and linearity, the signal is always fraught with an error caused by the signal transformation. The uncertainty caused by this errors is calculated in section 2.3.3.

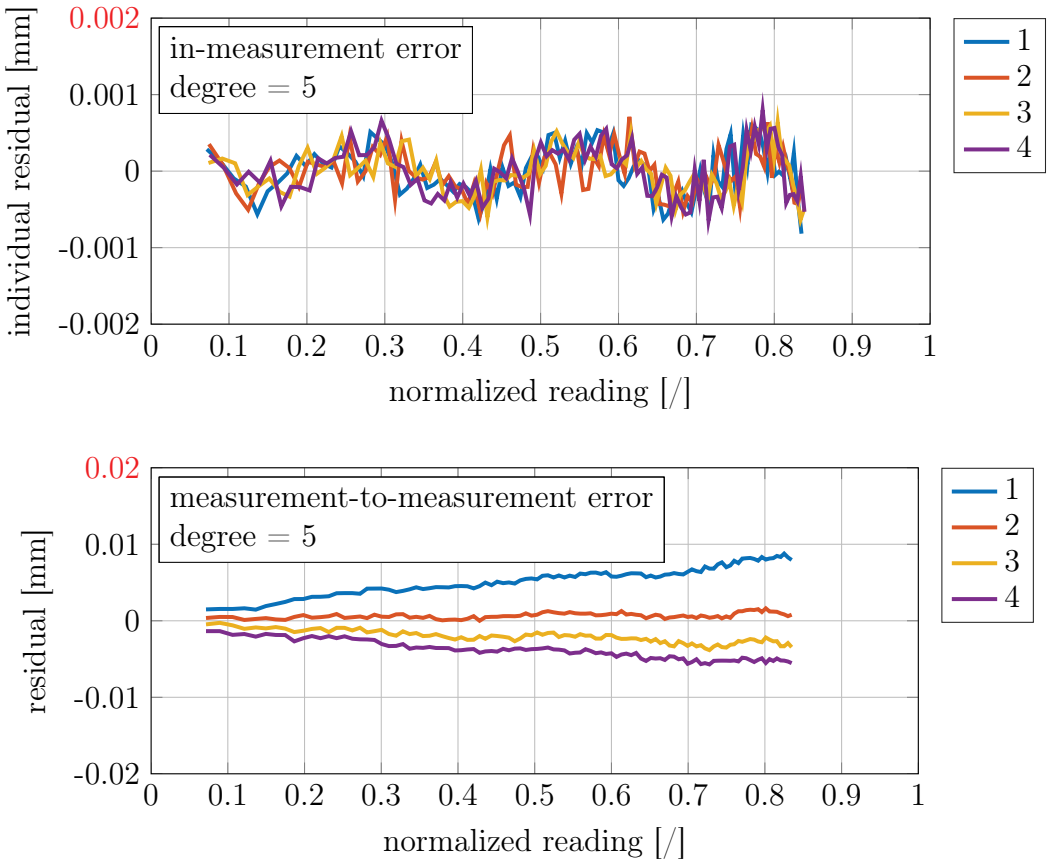

Figure 3.14.: Calibration data of displacement sensor 1 fitted with polynomial of degree = 5.

The figure 3.14 shows the remaining residual of a polynomial fit of degree = 5. The residuals shown, are computed by fitting each calibration run individually and represent an in-measurement error. When comparing several calibration runs of one sensor, a measurement to measurement error can be detected after four calibration runs.

To visualize hysteresis errors the calibration is performed in increasing and decreasing measurement distance for displacement sensor 1, as suggested in the ASTM standard E2309 [23]. This is why four calibration runs are performed on the calibration tool with displacement sensor 1 to investigate the measurement to measurement errors. Each run is one calibration set in ascending and descending measurement distance. Figure 3.15 shows, that the measurement to measurement error changes from the first to the fourth calibration run. In this figure, the measurement to measurement error is plotted with respect to a mean value over all calibration runs. While in the first run the residual is about +4 µm, it changes at every iteration and is about -3 µm at the 4th run. This indicates a slight offset shift with increasing iteration, which is referred to as the sensor *drift*.

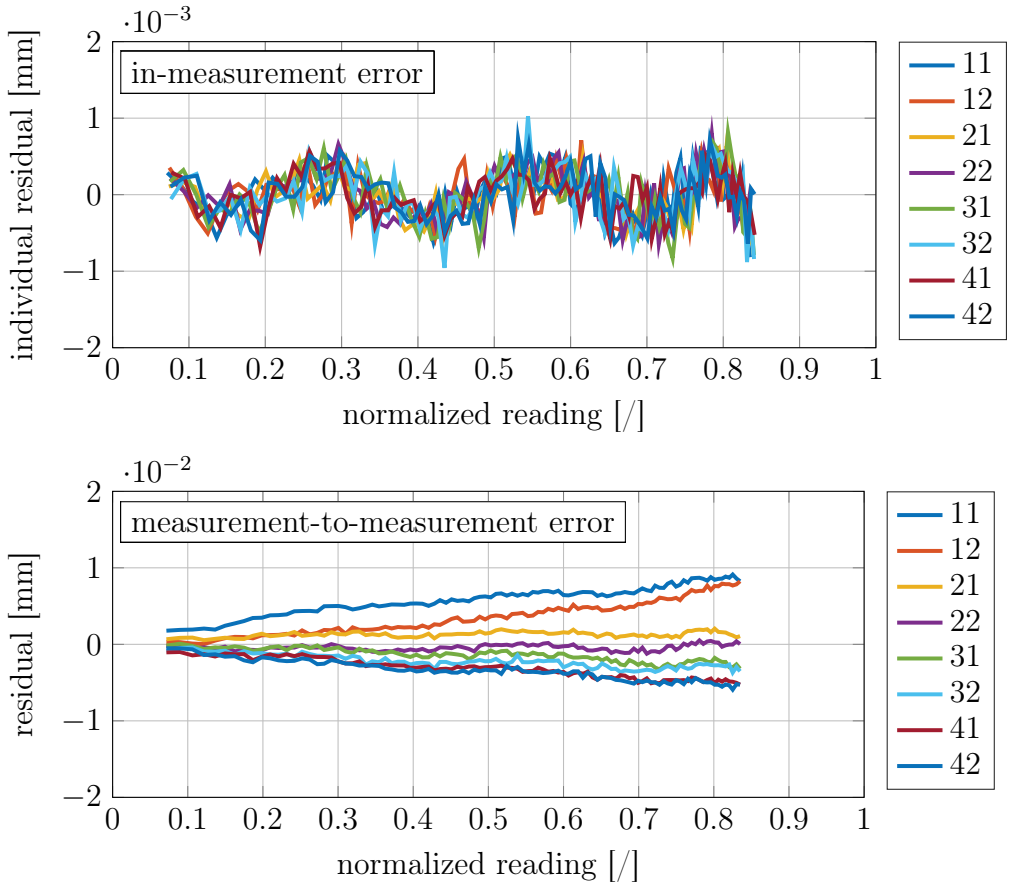

Figure 3.15.: Residuals of four consecutive calibration runs.

When analyzing the up- and downscale data more closely, it appears, that the hysteresis error (the difference between the up- and downscale values) converges towards a boundary. This can be shown by fitting the data of one run (in ascending and descending measurement width) pairwise. The delta from the upscale and downscale values for each run are plotted. In figure 7.6 it can be seen, that the difference between upscale and downscale run decreases. This indicates, that after several repetitions the hysteresis error can be neglected.

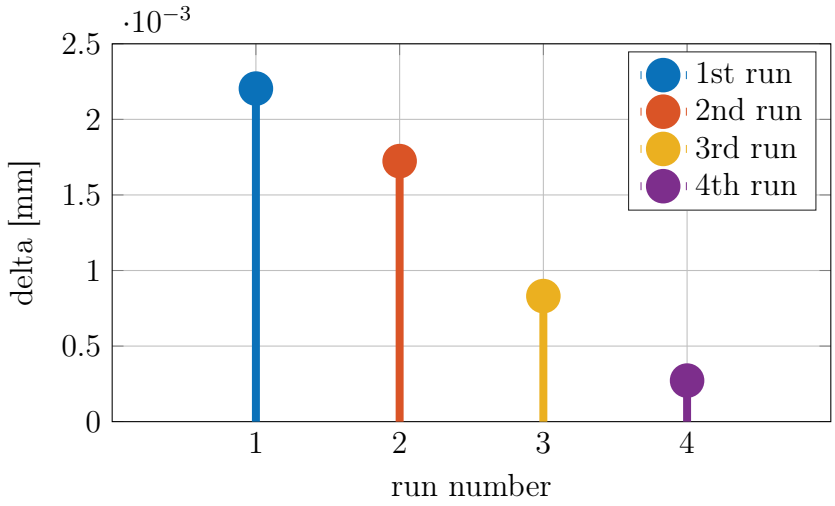

Figure 3.16.: Decrease of difference between calibration in ascending and descending order (delta) over four runs.

With the knowledge of the sensor behavior depicted in figure 3.15, that there is a signal drift over several runs, and the insight that the difference between upscale and downscale runs decreases with iteration, it can be assumed that there is some stationary behavior after a time t. However, from this experiment shown in 3.15 it cannot be determined, if the drift also has a lower boundary, or if it constantly shifts over time. This was investigated by switching the sensors on, and detecting the sensor signal without moving the sensor. Figure 3.17 shows, that the used sensors show a signal drift over time, which ends after a settling time and enters a constant level. This behavior can be observed for all three sensors at different temperatures. The signal drift also appears, when the sensor is fixed at the gauge block calibration tool, and not only on the test rig. It can be shown, that the detected drift is not due to creep of the test rig and also not dependent on the measurement target or the temperature. Therefore it can be considered as an intrinsic error and has to be included in the uncertainty analysis.

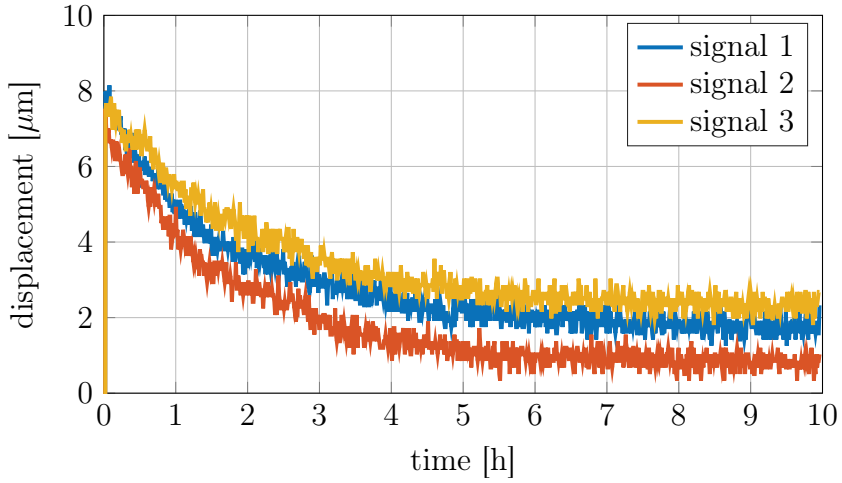

Figure 3.17.: Diagram of long time signal drift of displacement sensor 1 at room temperautre.

Calibration at Elevated Temperature

In this section the sensor calibration at elevated temperature is presented. The sensors are attached to the gauge block calibration tool and are positioned with gauge blocks, so that the maximum measurement distance of 1.5 mm is adjusted. The equipment is placed in the furnace and the test chamber is heated up. During the heating phase, the whole gauge block tool stretches due to thermal expansion. This is why at the beginning a change in displacement is detected. But this change of displacement may include both-changes due to thermal expansion and signal drifts. This is one reason why the design of the gauge block tool is as simple as possible. Because now the thermal expansions of the tool can be calculated easily and are considered in the calibration. After the first heating phase, the required time for isothermal measurement conditions passes, to detect the sensor signal. Then the furnace door is opened and the next pair of gauge blocks is put under the steel block. Since the heating takes longer, the higher the furnace temperature is, less data points are measured at 175°C. For 25°C and 100°C the step width is 100 µm, and for 175°C the step width is 200 µm. In figure 3.18 the raw data of the displacement sensors and the temperature sensor are plotted. The heating phases, the change of the gauge blocks and the isothermal measurement sections can be seen.

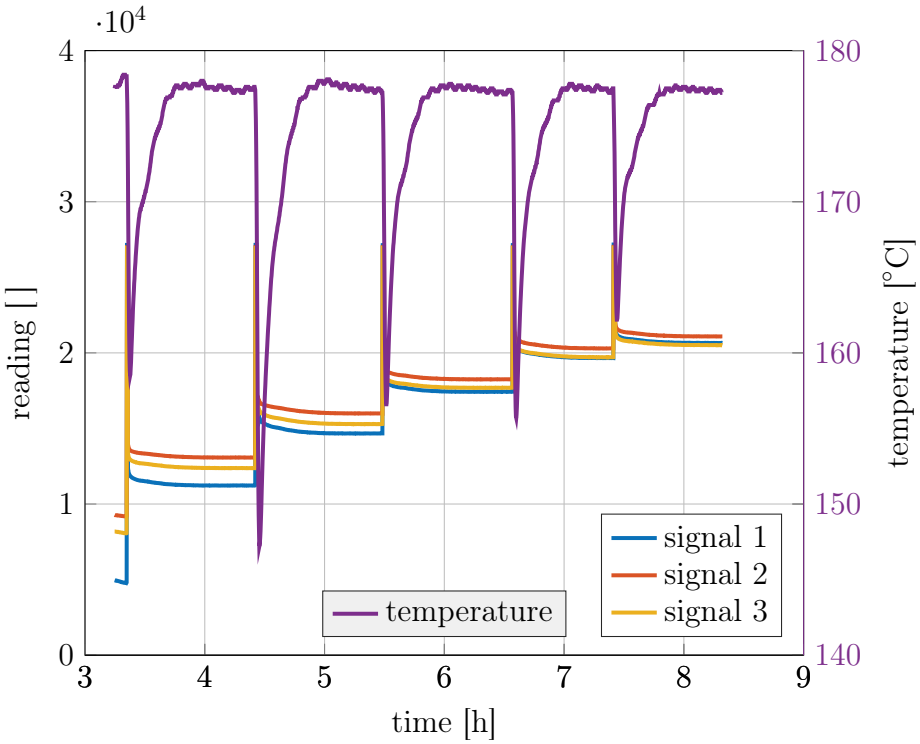

Figure 3.18.: Temperature signal and signal of three displacement sensors over time during a calibration on the gauge block tool at 100°C.

For the further evaluation the displacement signal of the isothermal sections of the measurement are used. In the following figure 3.19 the calibration data of the micrometer and gauge block calibration is shown. At room temperature both calibration methods show the same results. This indicates, that the gauge block calibration can be seen as a reliable standard. In this figure, the thermal expansions are not considered jet. This is one reason why at higher temperature a signal drift appears and the sensors show less reading. The second finding is, that the detected signal drift at room temperature also appears at elevated temperature.

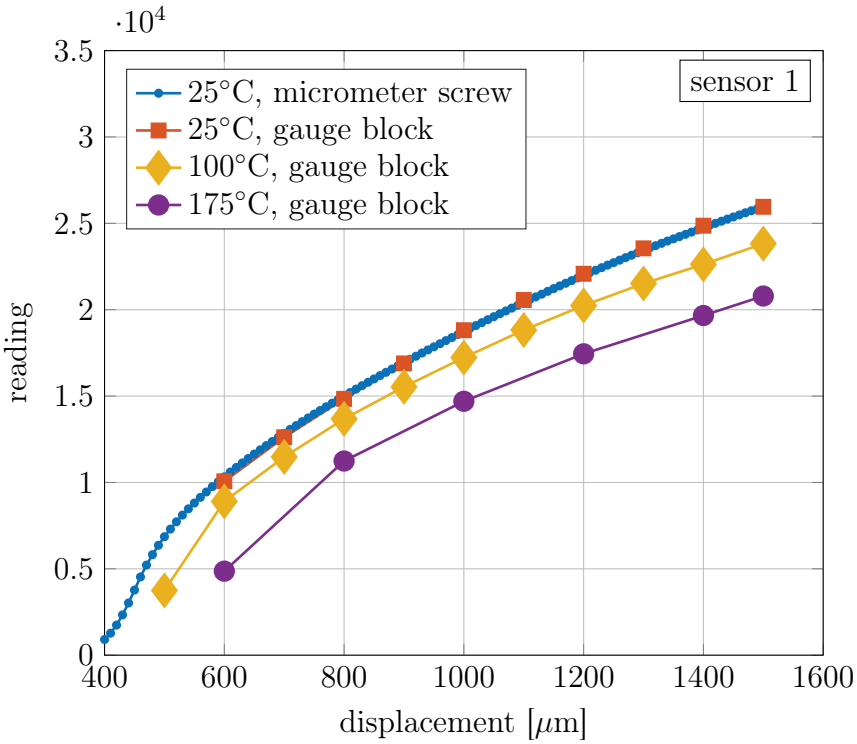

Figure 3.19.: Calibration data without consideration of thermal expansion at 25°C, 100°C and 175°C performed on gauge block calibration tool and comparison of micrometer screw and gauge block calibration at 25°C of displacement sensor 1.

Now the correction of the thermal expansion is applied to the calibration data. The thermal expansion coefficient for steel α is 1.310^{-5} 1/K. The height of the steel block is 30 mm and the height of the two outer steel columns is 50 mm. For the 100°C measurement the temperature increase while heating $\Delta T_{100°C}$ is 73°C, and for 175°C the temperature difference $\Delta T_{175°C}$ is 123°C.

$$\Delta\varepsilon = \alpha . \Delta T . \Delta l \tag{3.1}$$

$$\Delta\varepsilon_{100°C,steelblock} = 1.3\,10^{-5} . 73 . 30\,000 = 28.47\ \mu m \tag{3.2}$$

$$\Delta\varepsilon_{175°C,steelblock} = 1.3\,10^{-5} . 123 . 30\,000 = 47.97\ \mu m \tag{3.3}$$

$$\Delta\varepsilon_{100°C,steelcolumns} = 1.3\,10^{-5} . 73 . 50\,000 = 47.49\ \mu m \tag{3.4}$$

$$\Delta\varepsilon_{175°C,steelcolumns} = 1.3\,10^{-5} . 123 . 50\,000 = 79.95\ \mu m \tag{3.5}$$

Due to the test setup, the thermal expansion of the steel columns and the steel block have to be combined to receive the actually measured thermal expansion.

$$\begin{aligned} \Delta\varepsilon_{100°C} &= \Delta\varepsilon_{100°C,steelcolumns} - \Delta\varepsilon_{100°C,gaugeblocks} \\ \Delta\varepsilon_{100°C} &= 47.49 - 28.47 = 19.02\mu m \\ \Delta\varepsilon_{175°C} &= \Delta\varepsilon_{175°C,steelcolumns} - \Delta\varepsilon_{175°C,gaugeblocks} \\ \Delta\varepsilon_{175°C} &= 79.95 - 47.97 = 31.98\mu m \end{aligned} \tag{3.6}$$

In the following figure 3.20 the calibration data shifted by the error due to thermal expansion of the equipment is depicted.

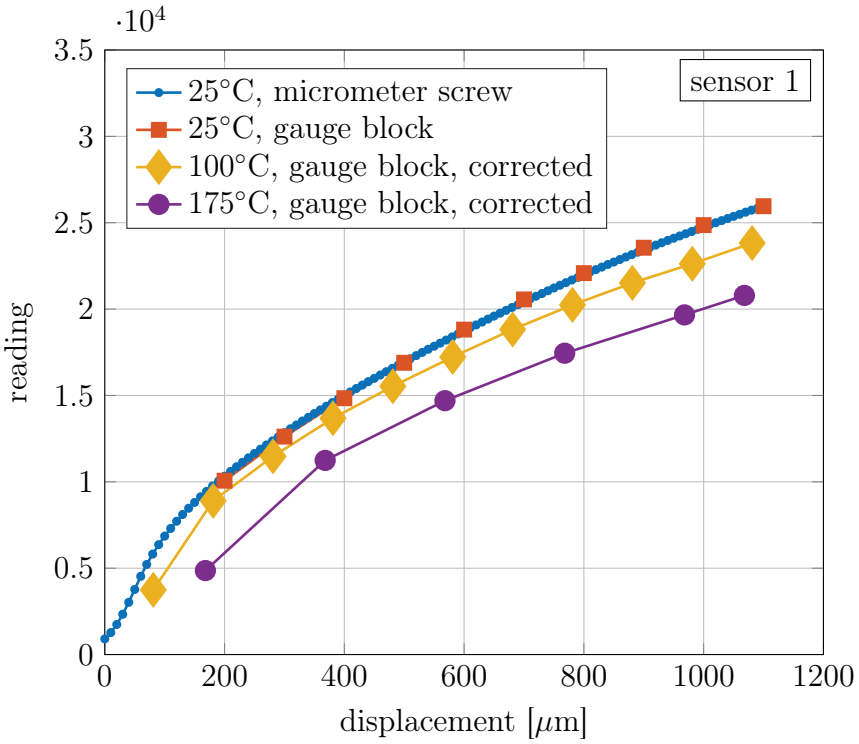

Figure 3.20.: Calibration data considering thermal expansion at 25°C, 100°C and 175°C performed on gauge block calibration tool and comparison of micrometer screw and gauge block calibration at 25°C of displacement sensor 1.

To implement the calibration at elevated temperature T_0 in the measurement data, a model for the calibration data has to be found, to get a correlation $y = f(x)$ between the reading in bit and the output in µm at T_0. Since at higher temperatures the time required for one calibration set increases due to the long heating phases between to measurement points, only few data points are available. The implementation of the calibration at elevated temperature is performed for a reference temperature T_{ref} of 100°C.

Therefore, a polynomial fit of degree = 2 is used to model the calibration data at T_{ref}. The assumption, that the sensor output also has a periodic behavior at elevated

temperature, as shown in figure 3.10 can be checked by plotting the residual from the second order fit at T_{ref} over the normalized reading (equivalent to figure 3.10) as depicted in figure 3.21. And the periodicity also can be found at 100°C. In the next step, a correlation between the reading in bit and the output in µm is to be found at T_{ref}. Therefore a polynomial fit of degree = 2 is modeled at T_{ref} for the three sensors and is used as calibration model at 100°C. The uncertainty, that increases with the polynomial fit of degree = 2 as shown above, has to be considered in the uncertainty calculations.

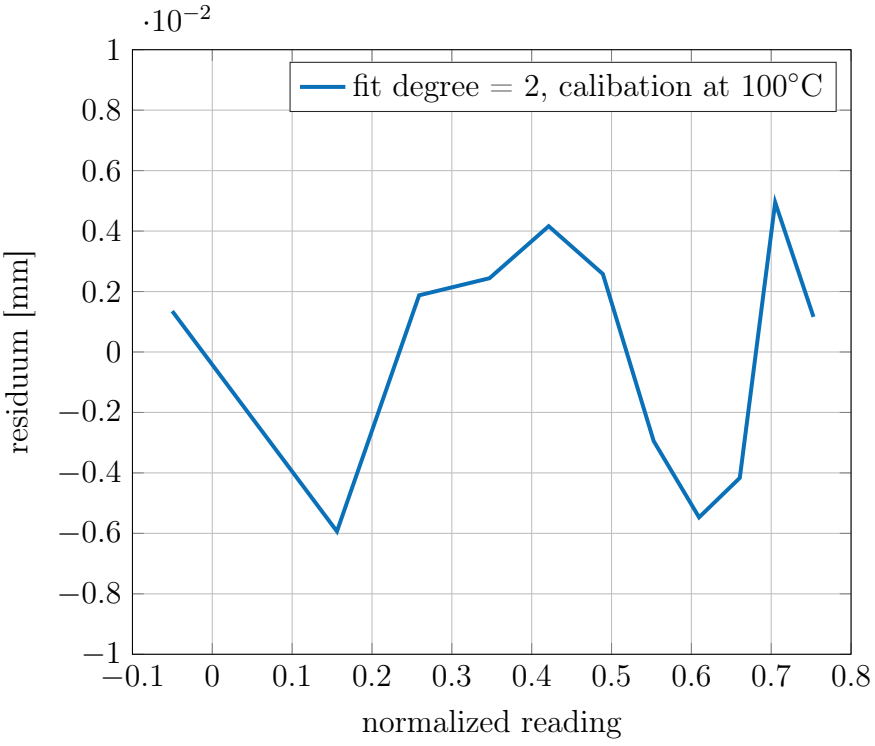

Figure 3.21.: Residual of calibration data from displacement sensor 1 at 100°C fitted with a polynomial of degree = 2.

3.2.2. Calibration of Load Cells

The calibration of the used load cell from Althen GmbH (Kelkheim, Germany), type ALF256-Z4466-2,5kN with the amplifier system SG-IP-24E-B10, is documented in this chapter. A gauge strain measurement mechanism is used, due to the higher thermal stability and better long term properties compared to piezo electric systems. The measurement system (load cell and amplifier combined) covers a range from -2.5 kN in compression to 2.5 kN load in tension and gives a corresponding signal from -10 to +10 V. To check the linearity of the signal output, it is attached to a conventional test equipment. Therefore, a universal testing machine of the type Z010, by Zwick GmbH & Co.KG (Ulm, Germany), with a ± 10 kN type KAF-W, by A.S.T. GmbH Mess- und Regeltechnik (Dresden, Germany) load cell is used. The load cell ALF256 is attached to the Z010 equipment and tested in a force controlled procedure. The load signal recorded by the conventional equipment in N is correlated to the reading of the used load cell in Bit. A linear regression curve is fitted to the documented data of the two load cells, depicted in figure 3.22, and is implemented in the developed test rig software. Due to readability the further proceedings of the load cell calibration are presented for load cell 1. The diagrams for load cell 2 can be found in the appendix 7.

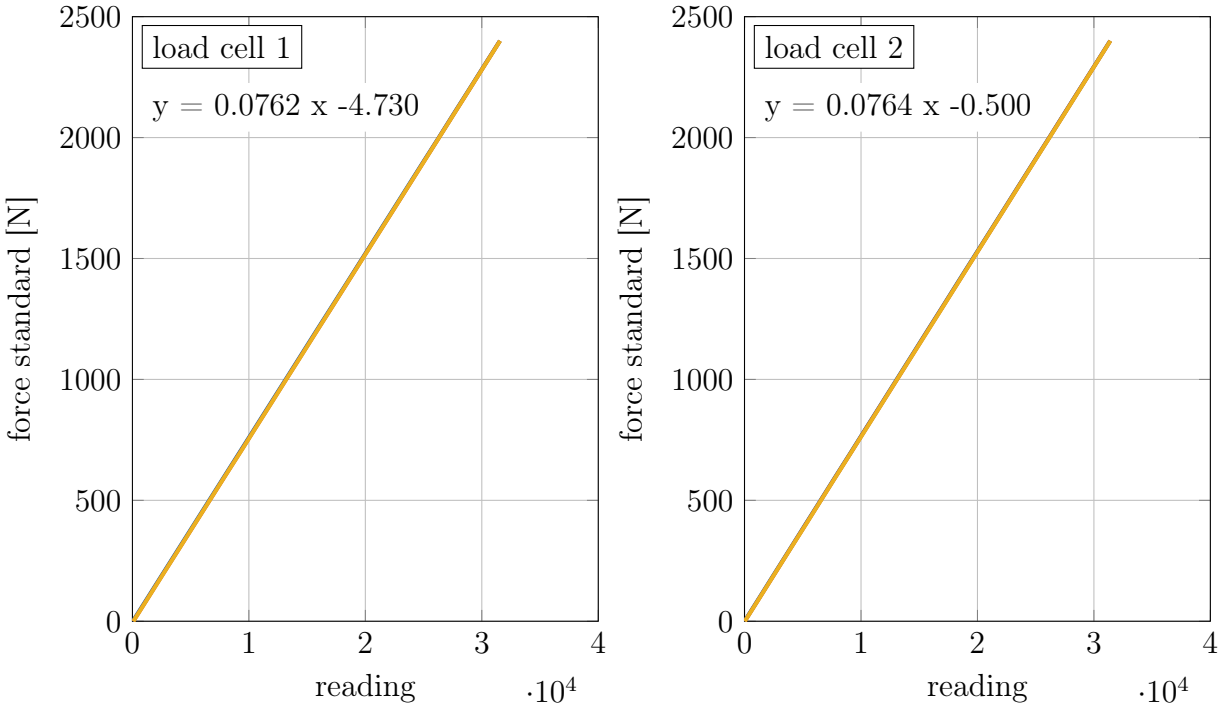

Figure 3.22.: Left figure: Calibration data of load cell 1 at room temperature, with equation of linear regression model. Right figure: Calibration data of load cell 1 at room temperature, with equation of linear regression model.

In figure 3.22 it can be seen, that there are slight differences in the regression curves of the two load cells. To further investigate the quality of the linear regressions a closer look is taken at the residuals. To get a reference for the quality of the fit, and whether the fit method or other sources cause the residuals a closer look has to be taken at the standard first. As standard the load cell type KAF-W 10 with 10 kN measurement range is used. In the calibration protocol of the KAF-W load cell an uncertainty U in the compression regime of 0.2 % of the measured value is documented. This is an absolute error of 5 N for a measurement value of 2500 N, as maximum value of the calibration procedure. So the uncertainty of the standard is higher, than the computed design stage uncertainty $u_{l,d}$ in section 3.3.2. This is why the uncertainty of the standard is depicted in figure 3.23 to give a reference. Further investigations on the uncertainty of the load measurement are documented in section 3.3.2.

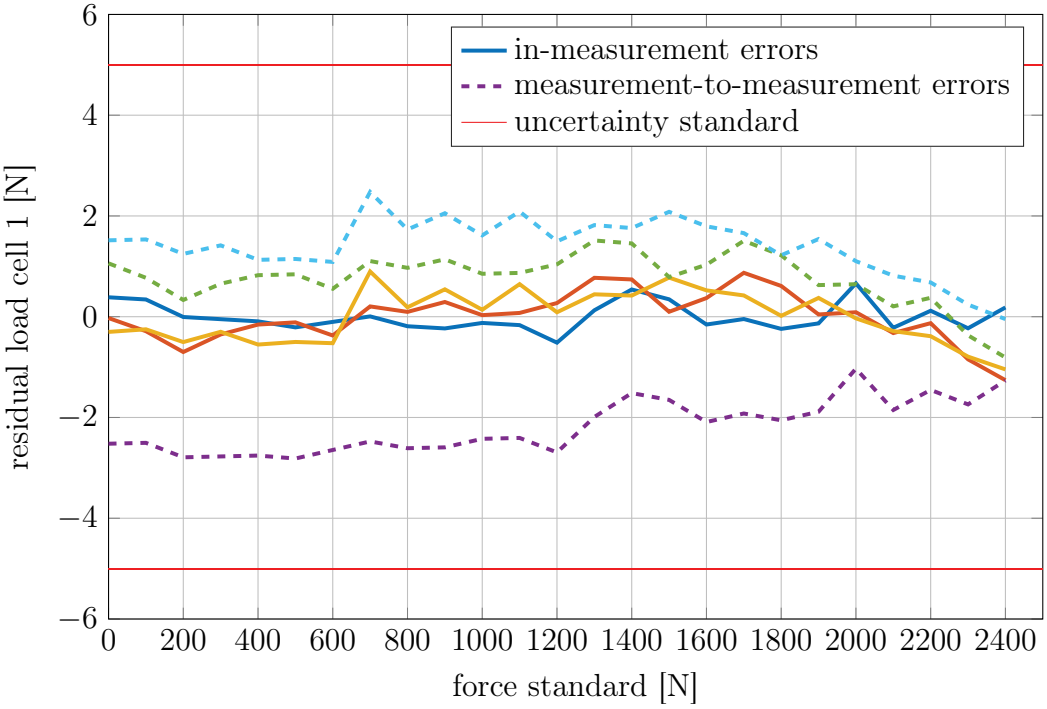

Figure 3.23.: Residuals of linear regression for load cell 1.

During the load cell calibration not only the signal output as a function of applied load is calibrated but also the deformation of the load cell as a function of the applied load. The measurement principle is, that an applied load leads to a defined deformation of small gauge strains. The deformation leads to a change in resistance, which can be detected. So it is a property of the measurement method, that a deformation of the load cell appears during measurement. However, since the specimen and the load cell are positioned in series on the chosen test setup, this deformation is also included in the detected displacement during a measurement. This is why the deformation of the

load cell, as a function of the applied load is characterized. During the calibration on the Zwick Z010 not only the force signal of the universal testing machine, but also the displacement signal of the crossbeam was detected. This displacement signal was not chosen for further investigations, since the compliance of the universal testing machine is included in this data and the cross beam displacement measurement uncertainty is to high.

Therefore, a different way of characterizing the displacement of the load cell was chosen. The displacement of the load cell was characterized on the test rig itself. In this characterization results not only the load cell compliance is contained, but the whole test rig compliance as suggested in [7].

3.3. Uncertainty Analysis

In the following an uncertainty analysis for the measurement system and it's components is performed. Therefore a design stage uncertainty for each measurement device is computed. The theory and the equations used are explained in chapter 2. For the displacement sensor the uncertainty is referred to as u_d, for the load cell as u_l and for the pressure valve as u_p.

3.3.1. Displacement Sensor Uncertainty Analysis

The design stage uncertainty u_d of the sensors is dominated by the electrical components used, such as the signal amplifier and the analog digital converter. It represents an estimate for the measurement device's intrinsic uncertainty and can be estimated without any measurement data. The manufacturers specifications given in the data sheets are used as data basis for the computation of the design stage uncertainty and are listed in table 3.1.

Table 3.1.: Manufacturer specifications of signal amplifier and analog digital converter.

Signal Amplifier	Symbol	Uncertainty
resolution (0.08 % f.s.o)	$u_{d,amp,0}$	1.2 µm
hysteresis [1](0.97 % f.s.o)	$u_{d,amp,h}$	14.55 µm
Analog Digital Converter	**Symbol**	**Uncertainty**
resolution ± 12 Bit	$u_{d,ADc,0}$	0.69 µm
gain (0.08 % of reading)	$u_{d,ADc,gain}$	1.2 µm
linearity (0.025 % of 20V)	$u_{d,ADc,lin}$	0.75 µm
offset (0.015 % of 20V)	$u_{d,ADc,o}$	0.45 µm

[1] hysteresis errors is dealt with separatly.
f.s.o, full-scale operating range.

The *zero order uncertainty* of the amplifier and the AD converter is given by their resolutions $u_{d,amp,0}$ and $u_{d,ADc,0}$. The *instrument uncertainty* $u_{d,c}$ represents the occurring uncertainties over the whole measurement range. An estimate for the design stage uncertainty $u_{d,d}$ for both, the amplifier and the AD converter, can be computed by the equation 2.12 shown in chapter 2.3.

$$u_d = \sqrt{u_0^2 + u_c^2}.$$

Consequently, the design stage uncertainty of the amplifier, $u_{amp,d}$ is given by the square root of the sum of the zero order uncertainty $u_{amp,0}$ and the instrument uncertainty $u_{amp,c}$.

$$u_{d,amp,d} = \sqrt{u_{d,amp,0} + u_{d,amp,c}}. \tag{3.7}$$

So the amplifiers zero order uncertainty and the design stage uncertainty are given by

$$u_{d,amp,0} = \sqrt{0.6^2} = \pm 0.6\,\mu m, \tag{3.8}$$

$$u_{d,amp,d} = \pm 0.6\,\mu m. \tag{3.9}$$

Analog the AD converter uncertainty $u_{ADc,d}$ can be computed as the square root of the square sum of the zero order uncertainty $u_{ADc,0}$ and the instrument uncertainty $u_{ADc,c}$, as given by the equation 3.12.

$$u_{d,ADc,0} = \sqrt{0.69^2} = \pm 0.69\,\mu m \tag{3.10}$$

$$\begin{aligned} u_{d,ADc,c} &= \sqrt{u_{d,ADc,gain}^2 + u_{d,ADc,lin}^2} \\ u_{d,ADc,c} &= \sqrt{1.2^2 + 0.75^2} = \pm 1.42\,\mu m \end{aligned} \tag{3.11}$$

$$u_{d,ADc,d} = \sqrt{0.69^2 + 1.42^2} = \pm 1.58\,\mu m \tag{3.12}$$

Since the sensor measurement signal passes through both, the amplifier and the converter, both have to be considered in the displacement sensor uncertainty u_d, d. Therefore a combined design stage uncertainty u_d, d is computed as follows:

$$\begin{aligned} u_{d,d} &= \sqrt{u_{d,amp,d}^2 + u_{d,ADc,d}^2} \\ &= \sqrt{0.6^2 + 1.58^2}\,\mu m \\ u_{d,d} &= \pm 1.69\,\mu m. \end{aligned} \tag{3.13}$$

The combined design stage uncertainty u_d is the minimal achievable uncertainty with this measurement equipment without considering calibration and data reduction errors. During the calibration process, which can be considered as a measurement itself, a given measurement distance is applied and the standard as well as the displacement sensor provide information about the measurement distance. The standard, a micrometer screw, provides the reference value for the displacement sensor. However this reference value cannot be determined with infinite accuracy and is also fraught with uncertainty. Hence an estimate for the uncertainty of the standard is required to calculate the calibration uncertainty.
Since data sheet for the analog micrometer screw only provides information about increments marked on the screw, but no details about a precision error or linearity, assumptions for those uncertainties are made. It is assumed, that considering linearity and

reading error a uncertainty of 2 µm and 95% confidence can be achieved. Considering the calibration uncertainty u_{cal} the estimate for the displacement measurement uncertainty u_d can be improved.

$$u_{cal} = \pm 1\,\mu m \tag{3.14}$$

$$\begin{aligned} u_d &= \sqrt{u_{d,d}^2 + u_{cal}^2} \\ &= \sqrt{1^2 + 1.69^2}\,\mu m \\ u_d &= \pm 1.96\,\mu m \end{aligned} \tag{3.15}$$

In this uncertainty calculations the uncertainty due to hysteresis and signal drifts was not considered. The hysteresis influence is shown in several measurements in section 3.2.1. The uncertainty due to hysteresis u_{hyst} is assumed conservatively by it's maximum value of 2.5 µm (documented in figure 7.6). The uncertainty due to signal drifts u_{drift} is estimated with 6 µm (depicted in figure 3.17). So the uncertainty for the displacement measurement can be computed as in equation 3.18:

$$\begin{aligned} u_{disp} &= \sqrt{u_d^2 + u_{hyst}^2 + u_{drift}^2} \\ &= \sqrt{1.96^2 + 2.5^2 + 6^2}\,\mu m \\ u_d &= \pm 6.78\,\mu m. \end{aligned} \tag{3.16}$$

Displacement Sensor Uncertainty Analysis at Elevated Temperature

In this section the findings of the sensor calibration at elevated temperature are implemented. Due to the reduced amount of data points in the calibration at elevated temperature, a polynomial fit of degree = 2 has to be performed. In this model the periodicity of the sensors behavior over the measurement range can not be considered. Therefore it must be considered in the uncertainty due to the data reduction. As depicted in figure 3.21 the residual of a polynomial fit of second degree of the calibration data from sensor 1 at 100°C is maximum ± 6 µm.

The uncertainty of the standard can be neglected in this calibration since the gauge block tools are manufactured with a precision of maximum ± 0.1 µm and deviations in the steel block are eliminated since the displacement is measured relatively.

Since the uncertainty due to a data reduction error at 100°C is much lower, than neglecting the temperature drift of the displacement sensor entirely, the new calibration model is implemented at 100°C even though the second degree polynomial model does not consider periodicity. Since the design stage uncertainty and the uncertainties due to signal drifts and hysteresis do not change with temperature the uncertainty due to data reduction $u_{d,red}$ is added to the displacement sensor uncertainty u_{disp}.

$$\begin{aligned} u_{disp,T_{ref}} &= \sqrt{u_d^2 + u_{hyst}^2 + u_{drift}^2 + u_{d,red}^2} \\ &= \sqrt{1.96^2 + 2.5^2 + 6^2 + 6^2}\,\mu m \\ u_{disp,T_{ref}} &= \pm 9\,\mu m. \end{aligned} \tag{3.17}$$

This leads to an overall displacement measurement uncertainty of ± 9 µm at a reference temperature of 100°C . For other temperatures, the calibration procedure on the gauge block tool has to be performed. A new model for the calibration data has to be found, and the gained uncertainty due to data reduction has to be implemented depending on the temperature.

3.3.2. Load Cell Uncertainty Analysis

Similar to the displacement sensor uncertainty analysis, the load cell uncertainty analysis is performed. Therefore, a design stage uncertainty is computed. In the table 3.2 the sensor specifications from the data sheet are listed.

Table 3.2.: Manufacturer specifications of signal amplifier and analog digital converter.

Signal Amplifier	Symbol	Uncertainty
linearity (± 0.05 % f.s.o)	$u_{l,amp,lin}$	1.25 N
hysteresis (± 0.05 % f.s.o)	$u_{l,amp,hyst}$	1.25 N
output signal at zero load (± 4 % f.s.o)	$u_{l,amp,o}$	100 N
creep (20 min) (± 0.05 % of reading)	$u_{l,amp,creep}$	1.25 N
reproducibility (± 0.02 % f.s.o)	$u_{l,amp,rep}$	0.5 N
Analog Digital Converter	**Symbol**	**Uncertainty**
resolution ± 12 Bit	$u_{l,ADc,0}$	0.92 N
gain (0.08 % of reading)	$u_{l,ADc,gain}$	2 N
linearity (0.025 % of 20V)	$u_{l,ADc,lin}$	1.25 N
offset (0.015 % of 20V)	$u_{l,ADc,o}$	0.75 N

f.s.o, full-scale operating range.

For the signal amplifier the design stage uncertainty $u_{amp,d}$ is computed as follows:

$$u_{l,amp,d} = \sqrt{u_{l,amp,0}^2 + u_{l,amp,c}^2} \tag{3.18}$$

The zero order uncertainty $u_{l,amp,0}$ is considered to be 0. So the instrument uncertainty $u_{l,amp,c}$ is computed in equation 3.19 and the resulting design stage uncertainty for the load cell amplifier is given in equation 3.20.

$$u_{l,amp,c} = \sqrt{u_{l,amp,lin}^2 + u_{l,amp,hyst}^2 + u_{l,amp,rep}^2} \tag{3.19}$$

$$u_{l,amp,d} = \sqrt{1.25^2 + 1.25^2 + 0.5^2} = \pm 1.84\,N \tag{3.20}$$

The design stage uncertainty for the AD converter is performed similar to upper section 3.3.2.

The desgin stage uncertainty for the AC converter, $u_{l,ADc,d}$, in N is calculated in equation 3.21:

$$u_{l,ADc,d} = \sqrt{u_{l,ADc,0}^2 + u_{l,ADc,c}^2}. \tag{3.21}$$

The zero oder uncertainty, $u_{l,ADc,0}$, and the instrument uncertainty, $u_{l,ADc,c}$, of the AD converter are used tio estimate the design stage uncertatinty, $u_{l,d}$, as given by equation 3.26.

$$u_{l,ADc,0} = \pm 0.92\,N \tag{3.22}$$

$$u_{l,ADc,c} = \sqrt{u_{l,ADc,gain}^2 + u_{l,ADc,lin}^2} \tag{3.23}$$

$$u_{l,ADc,c} = \sqrt{2^2 + 1.25^2}\,N u_{l,ADc,c} \quad = \pm 2.36\,N \tag{3.24}$$

$$\begin{aligned} u_{l,ADc,d} &= \sqrt{0.92^2 + 2.36^2}\,N \\ u_{l,ADc,d} &= \pm 2.53\,N. \end{aligned} \tag{3.25}$$

$$\begin{aligned} u_{l,d} &= \sqrt{u_{l,amp,d}^2 + u_{l,ADc,d}^2} \\ u_{l,d} &= \sqrt{1.84^2 + 2.53^2} = \pm 3.13\,N. \end{aligned} \tag{3.26}$$

The calculated design stage uncertainty for the load cell of 3.13 N is 0.13 % of the full measurement range of 2500 N.

To estimate an uncertainty for the load measurement errors due to calibration and data reduction must be included. Therefore the uncertainty of the calibration standard must be investigated. The uncertainty of the standard is documented in section 3.2.2. The uncertainty of the standard $u_{l,cal}$ is considered conservatively in the measurement uncertainty $u_{l,d}$, by assuming that $u_{l,d}$ is equal to $u_{l,cal}$ even if the design stage uncertainty $u_{l,d}$ is lower.

The temperature effects on the load cell uncertainty as well as on the uncertainty of the pressure valve, could not be determined in calibration tests similar to the displacement sensors. However, the uncertainty of the load cells and the pressure valves are estimated differently at elevated temperature, which is shown in section 4.1.

3.3.3. Pressure Valve Uncertainty Analysis

In the following section the design stage uncertainty for the pressure value is computed. The necessary information given by the data sheet is listed in the table 3.3.

Table 3.3.: Manufacturer specifications of signal amplifier and analog digital converter.

Signal Amplifier	Symbol	Uncertainty
linearity (± 0.5 % p_{2max})	$u_{p,amp,lin}$	0.05 bar
hysteresis (± 0.2 % p_{2max})	$u_{p,amp,hyst}$	0.02 bar
reproducibility (± 0.2 % p_{2max})	$u_{p,amp,rep}$	0.02 bar
responsiveness (± 0.2 % p_{2max})	$u_{p,amp,rspv}$	0.02 bar
Analog Digital Converter	**Symbol**	**Uncertainty**
resolution ± 12 Bit	$u_{p,ADc,0}$	0.0037 bar
gain (0.08 % of reading)	$u_{p,ADc,gain}$	0.008 bar
linearity (0.025 % of 20V)	$u_{p,ADc,lin}$	0.005 bar
offset (0.015 % of 20V)	$u_{p,ADc,o}$	0.003 bar

f.s.o, full-scale operating range.

The design stage uncertainty for the signal amplifier $u_{p,amp,d}$ is given by the equation :

$$u_{p,amp,d} = \sqrt{u_{p,amp,0}^2 + u_{p,amp,c}^2}. \tag{3.27}$$

The responsiveness (or sensitivity), which is the smallest amount of change that can be detected in a measurement, is seen as part of the $u_{p,amp,c}$ uncertainty. So the $u_{p,amp,d}$ can be computed as shown in equation 3.27.

$$\begin{aligned} u_{p,amp,c} &= \sqrt{u_{p,amp,lin}^2 + u_{p,amp,hyst}^2 + u_{p,amp,rep}^2 + u_{p,amp,rspv}^2} \\ u_{p,amp,c} &= \sqrt{0.05^2 + 0.02^2 + 0.02^2 + 0.02^2}\, bar \\ u_{p,amp,c} &= \pm 0.061\, bar. \end{aligned} \tag{3.28}$$

The design stage uncertainty for the amplifier of the pressure valve is

$$u_{p,amp,d} = \pm 0.061\, bar. \tag{3.29}$$

And for the AD converter the zero order uncertainty, $u_{p,ADc,0}$ in bar is given by the resolution and is

$$u_{p,ADc,0} = \pm 0.0037\, bar. \tag{3.30}$$

In the following equation 3.31 the instrument uncertainty for the AD converter is computed.

$$\begin{aligned} u_{p,ADc,c} &= \sqrt{u_{p,ADc,lin}^2 + u_{p,ADc,gain}^2} \\ u_{p,ADc,c} &= \sqrt{0.005^2 + 0.008^2}\, bar \\ u_{p,ADc,c} &= \pm 0.0094\, bar \end{aligned} \tag{3.31}$$

Now, analog to equation 3.27, the design stage uncertainty $u_{p,ADc,d}$ can be computed for the AD converter.

$$\begin{aligned} u_{p,ADc,d} &= \sqrt{u_{p,ADc,0}^2 + u_{p,ADc,c}^2} \\ u_{p,ADc,d} &= \sqrt{0.0037^2 + 0.0094^2} bar \\ u_{p,ADc,d} &= \pm 0.010 bar \end{aligned} \tag{3.32}$$

Now the design stage uncertainty $u_{p,d}$ for the pressure valve can be calculated, as documented in equation 3.32.

$$\begin{aligned} u_{p,d} &= \sqrt{u_{p,amp,d}^2 + u_{p,ADc,d}^2} \\ u_{p,d} &= \sqrt{0.061^2 + 0.010^2}\, bar \\ u_{p,d} &= \pm 0.062\, bar \end{aligned} \tag{3.33}$$

The design stage uncertainty of the pressure signal, detected by the CPU of 0.062 bar is 0.62% of the whole signal range from 0 to 10 bar.

The uncertainty of the pressure valve also has to be considered in the boundaries of the chosen regulation mechanism. Since the regulation can not be more accurate than the signal detection. The pressure regulation is performed with a potential function of the structure:

$$p = p_{target}\,(1 - e^{\frac{-t}{\tau}}) \tag{3.34}$$

The influence of the chosen time constant on the regulation speed is depicted in figure 3.24.

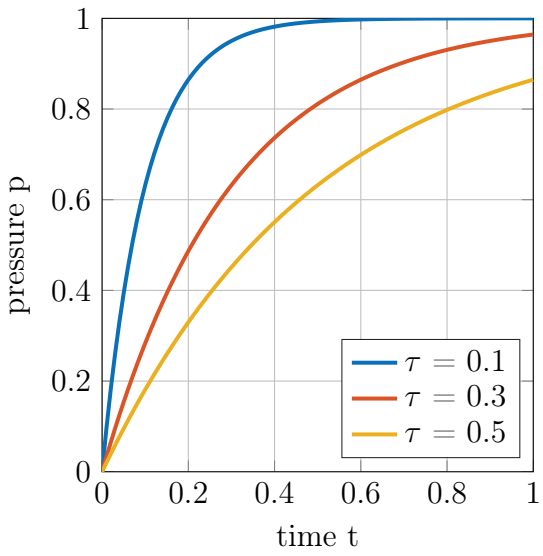

Figure 3.24.: Influence of time constant τ on the pressure regulation over time t.

3.3.4. Test Rig Uncertainty Analysis

With the information gained from the individual uncertainties of the sensors, an uncertainty for the test rig can be estimated. Therefore the mechanical test setup is again taken into consideration.

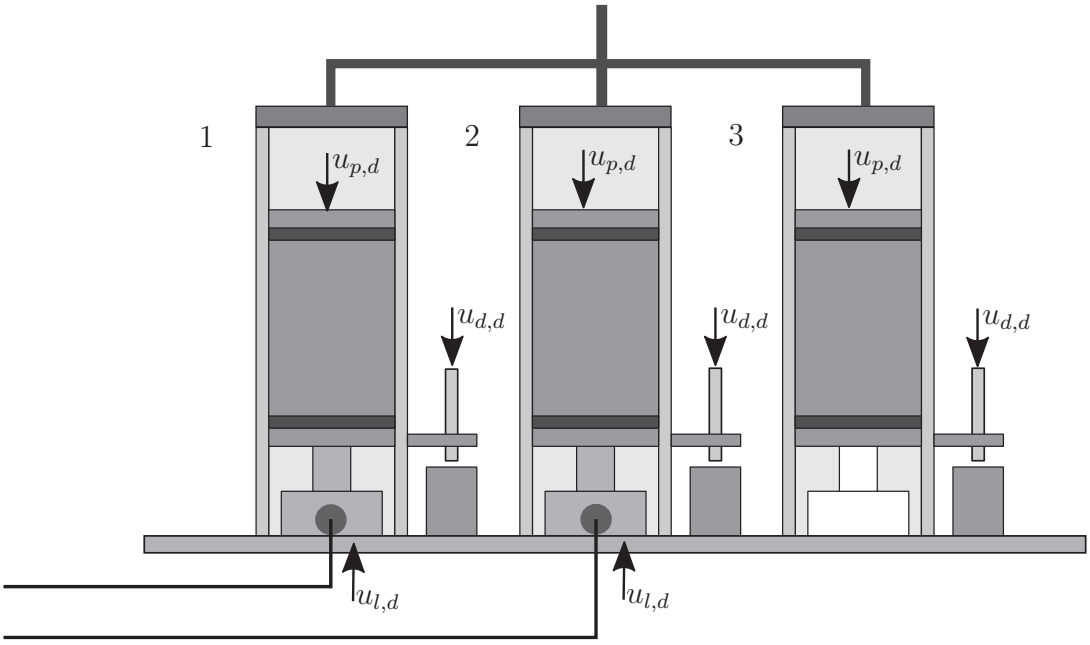

Figure 3.25.: Schematic picture of the test battery with the design stage uncertainties of the pressure value $u_{p,d}$, the displacement sensors $u_{d,d}$ and load cells $u_{l,d}$

The first effect that has to be considered is the combination of the uncertainty in the load application $u_{p,d}$ (caused by the pressure value) and by the load measurement $u_{p,d}$. To get a better comparison between the two uncertainties, the uncertainty in the pressure value $u_{p,d}$ in bar is converted to an uncertainty $u_{p,d}$ in N. Therefore the piston diameter A_{piston} is used.

$$\begin{aligned} A_{piston} &= \frac{50^2\pi}{4} = 1963.5\, mm^2 \\ u_{p,d} &= 0.062\, 10^5\, Pa \\ u_{p,d} &= \frac{0.062}{10}\, MPa \\ u_{p,d,N} &= \frac{u_{p,d}}{10} A_{piston} \\ u_{p,d,N} &= \frac{0.062}{10} 1963.5\, N \\ u_{p,d,N} &= \pm 12.2\, N \end{aligned} \tag{3.35}$$

According to equation 3.35 the pressure valve regulates the pressure with an uncertainty of ± 12.2 N. but the load cell can detect the applied force with an uncertainty of ± 5 N. Therefore, the load cell can be used, to determine the applied pressure in the pipe system. To investigate the pressure regulation and the load application more closely, a test procedure is used, to characterize the compliance of each test rig. The specimen and the specimen cup were removed, and the piston is in direct contact with the load cell or the dummy, as in figure 3.26. Now, pressure is applied and the signal of the pressure valve, the temperature and the signal of the displacement sensor are detected. The pressure is applied stepwise, with decompression to 0 bar after each step, as shown in the diagram of figure 3.26 . The stress levels of 1, 2.5, 5, 7.5, 10, 12.5 and 15 MPa are applied.

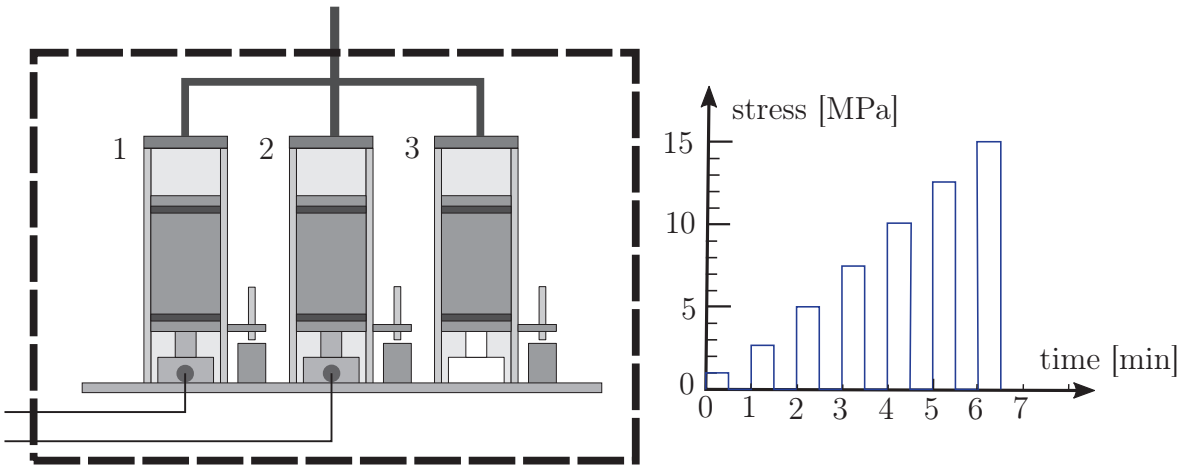

Figure 3.26.: Left picture: Test setup for stepwise determination of test rig compliances. Right picture: digramm of applied stress in MPa over time.

The target value for the pressure p_{tv} the current value of the pressure valve p_{cv} and the load signals of load cell 1 and load cell 2 are analyzed during the test procedure. By comparing p_{tv} and p_{cv} a measure for the quality of the pressure regulation is gained. By comparing the p_{tv} and the load signals a measure for the absolute regulation error is gained. The difference between the current pressure value p_{cv} and the detected load signal gives a measure for the deviation between the load cell calibration and the pressure value calibration.

In the following figure 3.27 the difference between the target value p_{tv} and the current value p_{cv} of the pressure value depending on the applied pressure p_{tv} is plotted. The left axis shows the difference $\Delta\, p_{cv} - p_{tv}$ in bar, while the right axis shows the difference Δ in N, as calculated by the equation 3.35.

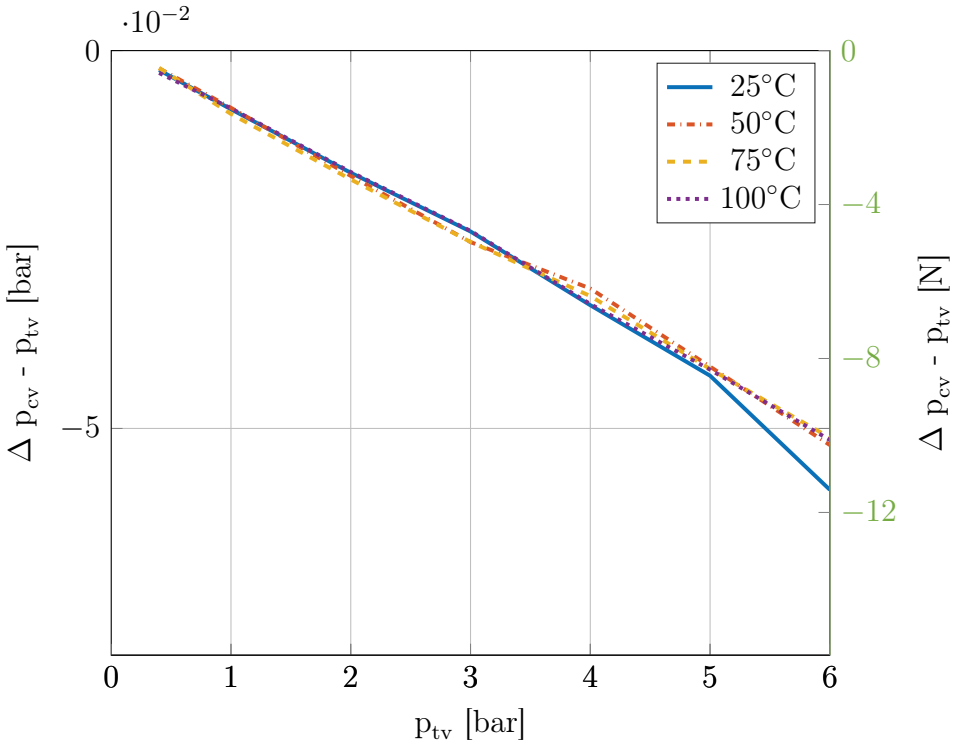

Figure 3.27.: Difference between the current pressure value p_{cv} and the target value p_{tv} plotted depending on the target pressure value p_{tv} in bar.

The plotted data show, that the maximum deviation between the target value and the current pressure value is less than the uncertainty $u_{p,d}$, which is ± 0.062 bar, and can therefore be considered as insignificant. Furthermore, the difference $\Delta\ p_{cv}$ - p_{tv} does not depend on the temperature. With this finding, the assumption, that the pressure regulated load application is also applicable at elevated temperature could be proven. The minor difference between the target value and the actual value can be caused by leakage of the pressure system and the decreasing stiffness of the sealing element at elevated temperature.

The upper part of figure 3.28 shows the deviation between the current value of the pressure valve p_{cv} and the load cell signal 1. The lower part shows the deviation between the measured load of load cell 1 and the target value p_{tv} in N (see equation 3.35). The difference between the two plots is the deviation between p_{tv} and p_{cv} of 12 N, which is exactly the discrepancy due to the pressure loss in the system.

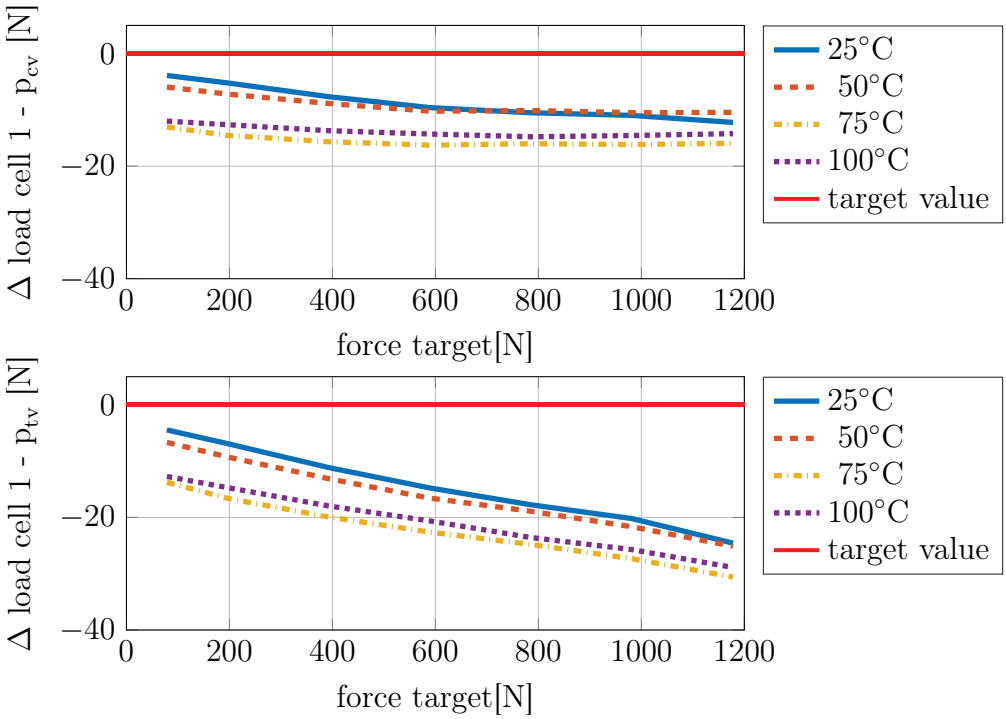

Figure 3.28.: Upper part: Difference between the signal of load cell 1 and the current pressure p_{cv} in [N]. Lower part: Difference between signal of load cell 1 and the target pressure p_{tv} in [N].

Since during loading not only the specimen, but also the load cells and the specimen cups get compressed, a measure for the test rig compliance is needed. It is assumed, that the load cells and the dummy cell show different deformations under compression. In the previous sections, the uncertainties for the displacement sensors and the load cells are discussed. Now the displacement sensors are used, to determine differences between the compliances in the three test rigs. For each rig, a compliance curve is to be measured, which documents the deformation of the rig depending on the applied load. Thus, the measured deformation of the test rig in a compression creep test on a specimen is known, and can be considered in the measurement data evaluation.

To get more information about the deviation of each test rig and between the measurements with one sensor, and the deviation between the different sensors, three different test configurations are investigated. Therefore, the position of the displacement sensors are changed cyclically on the test bench. In the table 3.4 the sensor number is listed for each test rig depending on the test configuration.

Table 3.4.: Overview table for test configurations of compliance measurements.

Test Rig No.	1	2	3
	Sensor No.		
configuration 1	1	2	3
configuration 2	3	1	2
configuration 3	2	3	1

For each configuration six runs were performed. The standard deviation within the six runs can be seen as a measure for the repeatability of the experiment. The difference between the results of each sensor on one rig represents the deviation between the sensors. And the evaluated compliances including all runs and all sensors on one test rig are seen as a measure of the individual test rig behavior. With this test procedure the calculated uncertainty for the test rig can be checked. For the data evaluation of this test, the displacement data at the given stress levels are extracted. The noise of each individual measurement is evaluated at the different stress levels, to see if it increases with the measurement distance. The deviation between the six runs at constant stress levels, and the deviation between the six runs of the three sensors on one rig are also evaluated by this routine. The results are depicted in chapter 4.1.

To investigate the performance of the test rig at elevated temperature, the test procedure as depicted in the diagram of figure 3.26 was performed at 50°C, 75°C and 100°C. The test results of the temperature calibration are depicted in chapter 4.1.

4. Results and Discussion

In the following chapter, the results of this thesis are presented. After the development, the uncertainty calculations and the performed calibration, a test rig compliance can be estimated. The test rig compliance C_m is introduced first. The creep measurement results on PTFE specimens are presented in the second section.

4.1. Test Rig Compliance

After the measurement uncertainties for the displacement and the load sensors and the regulation valve are computed, the gained information has to be combined to estimate the test rig compliance C_m. The test rig compliance is one of the most important outcomes, because it influences the test results significantly. Depending on the load, this influence can be much higher, than any calculated measurement uncertainty. The results of the performed test procedure, as depicted in figure 3.26, are presented in this chapter. For each configuration (as in table 3.4) at least six runs were performed.

The results of the three displacement sensors on the test rig number 1 are presented in the following figure 4.1. The deviation between the measurements is maximum $\pm\,6\,\mu m$ as estimated in the performed calculations. Since the measurements are performed randomly on different days, high deviations might be caused due to the appearing signal drifts.

Not only the displacement but also the detected force signal is investigated to determine whether the test system is also applicable for unloading experiments and if the pressure in the piping system is applied evenly to both load cells. Due to readability the diagram for the load cell 2 can be found in the appendix. It can be shown, that the detected load signals show almost identical signals, which means that the pressure is applied evenly in the system. Therefore, the solution of attaching a variable number of test rigs to one test battery and detecting the displacement but not the load in all rigs is justified. In the following figure 4.2 the signal of load cell number 1 is depicted.

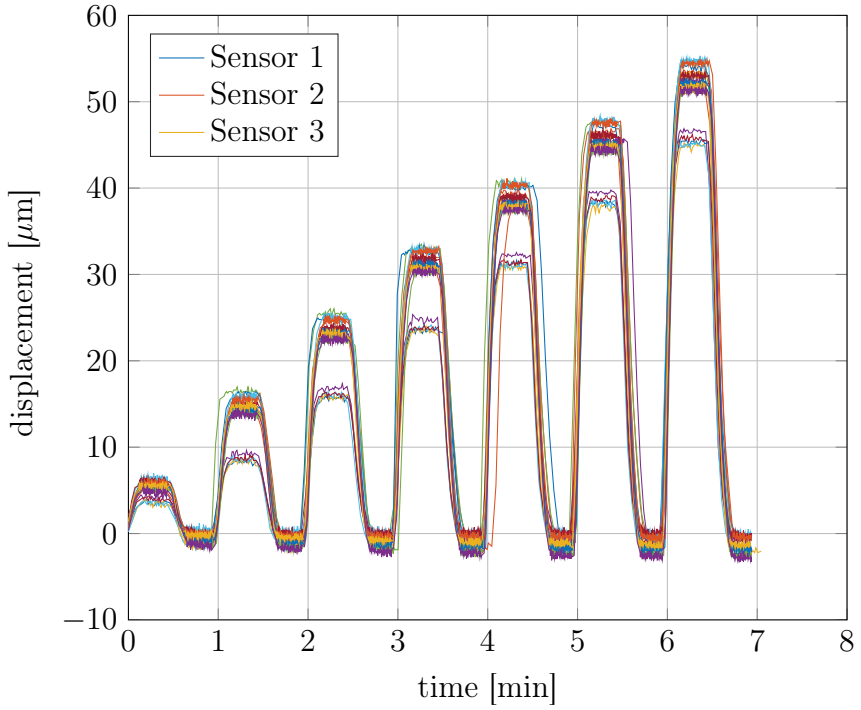

Figure 4.1.: Diagram of displacement signals of three displacement sensors on test rig 1.

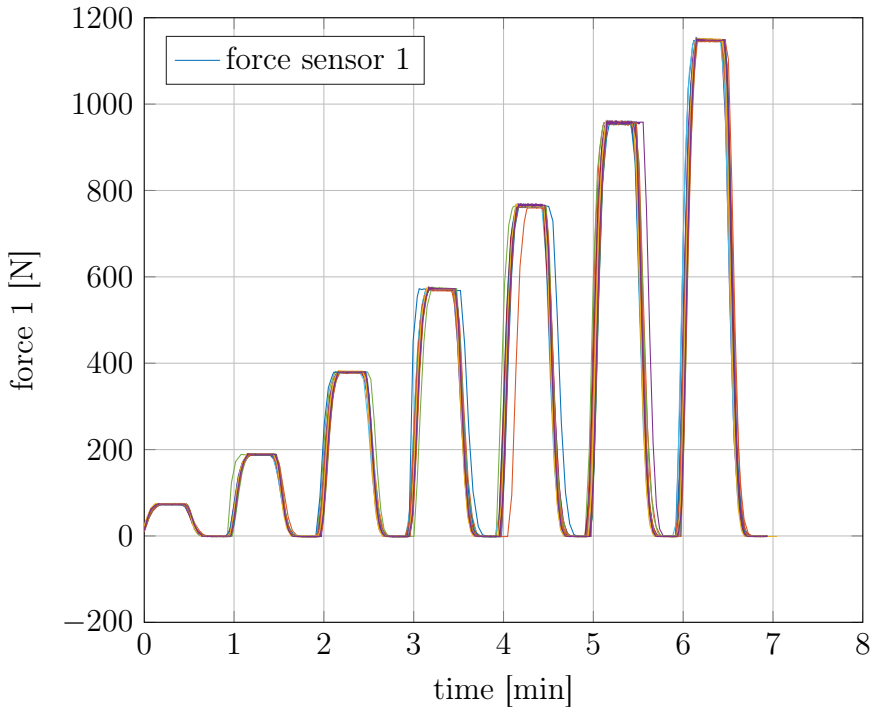

Figure 4.2.: Load signal of load cell number 1 during stepwise loading and unloading.

With the load signal also the pressure regulation can be controlled. None of the load cells shows overshooting during loading or unloading, which indicates that the pressure valve is able to control the pressure properly. This can also be seen by plotting the signal of the pressure valve during the experiments. The figure 4.3 shows the pressure signal over time.

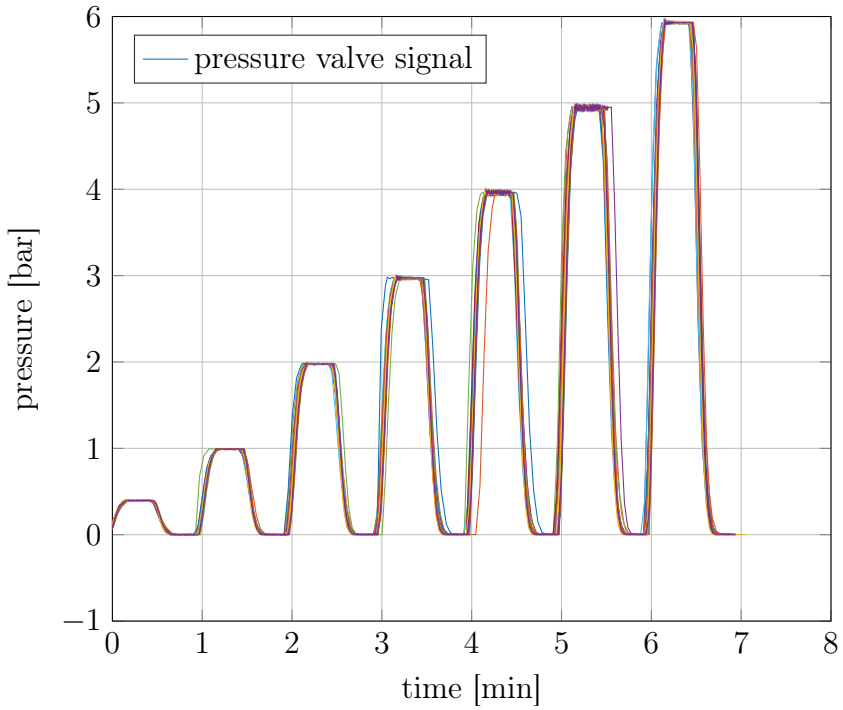

Figure 4.3.: Signal of pressure valve over time during stepwise loading and unloading.

To evaluate the data more closely, the measurement signals at the applied loads are extracted and the mean values and standard deviation within one measurement, and between all measurements on one test rig in all configurations are calculated. With the mean values of the displacement sensors on one test rig and the mean values of the load signal a correlation between the applied load and the deformation of the load cells can be investigated. Therefore, the displacements measured in the 3 configuration is plotted for each test rig in the following figures 4.4, 4.5 and 4.6. The red lines and error bars represent the mean value and the standard deviation of performed measurement runs on one test rig.

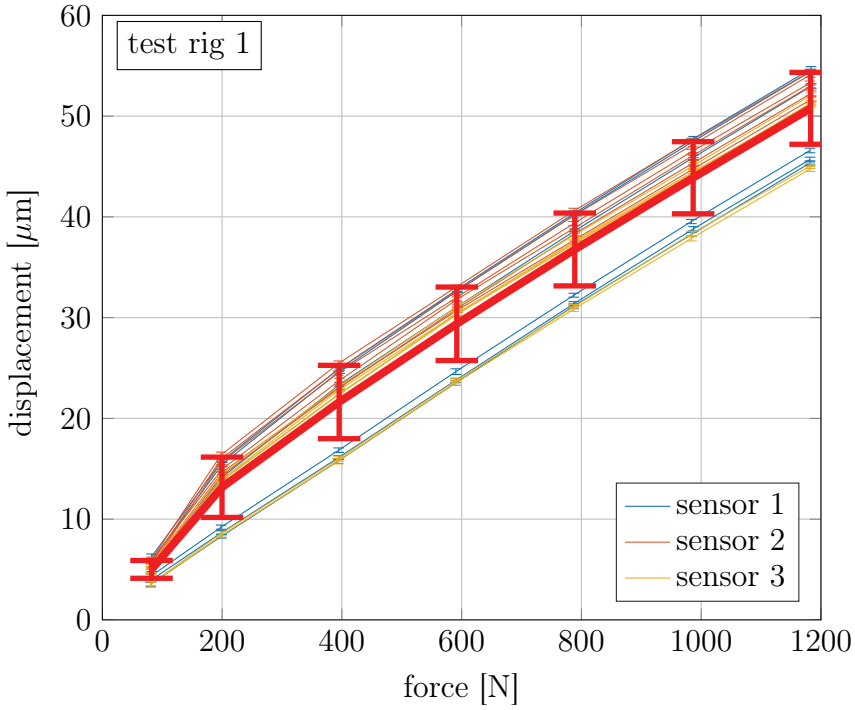

Figure 4.4.: Load dependent deformation of test rig number 1.

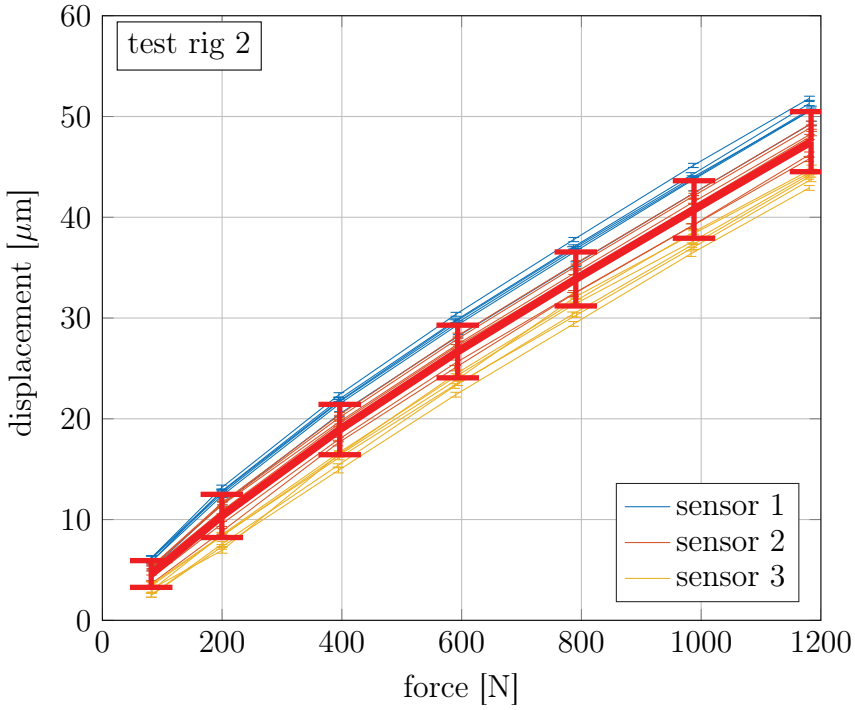

Figure 4.5.: Load dependent deformation of test rig number 2.

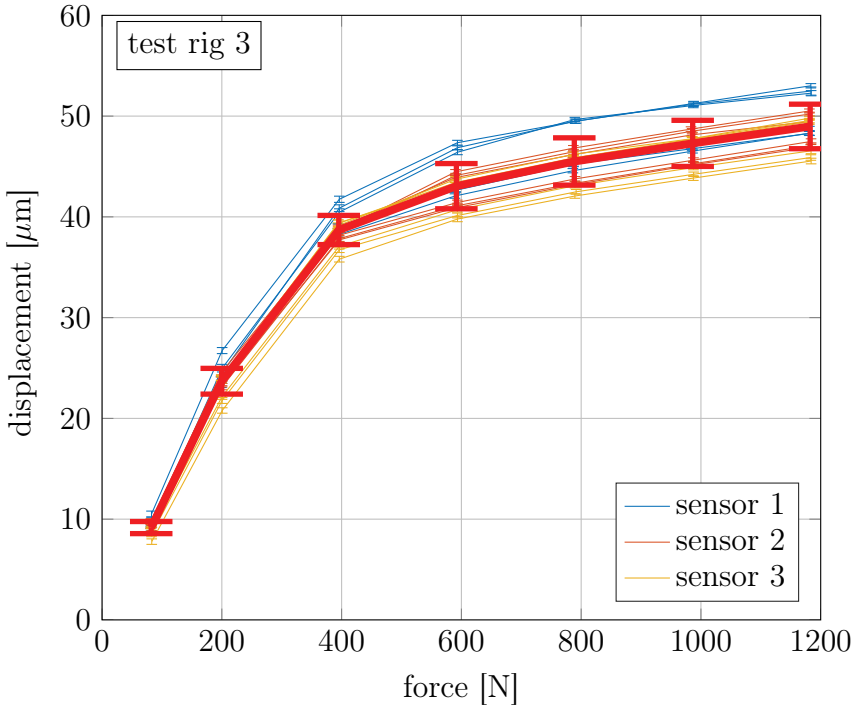

Figure 4.6.: Load dependent deformation of test rig number 3.

The measured test rig compliances can now be implemented in the data evaluation by applying linear regression curves to the results of test rig 1 and 2 and a polynomial model to the result of test rig 3. The load dependent displacements of the test systems is subtracted from the measurement results in the creep experiments presented in the following chapter.

The insights, that can be gained from this measurement procedure, can be summarized: i.) The first finding is, that an entirely unloading is possible and there is no friction between the sealing element and the cylinder, that would make the piston stop or stick during unloading. ii.) Another important outcome is, that there are detectable differences between the test rigs, which appear when comparing figure 4.4, figure 4.5 and figure 4.6. The first and the second test rig show very linear behavior over the whole calibration range, while the third sensor shows nonlinear behavior after about 400 N applied load. A different behavior between the three test rigs was expected, since the first and the second test rig are equipped with a load cell and the third one is equipped with a steel dummy. iii.) The third finding is, that the test concept with pressurized air and additional dummy cells is applicable and can be used for reproducible creep measurements. iiii.) The forth finding is, that the all over standard deviation (depicted with red error bars) is between 5 µm and 10 µm, depending on the test rig and the applied load.

Temperature Dependent Test Rig Uncertainty Analysis

To investigate the test rigs behavior at elevated temperature, the same test procedure as depicted in figure 3.26 was used, but with the test setup placed in the furnace. The compliance calibration was performed at 50°C, 75°C and 100°C. Six runs were performed in the first configuration (as shown in table 3.4). The results of this calibration procedure are presented in figure 4.7.

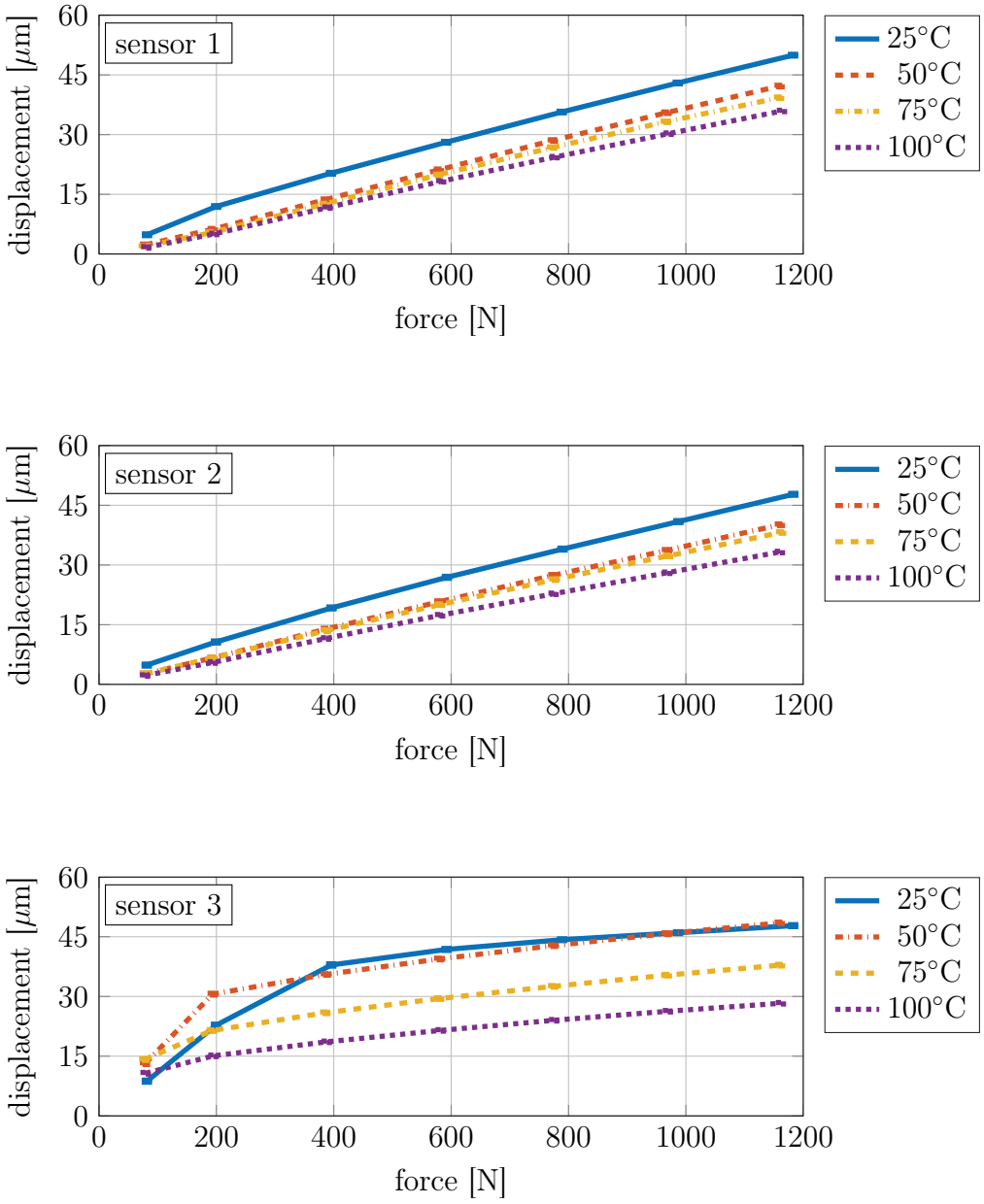

Figure 4.7.: Displacement signals of sensor 1, 2 and 3 during test rig compliance calibration as a function of the applied load and the test temperature.

The results show, that with increasing temperature the displacement measured by the system decreases. This would indicate, that the test rig compliance would not increase at higher temperatures but decrease and the system would get stiffer. Since the test setup contains no components, that could show a significant stiffness increase at 175°C, a mechanical stiffness increase is an unlikely cause. This is why a closer look at the displacement sensors behavior at elevated temperature was taken in section 3.2.1.

The displacement sensor calibration at elevated temperature with the gauge blocks show, that with increasing temperature the detected displacement signal decreases. Which means, that at higher temperature less displacement for the same reference value is detected. This explains, why at higher temperatures the test rigs seem to stiffen- because of the temperature dependent sensor behavior. Therefore, a temperature correction of the measurement data at elevated temperature must be performed by applying a new calibration at elevated temperature as shown in section 3.2.1.

Due to the changed temperature calibration at elevated temperature, the uncertainty of the displacement measurement as well as the uncertainty of the test rig compliance increases slightly at elevated temperature, as calculated in section 3.2.1.

4.2. Creep Measurements

In the following section the results of selected creep experiments are presented. Measurements at 100°C at 2 MPa, 4 MPa and 10 MPa are compared to tests performed on a conventional test equipment. In this way, the test rigs performance can be investigated at low stress and deformation (2 MPa) and high deformations (10 MPa) and the implementation of the performed temperature calibration can be tested. In figure 4.8 the strain in % is plotted over the measurement time in hours for 3 measurements on the test rig, and for two runs on conventional equipment as control measurements. The control measurements are performed by the Institute of Material Science and Testing of Polymers at the Montanuniversität Leoben, but on the same specimen type (cylinders, 10 mm diameter and 10 mm height). These measurements, referred to as "Zwick 1" and "Zwick 2" are performed on a special attachment to a universal testing machine, which is documented in [8].

In the following figures 4.8 and 4.9 the test rig compliance and the calibration of the displacement sensors at elevated temperature is already implemented.

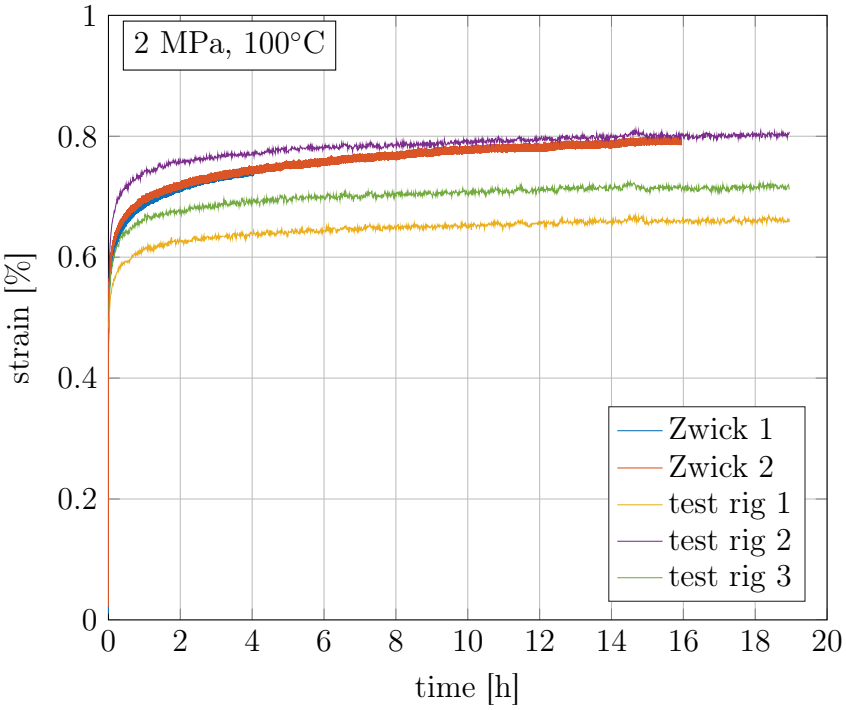

Figure 4.8.: Creep measurement of PTFE at 100° and 2 MPa.

In the comparison of the measurements at 2 MPa it can be seen, that the deviation between the three test rig measurements is about 0.15 % strain. As shown in chapter 3.2 the measurement uncertainty of the displacement sensors is ± 8 µm at room temperature and about ± 10 µm at 100°C. For the chosen specimen geometry of 10 mm height (± 0.1 mm tolerance) the deviation depending on the specimen height would be varying from 14.85 µm (0.15 % of 9.9 mm) to 15.15 µm (0.15 % of 10.1 mm). So a deviation of 0.15 % ranging from ± 7.43 µm to ± 7.58 µm at 100°C lies within the estimated measurement uncertainty of the displacement sensor of ± 10 µm. Therefore, in this measurement it can not be differentiated between deviations within the three specimens.

However, due to the small absolute displacement of 0.8 % during the measurement of 2 MPa an deviation of 0.15 % between the measurements is a relative measurement error of 19 %. This is why it is recommended, to use the developed test rig at higher absolute deformations to decrease the relative measurement error. Measurements at 2 MPa can be performed at 100°C to determine a creep compliance, but the measurement time should be longer, to increase the absolute measurement distance or higher specimens should be preferred.

To determine the deviation of the tests on the test rig at maximum measurement distance a creep test at 10 MPa stress and 100°C is performed as well. The measurement data is depicted in figure 4.9. If the absolute measurement distance increases, the relative deviation decreases significantly. In the 10 MPa measurement the absolute measurement

distance of 10.4 % strain is detected. The deviation between the three measurements performed on the test rig is 0.9 % strain, which is a relative deviation of 8.6% of the measurement distance. In absolute distances the maximum deviation between the three specimens in this test is 90 µm (0.9 % strain at 10 mm). With considering the determined measurement uncertainties for the displacement measurements in the previous sections the difference between specimens can clearly be measured.

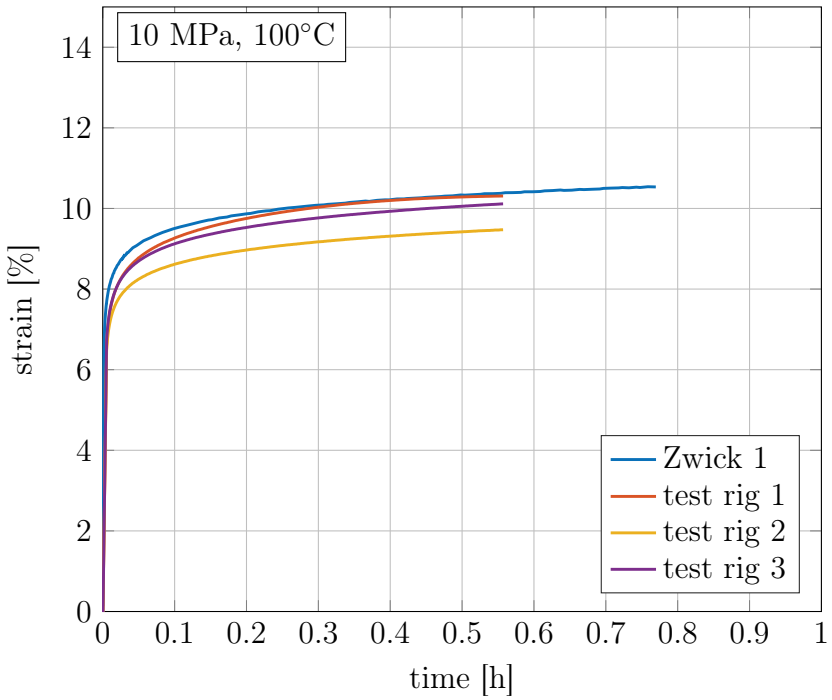

Figure 4.9.: Creep measurement of PTFE at 100°C and 10MPa.

With the selected creep experiments shown in this thesis at 100°C the limitations and possibilities of the developed measurement equipment can be visualized. The downsides and advantages of the developed test concept are discussed in the following section and an outlook for further development possibilities is given.

5. Summary

In this thesis a fully functional compressive creep testing machine is developed. By performing an extensive calibration and uncertainty analysis a reliable measuring certainty could be determined. The therefore resulting deviations in displacement and load measurement, that are to be expected, could be verified in various test procedures. The main influences on a creep experiment caused by the testing machine were investigated, such as time and temperature dependent sensor behavior and the machine compliance at selected temperatures. By carefully investigating these influences the measuring certainty can be determined also at elevated temperature.

It can be shown, that with diligent calibration the measurement quality can be improved significantly. With proper calibrated displacement sensor a compliance of the test machine can be measured. The measurement results are compared with the calculated results from the uncertainty analysis and a correlation can be shown. To investigate the behavior of the test machine, the displacement sensors are calibrated individually at elevated temperature and then the test rig compliance is again measured at higher temperature. With the performed temperature calibration creep measurements on PTFE are performed and compared with measurements on a conventional equipment. It can be shown, that with the developed test equipment reliable test results, that correlate well with data gained on conventional equipment, can be obtained.

The results show, that the selected concept of the piston moved by pressured air is applicable not only at room temperature but also at elevated temperature. The modular design allows reproducible simultaneous creep experiments. By adding a second pressure valve to the setup independent pressure circuits could be implemented and different test batteries could be applied with different pressures and measured simultaneously. If more reproductive test rigs are to be attached to the current setup, a balanced piping system should be implemented again to reduce uncertainties in the pressure distribution within system. This can be investigated by changing position of the load cells and performing experiments as presented in chapter 4.1.

However the currently implemented sensor calibration and the therefore arising measuring certainty should be considered when performing creep experiments. It is recommended, to avoid measurements with maximum deformations below 100 µm, since the relative measuring uncertainty prevents precise statements on the deviations between the three measurements. If small strains should be determined the applicability of the current sensor must be proven in a re-calibration or a different sensor type may be

implemented.

Due to the modular test setup not only creep experiments, but also relaxation experiments could be performed in future. On the presented test battery with 2 load cells two simultaneous relaxation experiments can be measured. Therefore an additional attachment to the setup must be made to stop the piston, that is applied with load, at a given position. With this setup, the specimen is compressed up to a defined height, and the load signal can be detected over time.

6. Bibliography

[1] F. Schwarzl. *Polymermechanik: Struktur und mechanisches Verhalten von Polymeren*. Berlin, Heidelberg: Springer Berlin Heidelberg, 1990.

[2] Wolfgang Grellmann. *Kunststoffprüfung*. 3. Aufl. München: Hanser, 2015.

[3] H. Domininghaus. *Kunststoffe: Eigenschaften und Anwendungen*. 7., neu bearb. und erw. Aufl. VDI-Buch. Berlin, Heidelberg, and New York, NY: Springer, 2008.

[4] G. W. Ehrenstein and R. P. Theriault. *Polymeric materials: Structure, properties, applications*. Munich and Cincinnati, OH: Hanser and Hanser Gardner Publications, 2001.

[5] P. Elsner, P. Eyerer, and T. Hirth. *Polymer Engineering: Technologien und Praxis*. Dordrecht: Springer, 2008.

[6] F. Schwarzl. "Zur molekularen Theorie der linearen und nichtlinearen Relaxationserscheinungen". In: *Kolloid-Zeitschrift* 165.1 (1959), pp. 88–96.

[7] ISO 604. *Bestimmung von Druckeigenschaften*. 2003.

[8] M. Jerabek. "Advanced Characterization of the Tensile and Compressive Behavior of PP and PP Composites: Dissertation". Dissertation. Leoben: Montanuniversität Leoben, 2009.

[9] M. Jerabek, Z. Major, and R. W. Lang. "Uniaxial compression testing of polymeric materials". In: *Polymer Testing* 29.3 (2010), pp. 302–309.

[10] M. Jerabek, Z. Major, and R. W. Lang. "Strain determination of polymeric materials using digital image correlation". In: *Polymer Testing* 29.3 (2010), pp. 407–416.

[11] ISO 3167. *Kunststoffe - Vielzweckprüfkörper*. 2003.

[12] R. Danzer et al. "Fracture of Ceramics". In: *Advanced Engineering Materials* 10.4 (2008), pp. 275–298.

[13] Zwick GmbH & Co. KG, 2016.08.03. *https://www.zwick.de/de/produkte*.

[14] 2016.08.03 Instron GmbH. *http://www.instron.de/de-de/testing-solutions/by-test-type/compression*.

[15] 2016.08.03 MTS Systems Corporation. *https://www.mts.com/en/products/index.htm*.

[16] Torsten Theumer and Franziska Heilenz. “Kriechprüfstand und Verfahren zu seiner Verwendung”. DE 10 2010 040 268 A1. 2012.

[17] Ruchtl, Peter, Dipl.-Ing. “Hebelarmprüfmaschine”. DE 10 2009 049 700 A1. 2011.

[18] Werner Hufenbach et al. “Vorrichtung zur einachsigen Druckprüfung schlanker Prüfkörper mittels einer von außerhalb der Vorrichtung gerichteten Einleitung von Druckkraft auf den Prüfkörper”. DE 10 2010 052 815 B4. 23.11.2010.

[19] Deutschland Bültmann GmbH. “Vorrichtung zum Aufbringen von Druck- und/oder Zugkräften auf im wesentlichen stabförmige Werkstücke aus elektrisch leitfähigem und/oder magnetisierbarem Material”. DE 201 22 031 U1. 2004.

[20] Uwe Beck. “Verfahren und Vorrichtung zur Ermittlung von durch Druck beeiflussbaren Eigenschaften eines Prüflings”. DE 10 2009 019 202 B4. 2010.

[21] ISO 527. *Kunststoffe- Bestimmung der Zugeigenschaften*. 2010.

[22] R. S. Figliola and D. E. Beasley. *Theory and design for mechanical measurements*. 5th ed. Hoboken, NJ: J. Wiley, 2011.

[23] ASTM E2309. *Standard Practices for Verification of Displacement Measuring Systems and Devices Used in Material Testing Machines*. 2016.

[24] Silvia Brunbauer, Andreas Kaufmann, and Martin Pletz. *FE Modelle zur indirekten Bestimmung des Reibkoeffizienten im Stauchversuch*. 25. Leobener Kunststoff-Kolloquium, April 2016.

7. Appendix

In the following chapter, all pictures and tables are added, which are not included in the thesis to increase readability.

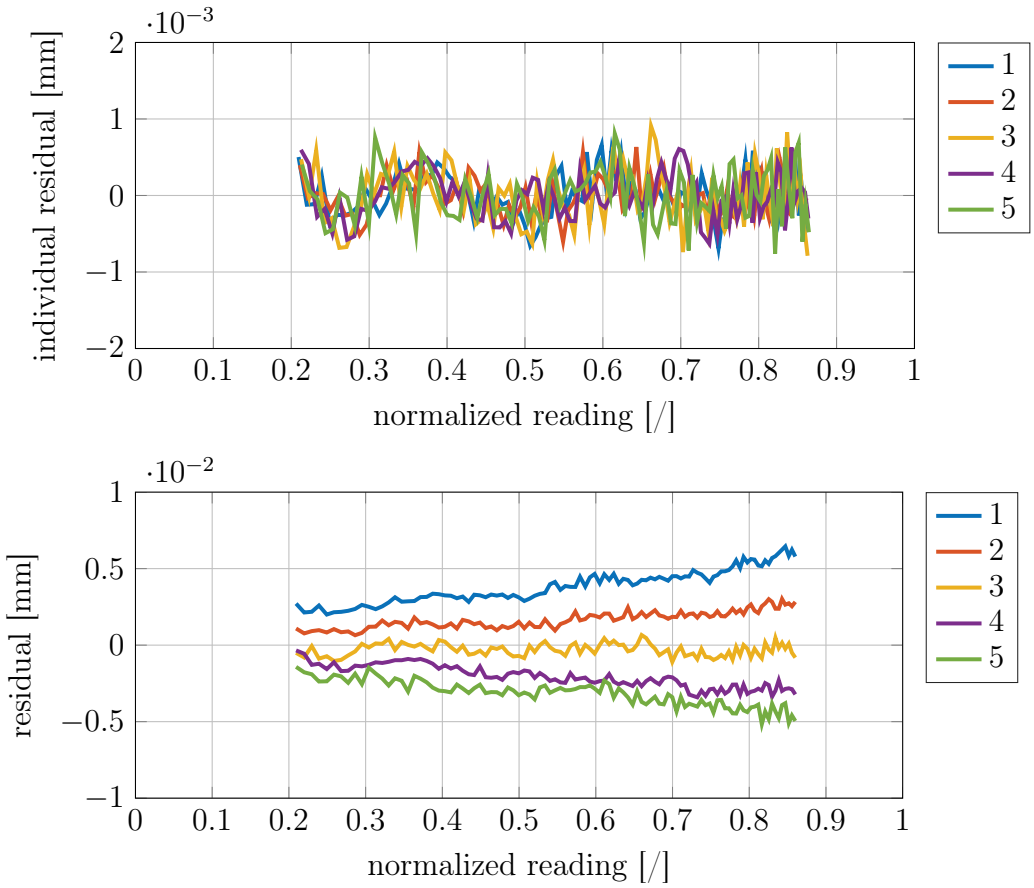

Figure 7.1.: In-measurement error and measurement-to-measurement error of displacement sensor 2, fitted with polynomial of dergee = 5.

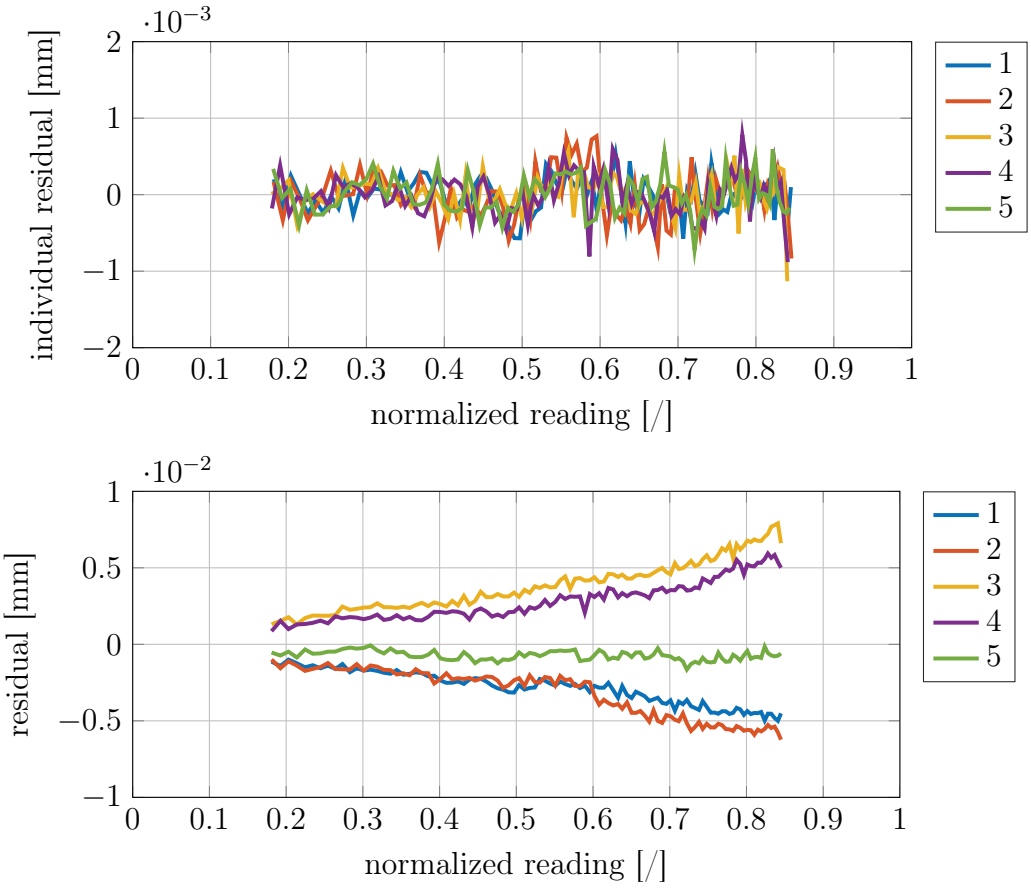

Figure 7.2.: In-measurement error and measurement-to-measurement error of displacement sensor 3, fitted with polynomial of dergee = 5.

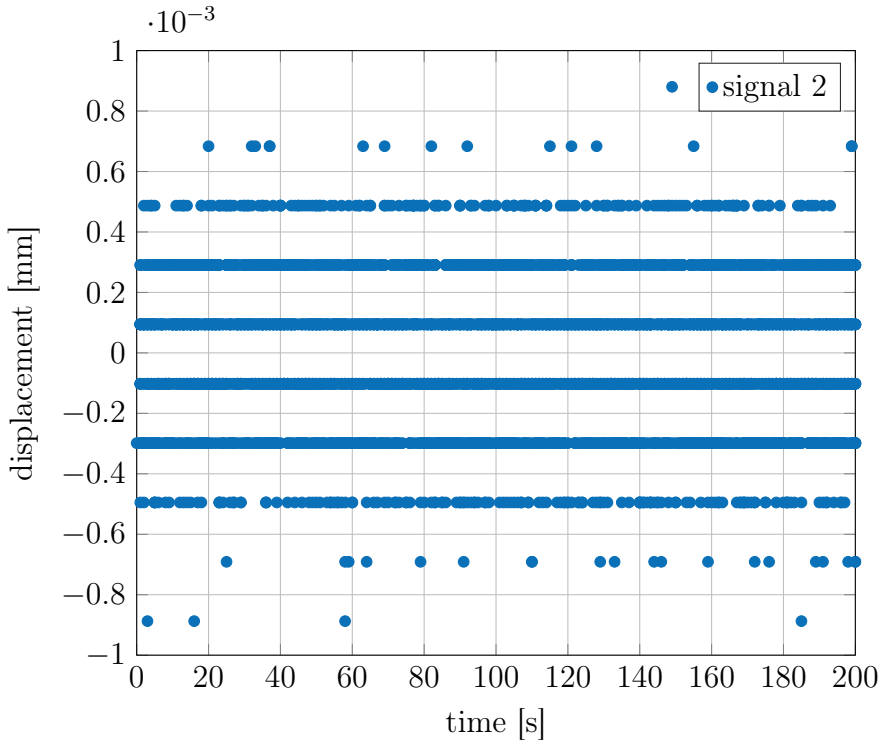

Figure 7.3.: Noise in a static test of displacement sensor 2 over time.

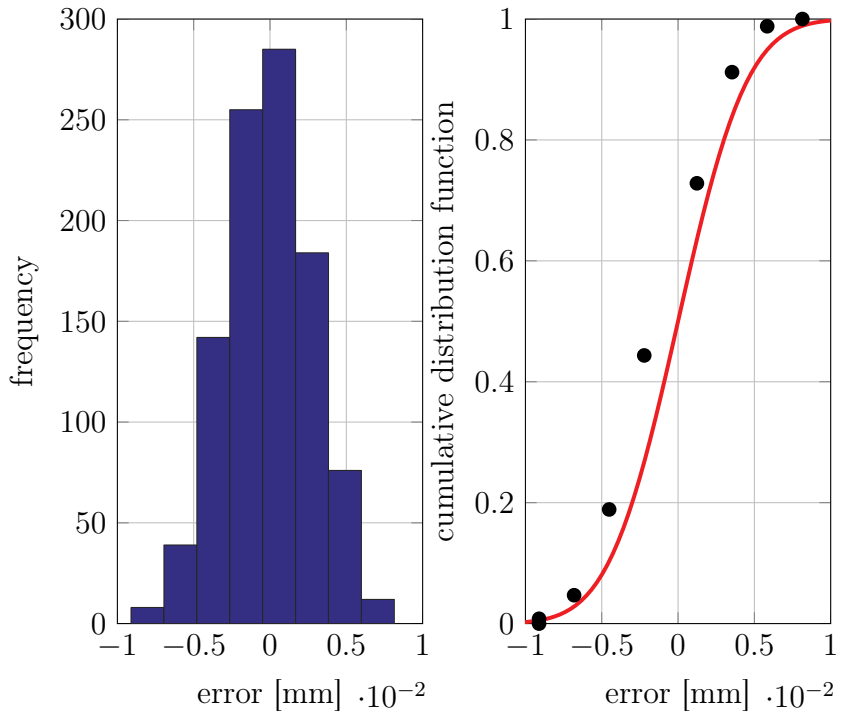

Figure 7.4.: Kolmogorow-Smirnow test for noise of displacement sensor 2.

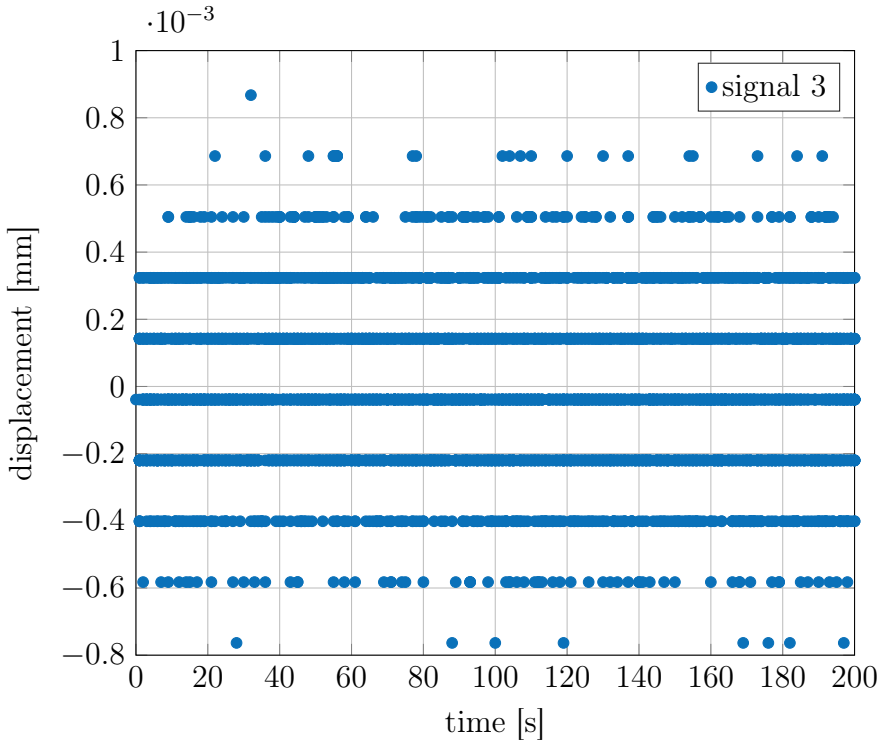

Figure 7.5.: Noise in a static test of displacement sensor 3 over time.

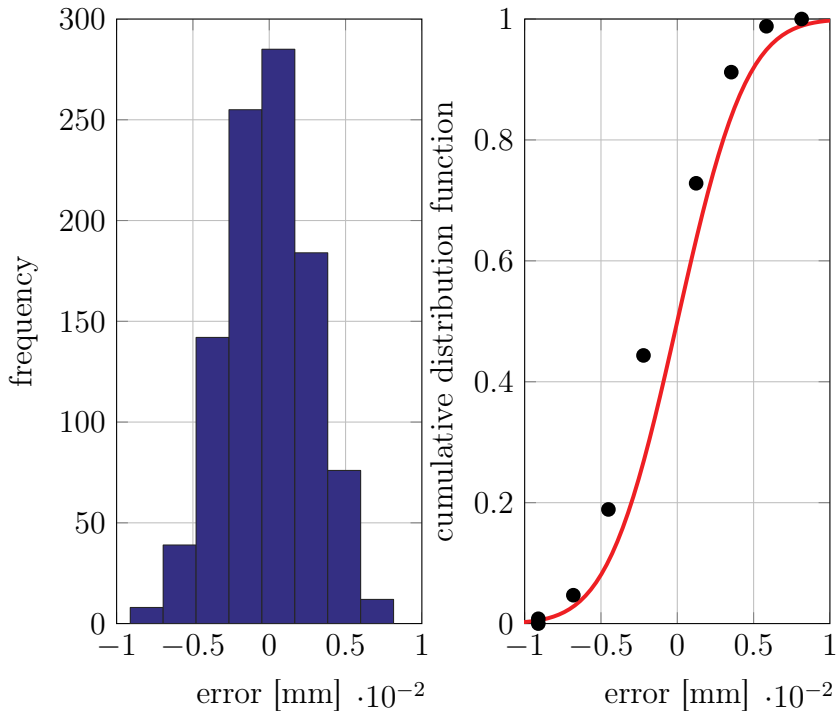

Figure 7.6.: Kolmogorow-Smirnow test for noise of displacement sensor 3.

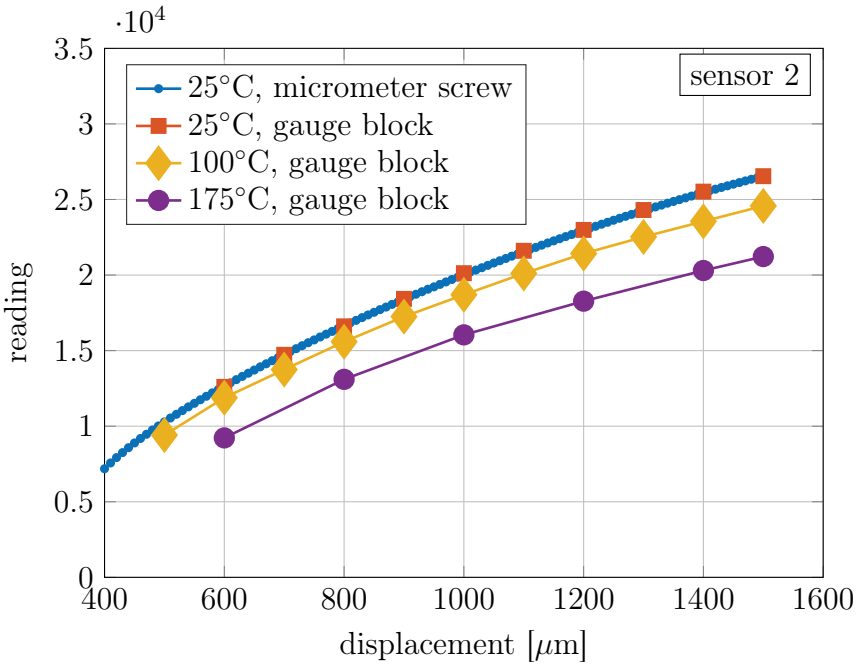

Figure 7.7.: Calibration data without consideration of thermal expansion at 25°C, 100°C and 175°C performed on gauge block calibration tool and comparison of micrometer screw and gauge block calibration at 25°C of displacement sensor 2.

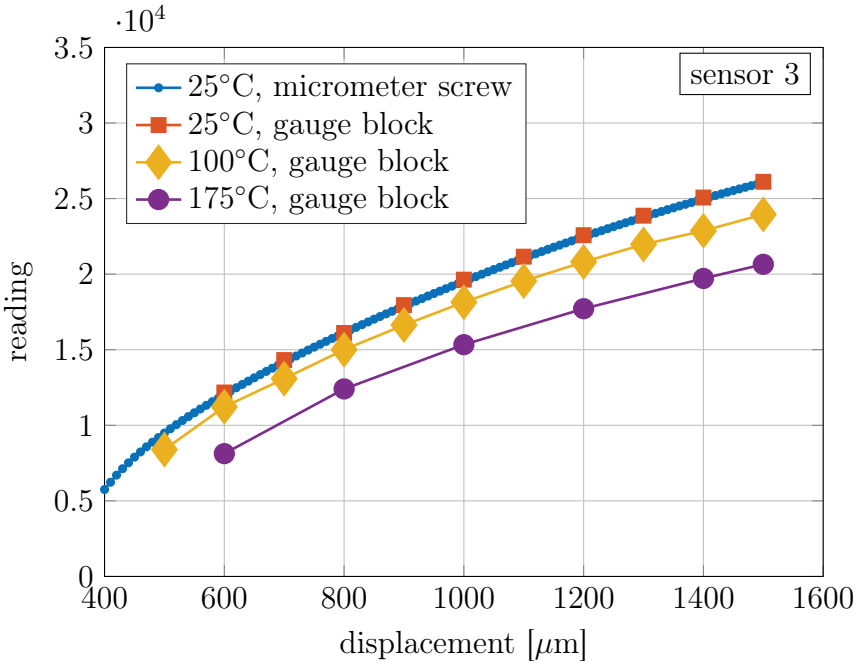

Figure 7.8.: Calibration data without consideration of thermal expansion at 25°C, 100°C and 175°C performed on gauge block calibration tool and comparison of micrometer screw and gauge block calibration at 25°C of displacement sensor 3.

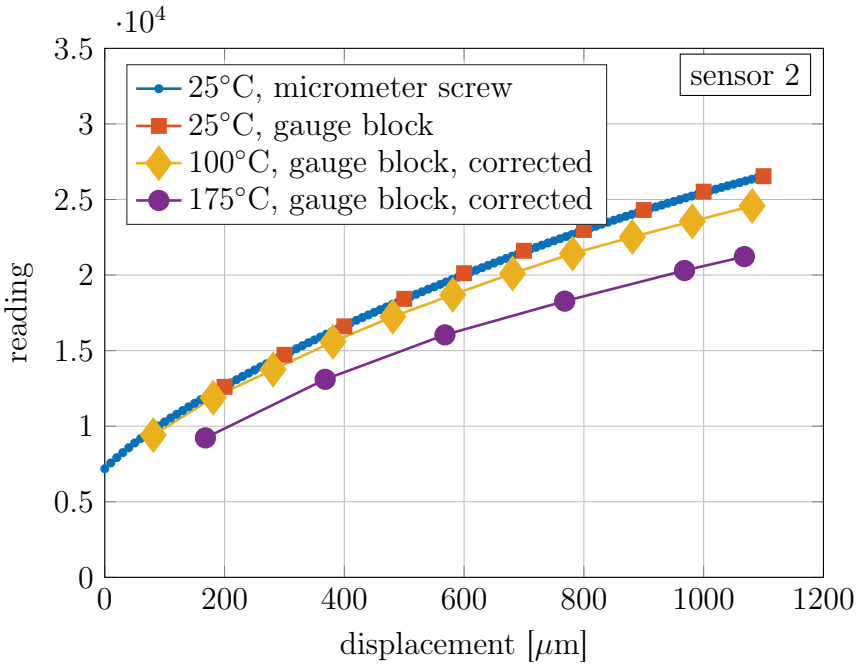

Figure 7.9.: Calibration data considering thermal expansion at 25°C, 100°C and 175°C performed on gauge block calibration tool and comparison of micrometer screw and gauge block calibration at 25°C of displacement sensor 2.

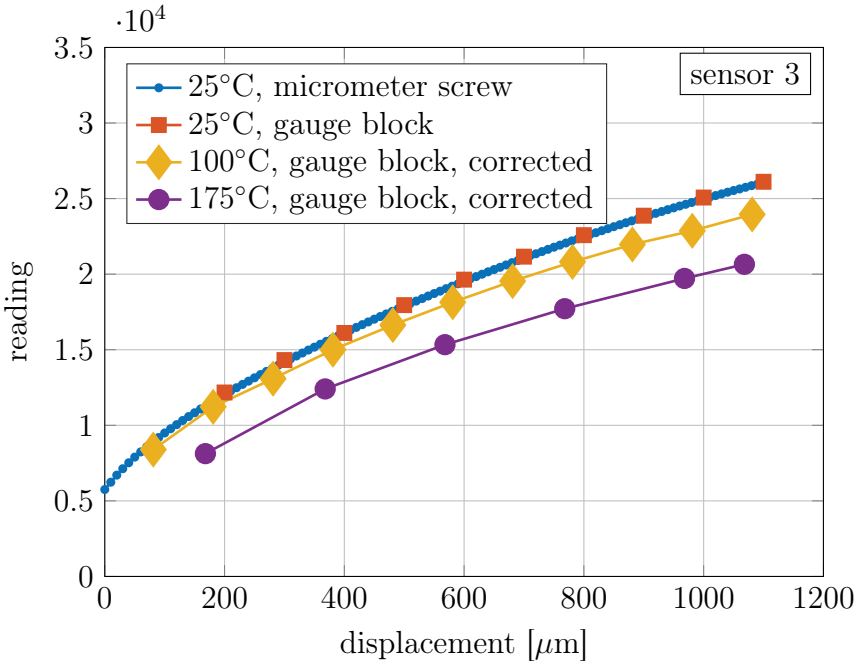

Figure 7.10.: Calibration data considering thermal expansion at 25°C, 100°C and 175°C performed on gauge block calibration tool and comparison of micrometer screw and gauge block calibration at 25°C of displacement sensor 3.

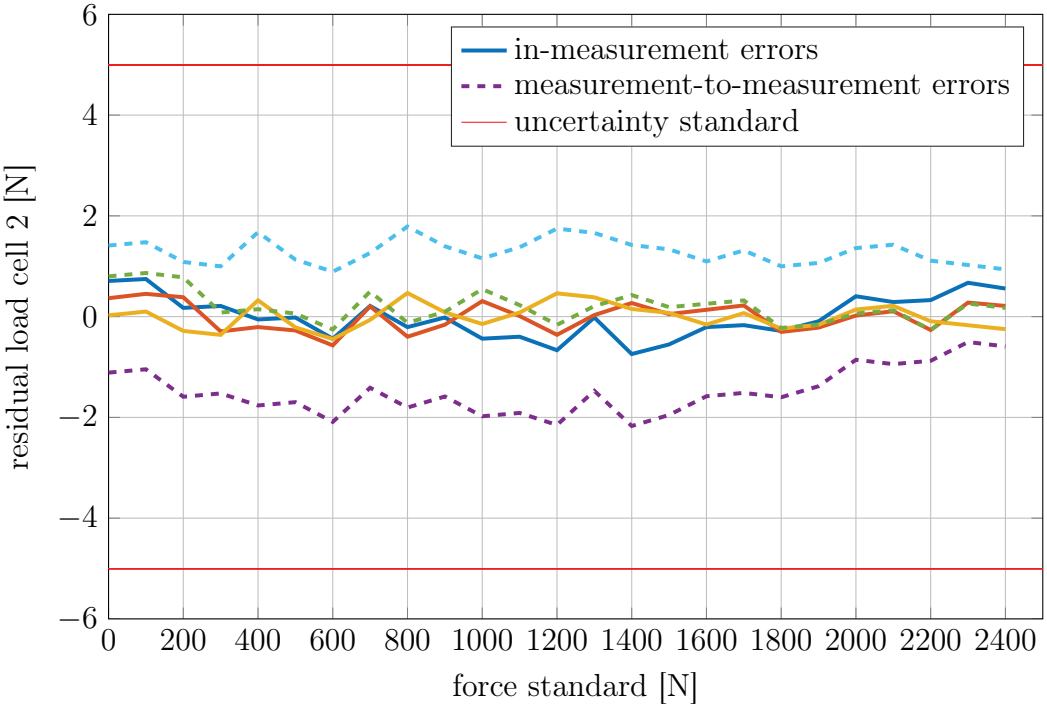

Figure 7.11.: Residuals of linear regression for load cell 2.

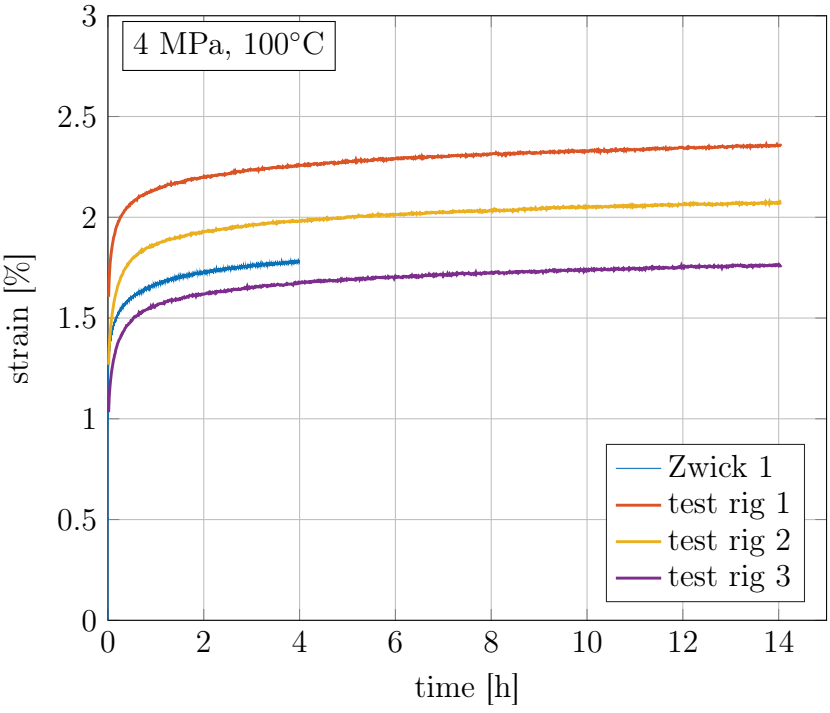

Figure 7.12.: Creep measurement of PTFE at 100°C and 4 MPa.

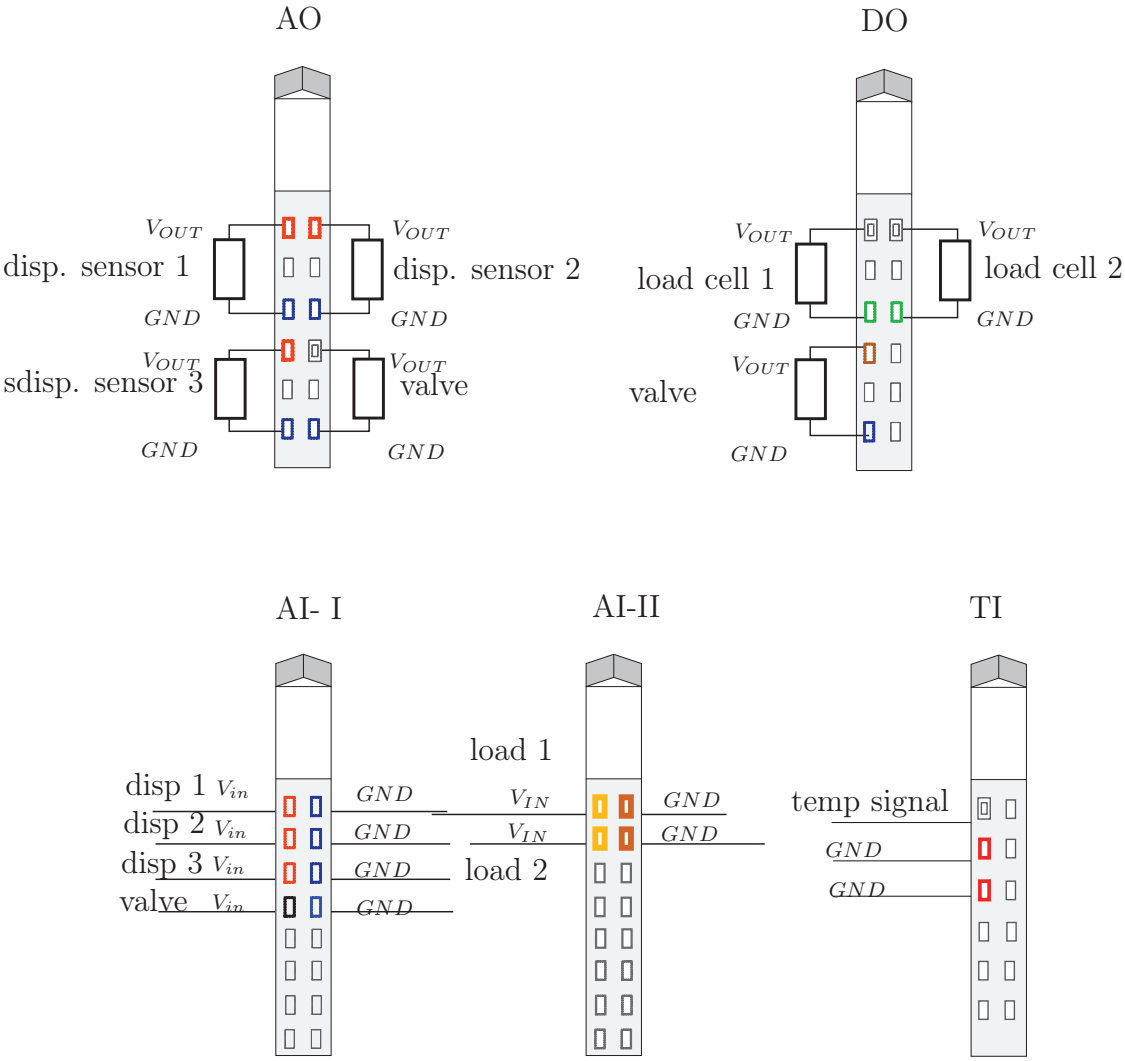

Figure 7.13.: Circuit diagram of analog input moduels I & II (AI-I and AI-II), analog output module (AO), digital output module (DO) and the temperature input module (TI).